Int J Fract (2016) 201:29–80
DOI 10.1007/s10704-016-0142-6

SPECIAL INVITED ARTICLE CELEBRATING IJF AT 50

Ductile failure modeling

Ahmed Amine Benzerga · Jean-Baptiste Leblond · Alan Needleman · Viggo Tvergaard

Received: 29 March 2016 / Accepted: 21 July 2016 / Published online: 27 July 2016

Abstract Ductile fracture of structural metals occurs mainly by the nucleation, growth and coalescence of voids. Here an overview of continuum models for this type of failure is given. The most widely used current framework is described and its limitations discussed. Much work has focused on extending void growth models to account for non-spherical initial void shapes and for shape changes during growth. This includes cases of very low stress triaxiality, where the voids can close up to micro-cracks during the failure process. The void growth models have also been extended to consider the effect of plastic anisotropy, or the influence of non-local effects that bring a material size scale into the models. Often the voids are not present in the material from the beginning, and realistic nucleation models are important. The final failure process by coalescence of neighboring voids is an issue that has been given much attention recently. At ductile fracture, localization of plastic flow is often important, leading to failure by a void-sheet mechanism. Various applications are presented to illustrate the models, including welded specimens, shear tests on butterfly specimens, and analyses of crack growth.

Keywords Ductile failure · Constitutive modeling · Micromechanics · Porosity evolution

A. A. Benzerga
Department of Aerospace Engineering, Texas A&M University, College Station, TX, USA

J.-B. Leblond
Institut Jean le Rond d'Alembert, Sorbonne Universités, Université Pierre et Marie Curie, Paris, France

A. Needleman (✉)
Department of Materials Science and Engineering, Texas A&M University, College Station, TX, USA
e-mail: needle@tamu.edu

V. Tvergaard
Department of Mechanical Engineering, The Technical University of Denmark, Lyngby, Denmark

1 Introduction

The role played by void nucleation, growth and coalescence in ductile fracture was identified in the 1940s (Tipper 1949). However, it was not until the 1960's that the phenomenology of this process was well documented (Rogers 1960; Beachem 1963; Puttick 1959; Gurland and Plateau 1963). In structural metals deformed at room temperature, the voids generally nucleate by decohesion of second phase particles or by particle fracture, and grow by plastic deformation of the surrounding matrix. Void coalescence occurs either by necking down of the matrix material between adjacent voids or by localized shearing between well separated voids, as has been described in a number of previous review papers (Garrison and Moody 1987; Tvergaard 1990; Benzerga and Leblond 2010).

The first micromechanical studies of void growth were carried out for a single void in an infinite elastic-plastic solid, either a circular cylindrical void (McClintock 1968) or a spherical void (Rice and Tracey 1969).

A numerical study for a material containing a periodic array of circular cylindrical voids (Needleman 1972) allowed for including the effect of the interaction with neighboring voids, both in the early growth stages and in the final stages approaching coalescence. This numerical study considered a representative unit volume, containing a single void, with appropriate boundary conditions to represent the full material. Such unit cell analyses have become an important tool in the analysis of several different aspects of ductile fracture. It is also appreciated that unit cells containing many voids have advantages over those with only one void, as they can account for differences in void size or spacing and also for localized plastic flow due to void clustering or due to instabilities.

One approach to modeling void evolution in plastic solids is to directly use isolated void growth analyses as in the models of Beremin et al. (1981a) and Johnson and Cook (1985). Such uncoupled models have been recently reviewed by Pineau et al. (2016). Another approach is to incorporate porosity evolution into the constitutive formulation and several porous plastic constitutive frameworks have been developed for analyzing ductile failure problems, (e.g. Gurson 1975, 1977; Rousselier 1981, 1987). Probably the most widely known and most widely used porous ductile material model is that developed by Gurson based on micromechanical studies (Gurson 1975, 1977), using averaging techniques similar to those applied by Bishop et al. (1945). Here, we focus on ductile failure modeling based on the Gurson framework (Gurson 1975, 1977) and its modifications. Some improvements were added to Gurson's model early on (Chu and Needleman 1980; Tvergaard 1981, 1982b; Tvergaard and Needleman 1984), resulting in a modified Gurson model (the so-called GTN model), which has since been used extensively to analyze a variety of problems. In many applications the material does not contain voids initially, so the representation of gradual void nucleation during the deformation process is important. Porous ductile material models were also developed early on by fitting experiments for powder metallurgy materials (Shima and Oyane 1976), and in fact the approximate yield surfaces obtained by these different methods are in rather good agreement for a given void volume fraction.

The Gurson model is limited by a number of assumptions, e.g. the voids are embedded in a standard Mises solid, and the voids are taken to remain spherical independent of the stress state. At low stress triaxiality, i.e. low mean tensile stress relative to the effective Mises stress, voids tend to elongate, and this can have a strong influence on predictions of ductile failure. Early studies that extended the Gurson model to account for void shape effects are given by Gologanu et al. (1993, 1994, 1997). Other early work on the effect of shape changes was presented by Ponte Castañeda and Zaidman (1994). Regarding the effect of anisotropy the Gurson model was extended by Benzerga and Besson (2001) to consider a spherical void embedded in an elastic-plastic matrix that obeys Hill's quadratic yield condition (Hill 1948). This model was further extended by Keralavarma and Benzerga (2008, 2010) to also account for non-spherical voids embedded in the same anisotropic solid.

The final failure in void containing materials typically occurs by void coalescence, where the ligament between neighbor voids necks down to zero thickness and leaves the characteristic fibrous fracture surface. An important contribution to the modeling of this mechanism has been given by Koplik and Needleman (1988). However, quite often the final failure is associated with a shear band instability (Rice 1976; Needleman and Rice 1978), leading to a so-called void-sheet failure, where voids grow to coalescence inside a narrow layer of material (Rogers 1960) and the fracture surface shows that the voids have been smeared out during coalescence. In materials containing two size scales of voids or inclusions from which voids nucleate, it is sometimes observed that plastic flow localization develops between two larger voids and that final failure involves void-sheet failure by the small scale voids between the larger voids (Cox and Low 1974; Van Stone et al. 1985). In a model of this phenomenon the small scale voids have been represented in terms of the Gurson model and localization leading to void-sheet failure between larger voids has been predicted (Tvergaard 1982a).

Recently there has been increasing interest in the behavior of porous materials under low stress triaxiality, such as simple shear, where the standard material models do not predict void growth to coalescence. Full three dimensional analyses for shear specimens containing spherical voids have been carried out by Barsoum and Faleskog (2007a) in order to model experiments on ductile fracture in double notched tube specimens loaded in combined tension and torsion (Barsoum and Faleskog 2007b). In plane strain cell model analyses for a material containing a periodic array of cir-

cular cylindrical voids (Tvergaard 2008, 2009, 2012; Dahl et al. 2012), it has been found that in stress states similar to simple shear the voids flatten out to micro-cracks, which rotate and elongate until interaction with neighboring micro-cracks gives coalescence; stresses pass through a maximum so that failure is predicted. This mechanism has also been found in three dimensions for initially spherical voids (Nielsen et al. 2012). Thus, under high stress triaxiality the void volume fraction increases until ductile fracture occurs, whereas the void volume fraction disappears under low stress triaxiality, as the voids become micro-cracks. The significant void shape changes at low stress triaxiality are accounted for in the models of Gologanu et al. (1993, 1994, 1997) and Ponte Castañeda and Zaidman (1994) mentioned above, but to deal with failure in simple shear the models must be extended to describe void closure into micro-cracks and the interaction between these micro-cracks.

The early constitutive models for porous ductile solids did not incorporate an effect of the third stress invariant J_3, but recently there has been more focus on this through the effect of the Lode parameter. It has been found in some fracture tests under loads including shear (Bao and Wierzbicki 2004; Barsoum and Faleskog 2011) that the effective plastic strain to failure does not decrease monotonically with increasing stress triaxiality. This has been further investigated by Xue et al. (2013), where tension-torsion fracture experiments are modeled using an extension of the Gurson model by Nahshon and Hutchinson (2008), which has been made J_3 dependent by adding an extra damage term that allows for failure prediction even at zero hydrostatic tension. This extension of the Gurson model (Nahshon and Hutchinson 2008) has been compared with cell model studies for voids in shear fields (Tvergaard and Nielsen 2010) and it has been found that the model can capture quantitative aspects of softening and localization in shear. Xue et al. (2013) modeled tension-torsion fractures by finding the localization strain in a shear stress state with varying amounts of superposed tensile stress, and showed that the failure strain does not vary monotonically with the stress triaxiality. On the other hand, it has been found in other recent fracture tension-torsion experiments (Haltom et al. 2013; Papasidero et al. 2015) that the strain to failure decreases monotonically with stress triaxiality. Improved ductile failure modeling is therefore needed to gain insight into the fundamental reasons for such conflicting reports.

Recent reviews of the field are available (Benzerga and Leblond 2010; Besson 2010). Nevertheless, developments that have occurred in the past five years, notably pertaining to the influence of void shape effects at low triaxiality, the micromechanically-based modeling of void coalescence and new applications, justifies a review paying special attention to these aspects.

The paper focuses on studies extending and using the framework orginated by Gurson (1975, 1977) and is organized as follows. Section 2 gives the current framework, through an introduction to the Gurson and GTN models. Section 3 discusses void nucleation, while Sect. 4 presents a number of models for void growth. Studies of void coalescence are discussed in Sect. 5. Localization of plastic flow is introduced in Sect. 6, and finally applications of the ductile failure models are presented in Sect. 7.

2 Current framework

The Gurson flow potential (Gurson 1975, 1977) was obtained from the approximate homogenization and limit-analysis of a hollow sphere made of a rigid, ideal-plastic Mises solid. It was subsequently modified by Tvergaard (1981) and Tvergaard and Needleman (1984) to take the form

$$\Phi(\boldsymbol{\sigma}, f^*) = \frac{\sigma_{eq}^2}{\bar{\sigma}^2} + 2q_1 f^* \cosh\left(\frac{3q_2\sigma_m}{2\bar{\sigma}}\right) - 1 - q_3 f^{*2} = 0 \tag{1}$$

during plastic flow.

Here, $\sigma_{eq} = (\frac{3}{2}\boldsymbol{\sigma}' : \boldsymbol{\sigma}')^{1/2}$, $\sigma_m = \frac{1}{3}\mathrm{tr}\,\boldsymbol{\sigma}$ ($\boldsymbol{\sigma}$ is the Cauchy stress tensor and $\boldsymbol{\sigma}'$ its deviator), $\bar{\sigma}$ is the matrix flow strength, the $q_i, i = 1, 2, 3$ are Tvergaard's (1981) parameters (in practice $q_3 = q_1^2$ is generally used) and f^* is given by

$$f^* = \begin{cases} f, & f < f_c \\ f_c + (1/q_1 - f_c)(f - f_c)/(f_f - f_c), & f \geq f_c \end{cases} \tag{2}$$

where f is the porosity (the void volume fraction) and f_c and f_f are specified parameters. The constant $1/q_1 = f_u$ is the value of f^* at zero stress carrying capacity, i.e. at material failure. As $f \to f_f$ and $f^* \to f_u$ the material loses all stress carrying capacity.

The rate of deformation tensor, $\mathbf{D}$, the symmetric part of $\dot{\mathbf{F}} \cdot \mathbf{F}^{-1}$ (where $\mathbf{F} = \partial\bar{\mathbf{x}}/\partial\mathbf{x}$ with $\mathbf{x}$ and $\bar{\mathbf{x}}$ being the positions of a material point in the reference and current states, respectively), is written as the sum of an

elastic part (most commonly in applications a hypoelastic part), $\mathbf{D}^e$, and a plastic part, $\mathbf{D}^p$ with the plastic flow rule given by

$$\mathbf{D}^p = \dot{\Lambda}\frac{\partial \Phi}{\partial \boldsymbol{\sigma}}(\boldsymbol{\sigma}, f) \tag{3}$$

For a rate independent matrix material

$$\dot{\Lambda}\begin{cases} = 0 & \text{if } \Phi(\boldsymbol{\sigma}, f) < 0 \\ \geq 0 & \text{if } \Phi(\boldsymbol{\sigma}, f) = 0 \end{cases} \tag{4}$$

while for a rate dependent matrix material, $\dot{\Lambda}$ is a non-negative function of state.

Assuming small elastic strains, the constitutive relation can be expressed in terms of the Cauchy stress $\boldsymbol{\sigma}$ and the rate of deformation tensor $\mathbf{D}$ in the form

$$\hat{\boldsymbol{\sigma}} = \mathbf{L}^{el} \cdot (\mathbf{D} - \mathbf{D}^p). \tag{5}$$

Here the Jaumann rate of Cauchy stress $\hat{\boldsymbol{\sigma}}$ is given by

$$\hat{\boldsymbol{\sigma}} = \frac{D\boldsymbol{\sigma}}{Dt} + \boldsymbol{\sigma} \cdot \boldsymbol{\Omega} - \boldsymbol{\Omega} \cdot \boldsymbol{\sigma} \tag{6}$$

where $D\boldsymbol{\sigma}/Dt$ is the material time derivative of Cauchy stress and $\boldsymbol{\Omega}$ is the antisymmetric part of $\dot{\mathbf{F}} \cdot \mathbf{F}^{-1}$.

With the moduli $\mathbf{L}^{el}$ taken as constants, as generally done in practice, the relation Eq. (5) is a hypoelastic relation not a hyperelastic relation. However, if needed, a hyperelastic relation can be expressed in the form Eq. (5) but the elastic moduli are then stress dependent.

The evolution of the void volume fraction has two terms; a growth term from approximate matrix incompressibility (elastic volume change neglected) and a term arising from void nucleation, so that

$$\dot{f} = (1 - f)\,\mathrm{tr}\,\mathbf{D}^p + \dot{f}_{\mathrm{nuc}} \tag{7}$$

It is worth noting that the term $(1 - f)\,\mathrm{tr}\,\mathbf{D}^p$ that accounts for void growth is one of the rare rigorous equalities (presuming no elastic volume change) derived from homogenization.

Another key relation of the framework is

$$\dot{W}^p = \bar{\sigma}\dot{\bar{\epsilon}} = (1 - f)\boldsymbol{\sigma} : \mathbf{D}^p \tag{8}$$

where $\dot{W}^p = \bar{\sigma}\dot{\bar{\epsilon}}$ is the plastic dissipation rate in the matrix material. There are two parts to this relation: (i) the statement that the macro or overall plastic dissipation rate is equal to the plastic dissipation rate in the matrix material; and (ii) that the plastic dissipation rate in the matrix material can be represented by the product of "average" values (or representative values) of flow strength and matrix plastic strain rate.

Note that Eq. (8) implies that during plastic flow

$$\dot{\Lambda} = \frac{\bar{\sigma}\dot{\bar{\epsilon}}}{(1 - f)\boldsymbol{\sigma} : (\partial \Phi/\partial \boldsymbol{\sigma})} \tag{9}$$

Although the analysis leading to Eq. (1) was based on the assumption of a perfectly plastic, rate independent matrix material, this framework is widely used to model porous materials with strain and strain rate hardening matrix materials.

Equations (1) to (8) together with a constitutive characterization of the matrix material provide a constitutive framework for analyzing porosity evolution in ductile solids. This framework, now generally referred to as the GTN relation, differs from a purely phenomenological damage mechanics framework in that, to some extent at least, it is based on micromechanical analyses. However, it is important to remember that the micromechanical analyses leading to the form of the flow potential, Eq. (1) and extensions that will be discussed subsequently, are obtained from analyses predicting the yield surface of a non-hardening, rate independent solid containing voids. The extensions to use Eq. (1) for other matrix constitutive characterizations, for example strain hardening and strain rate hardening matrix materials, are phenomenological as are the extensions to include the q_i parameters and void coalescence via Eq. (2). Thus, this framework as used is a cross between a micromechanically based model and a phenomenological damage mechanics theory.

The micromechanical basis of this material model can be regarded as pertaining to isothermal porosity evolution in lightly (strain and/or strain rate) hardening solids, mainly structural metals at room temperature. Even in this context there are potentially significant effects that will not be discussed in the following: (i) for sufficiently small voids the increased hardening due to the size dependence of plastic flow in metals delays void growth (e.g. Hussein et al. 2008; Segurado and Llorca 2009); (ii) the voids in structural metals typically nucleate from second phase particles and the constraint provided by the particle can enhance void growth at low values of the stress triaxiality (e.g. Fleck et al. 1989);

and (iii) at sufficiently high loading rates as can occur near a crack tip in a dynamically loaded component or structure material inertia can affect porosity evolution (e.g. Ortiz and Molinari 1992; Jacques et al. 2012).

A goal of recent analyses is to develop flow potentials that extend the micromechanical basis of this framework. For example, the form of Eq. (1) is based on analysis of spherical voids. The effects of void shape and void shape changes, which are particularly important at low values of the stress triaxiality, are not accounted for. An ultimate goal is to develop a unified, micromechanically based flow potential that incorporates void nucleation, void growth and void coalescence. Progress is being made on incorporating void coalescence but incorporating void nucleation is essentially unexplored.

The aim of the GTN relation is to provide a basis for predicting ductile failure/fracture or at least the reduction in strength due to porosity evolution. Modeling the localization of deformation and creation of new free surface requires the incorporation of a length scale into the formulation as will be discussed in several contexts subsequently.

3 Void nucleation

In ductile fracture formulations based on a single damage variable, namely the void volume fraction f, void nucleation is represented through a rate equation of the form of Eq. (7). This formulation goes back to Gurson (1975) and was further developed by Chu and Needleman (1980) who accounted for two possible contributions that we write as

$$\dot{f}_{\rm nuc} = \mathcal{D}\dot{\bar{\varepsilon}} + \mathcal{B}(c_1\dot{\sigma}_{\rm eq} + c_2\dot{\sigma}_{\rm m}), \tag{10}$$

with the first term representing strain-controlled nucleation (Goods and Brown 1979), and the second term representing stress-controlled nucleation (Argon et al. 1975; Beremin et al. 1981b), with the requirement that $c_1\dot{\sigma}_{\rm eq} + c_2\dot{\sigma}_{\rm m} > 0$. Generally the factor c_1 is taken as 1 or 0 and the factor c_2 is introduced here based on findings by Needleman (1987) using cell model analyses. On the basis of earlier studies (e.g., Goods and Brown 1979; Argon et al. 1975), it was suggested by Chu and Needleman (1980) that $\mathcal{D}$ and $\mathcal{B}$ are functions of $\bar{\varepsilon}$ and $c_1\sigma_{\rm eq} + c_2\sigma_{\rm m}$, respectively, and that they follow a normal distribution. For the strain controlled term,

$$\mathcal{D}(\bar{\varepsilon}) = \frac{f_{\rm N}}{s_{\rm N}\sqrt{2\pi}} \exp\Big[-\frac{1}{2}\Big(\frac{\bar{\varepsilon} - \epsilon_{\rm N}}{s_{\rm N}}\Big)^2\Big] \tag{11}$$

where $f_{\rm N}$ represents the volume fraction of void-nucleating particles, $\epsilon_{\rm N}$ is some average nucleation strain and $s_{\rm N}$ is a standard deviation.

For the stress controlled term, with σ_N the average nucleation stress,

$$\mathcal{B} = \frac{f_N}{s_N\sqrt{2\pi}} \exp\Big[-\frac{1}{2}\Big(\frac{c_1\sigma_{\rm eq} + c_2\sigma_m - \sigma_N}{s_N}\Big)^2\Big] \tag{12}$$

if $(c_1\sigma_{\rm eq} + c_2\sigma_m)$ is at its maximum over the deformation history. Otherwise $\mathcal{B} = 0$.

At a more fundamental level, an energy criterion is necessary for void nucleation (Goods and Brown 1979). When this criterion is satisfied, a sufficient condition may be formulated in terms of stresses. On the other hand, attainment of a critical strain is neither necessary nor sufficient for void nucleation. In addition, a strain-controlled criterion does not capture the dependence of void nucleation upon stress triaxiality, a fact that is inferred from both experiments (Beremin et al. 1981b) and analysis (Needleman 1987). It would also predict an increasing amount of void nucleation with decreasing stress triaxiality, simply because of the larger amounts of accumulated plastic strain at low triaxialities. In practice, however, use of a strain-controlled nucleation may be a convenient way of representing the outcome of a more basic stress-based criterion. An example in this regard was discussed by Needleman (1987).

Analyses of localization carried out within the framework of Rice (1976) indicated that strain-controlled and stress-controlled nucleation can lead to quite different predictions of macroscopic ductility, interpreted as the onset of a bifurcation in the set of governing partial differential equations (see Sect. 6 for details). Of particular significance is that the hydrostatic stress dependence of $\dot{f}_{\rm nuc}$ in Eq. (10) gives rise to non-symmetry of the tangent matrix, which favors early flow localization.

In ductile fracture formulations that employ additional damage variables, such as the void shape and orientation, Eqs. (7–10) may still be used. This model of nucleation does not refer to a specific nucleation mechanism and thus does not distinguish between particle debonding and particle cracking for instance. In some material systems, void nucleation is deformation

induced and may occur at twins (Kondori and Benzerga 2014; Rodriguez et al. 2016) or by cleavage in brittle phases (Joly et al. 1990). In such cases as well as for particle cracking, damage initiates in the form of penny-shape cracks. It is not clear what role, if any, the shape of incipient voids plays on subsequent fracture events but enhanced void nucleation formulations are needed to elucidate such effects. Also, the formulation in Eq. (10) rests on empirical experimental evidence, some basic analyses in the 1970's and early 1980's and further corroborated by the micromechanical simulations of Needleman (1987). In the latter, constitutive relations are specified independently for the matrix, the particle and the interface. However, the analyses were limited to axisymmetric loadings, spherical particles in a plastically isotropic matrix, with debonding as the only nucleation mechanism. There is a great deal of interest in recent years in ductile fracture at low triaxiality of stress states, and in particular under shear dominated loadings. Under such circumstances, additional complexity arises due to so-called void-locking effects (see Pineau et al. 2016 for an overview). There is a need to extend the analysis basis to account for particle shape effects, nucleation by cracking or at sites other than particles. Some of that has been accomplished (e.g. Xu and Needleman 1993; Hu and Ghosh 2008) but has not yet been translated into useful expressions for modeling void nucleation in a Gurson-type constitutive framework. It is worth mentioning in this context the work of Horstemeyer and co-workers (Horstemeyer and Gokhale 1999), who included the effects of the third stress invariant in a phenomenological void nucleation criterion, as well as the work of Lee and Mear (1999) who in the spirit of earlier work (Wilner 1988) conducted a large series of analyses providing a micromechanical basis to formulate a nucleation criterion that distinguishes particle debonding from particle cracking (see Benzerga and Leblond 2010).

There have been a limited number of micromechanical studies of the effects of particle size and distribution on void nucleation. A highly idealized two dimensional study of void clustering effects on void nucleation by inclusion debonding was carried out by Shabrov and Needleman (2002). The particle distributions in Fig. 1 were analyzed for applied overall in-plane stress states of $\sigma_{yy} = \sigma$ and $\sigma_{xx} = \rho\sigma$ so that the stress triaxiality increases with increasing values of ρ.

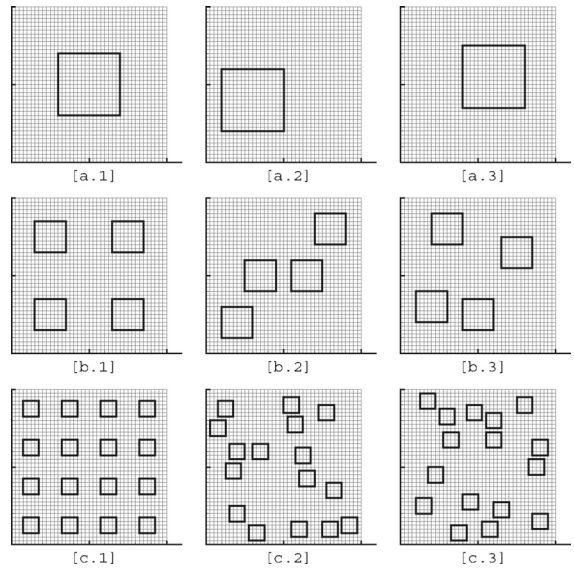

Fig. 1 Inclusion distributions analyzed by Shabrov and Needleman (2002). Each distribution has the same volume fraction. The particle size decreases as the distributions go from *row a* to *row b* to *row c*

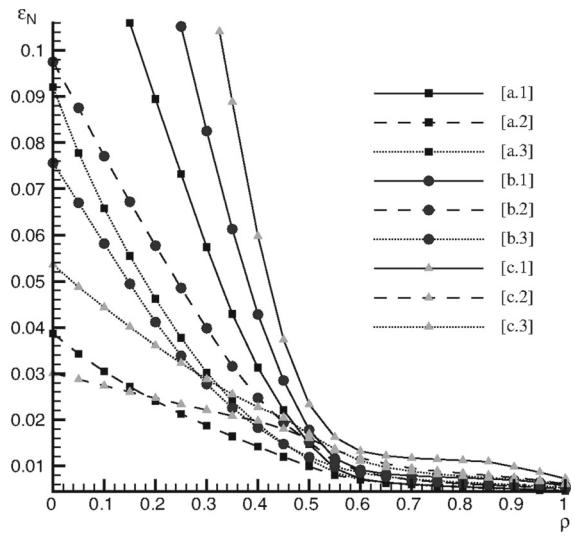

Fig. 2 The dependence of the void nucleation strain on the imposed stress ratio ρ. The distribution labels correspond to those in Fig. 1. From Shabrov and Needleman (2002)

Figure 2 shows the effects of particle size and distribution on the strain for void nucleation. The nucleation strain is more sensitive to particle size and distribution at smaller values of ρ (lower stress triaxiality values) and has relatively little sensitivity when the stress triaxiality is higher. Furthermore, Shabrov and Needleman

(2002) found that the value of c in Eq. (10) differed significantly from $c = 1$, the most commonly used value in applications, and varied somewhat with particle size and distribution. The dependence on c is significant since, as will be seen in Sect. 6, the localization of deformation can depend on the value of c. There is a need for more, and more realistic, micromechanical studies of void nucleation and a need to use such studies to develop physically based void nucleation criteria.

4 Void growth

4.1 Generalities

There are two basic methods to derive "homogenized" models for porous plastic materials depicting the second phase—void growth—of ductile fracture:

- The first was initiated by Gurson (1975, 1977), followed by many others (Gologanu et al. 1993, 1994, 1997; Benzerga and Besson 2001; Monchiet et al. 2006, 2008; Keralavarma and Benzerga 2008, 2010; Madou and Leblond 2012a, b, 2013; Madou et al. 2013). Its principle consisted in combining the theory of limit-analysis (equivalent to plasticity theory in the absence of elasticity and strain hardening) with homogenization of some "elementary cell" in some plastic porous material. The shape of this cell was "adapted" to that of the enclosed void: spherical/cylindrical for a spherical/cylindrical void, spheroidal and confocal with the void if spheroidal, ellipsoidal and again confocal with the void if ellipsoidal. Conditions of homogeneous boundary strain rate, as proposed by Mandel (1964) and Hill (1967), were used. The matrix was assumed to obey the Mises (isotropic) yield criterion or the (Hill 1948) (orthotropic) criterion.
- The second originated from homogenization methods extending the linear Hashin–Shtrikman bounds to nonlinear composites (Ponte Castaneda 1991; Willis 1991; Michel and Suquet 1992), and used a technique of "comparison" with some reference linear material. The early model of Ponte Castañeda and Zaidman (1994), in spite of its accuracy for deviatoric loadings, suffered from a notable overestimation of the overall yield limit under hydrostatic loading. This drawback was remedied in the more recent model of Danas and Ponte Castañeda (2009a, b) based on the "second-order homogenization method" (Ponte Castaneda 2002) . The Ponte Castañeda and Zaidman (1994) yield surface was also very recently improved by Agoras and Ponte Castañeda (2013, 2014) using an "iterative" approach devised by Ponte Castaneda (2012).

Both approaches are presented in the sequel but with major emphasis on the first one, which has been followed by most authors and used more widely for practical applications. As will be seen, a remarkable, though still incomplete degree of convergence between these approaches is apparent in very recent works.

Starting with the work of Gurson (1975, 1977) flow potentials for modeling room temperature ductile failure have mainly been based on analyses of isolated voids or idealized distributions of voids in a rate independent non-hardening solid. The analyses have focused on developing expressions for the onset of plastic yielding, i.e. yield surface. Presuming plastic normality at the microscale, the yield surfaces so computed serve as plastic potentials. It is as plastic potentials as in Eq. (3) that the derived expressions are typically used in applications.

4.2 Gurson's model

4.2.1 Original form

Gurson's (1975, 1977) model was derived from the approximate homogenization and limit-analysis of a hollow sphere made of some rigid, ideal-plastic material obeying the Mises yield criterion and the associated plastic flow rule, and subjected to conditions of homogeneous boundary strain rate (Mandel 1964; Hill 1967). The overall criterion thus obtained is given by Eq. (1) with $q_i = 1$ for $i = 1, 2, 3$ and $f^* \equiv f$.

Gurson (1975, 1977) also showed that as a consequence of homogenization combined with a classical result of limit-analysis, the normality property obeyed at the microscopic scale is preserved at the macroscopic scale; thus the overall flow rule is a direct consequence of the overall criterion, the overall plastic strain $\mathbf{D}^p$ being given by Eq. (3) with Eq. (4).

It is worth noting that Eq. (7) shows that the evolution of the internal parameter f is dictated by the flow rule and thus, by what precedes, by the flow potential. Therefore specifying this potential can, if void nucle-

ation is neglected, quite remarkably, completely define the model.

The Gurson model, in its original form, possesses the following nice properties, which may serve for an alternative, less rigorous but more intuitive derivation:

- the criterion reduces to that of von Mises in the limit of a zero porosity f;
- for a purely deviatoric loading ($\sigma_m = 0$), it predicts an overall yield stress equal to $(1-f)\bar{\sigma}$ (with $q_3 = q_1^2$ in Tvergaard's modification this becomes $(1-q_1 f)\bar{\sigma}$), in agreement with the elementary but rigorous inequality $\sigma_{eq} \leq (1-f)\bar{\sigma}$ resulting from the Cauchy-Schwartz inequality;
- for a purely hydrostatic loading ($\sigma_{eq} = 0$), it predicts an overall yield stress equal to $-\frac{2}{3}\bar{\sigma}\ln f$ (in Tvergaard's modification this becomes $-\frac{2}{3}\bar{\sigma}\ln(q_2 f)$), in agreement with the exact result for a hollow sphere resulting from an elementary calculation;
- for a low porosity f and a high triaxiality $T = \sigma_m/\sigma_{eq}$, combination of Eqs. (1, 3, 7) essentially yields (up to some multiplicative factor) the famous exponential void growth law of Rice and Tracey (1969), derived from the approximate limit-analysis of a single void embedded in an infinite matrix;
- it formally looks like (without being completely identical to) that for a hollow cylinder subjected to some axisymmetric loading under conditions of generalized plane strain, the exact form of which is also known from the work of Gurson (1975, 1977).

The original reasoning of Gurson (1975, 1977), which involved a somewhat dubious expansion in powers of a parameter which was not really small, was very recently reexamined and clarified by Leblond and Morin (2014) using more rigorous mathematics (see also Benallal et al. 2014). The main conclusions of this work were twofold:

- Gurson's criterion Eq. (1) provides a rigorous "upper bound" for the exact overall yield locus of the hollow sphere envisaged with the boundary conditions considered, and also as a consequence for that of a Hashin assembly of hollow spheres having identical porosities (the same conclusion was also reached by Benzerga and Leblond (2010), using a different argument);
- for the overall criterion, Gurson's expansion procedure converges very quickly, and his first-order criterion is almost identical to the final "converged" one; but this is less true for the overall flow rule, Gurson's first-order truncation of the series involving a 25 % maximum error on the porosity rate (further comments on this point are provided below).

4.2.2 *Extended forms*

In a sense, the first extension of Gurson's model defined by Eqs. (1, 3, 7) is due to Gurson himself, and pertains to strain hardening. He assumed hardening to be of isotropic type at the local scale, the yield stress in pure tension of the material being now, instead of a mere constant $\bar{\sigma}$, a given function $\sigma(\epsilon)$ of the Mises equivalent accumulated strain ϵ. Instead of extending his approximate homogenization of a hollow sphere made of ideal-plastic material to the hardenable case, he adopted a purely heuristic approach which consisted of assuming that his overall yield criterion Eq. (1) remained applicable to such a case, the parameter $\bar{\sigma}$ denoting now some "average value" of the local yield stress $\sigma(\epsilon)$. More precisely, he defined $\bar{\sigma}$ as the value of σ corresponding to some "average value", $\bar{\epsilon}$, of ϵ, for which he proposed Eq. (8) as an evolution law.

The meaning of Eq. (8) is that the plastic dissipation $(1-f)\boldsymbol{\sigma} : \mathbf{D}^p$ in the real, inhomogeneously strained material is heuristically identified to that, $\bar{\sigma}\dot{\bar{\epsilon}}$, in a fictitious, homogeneously strained material with equivalent accumulated strain $\bar{\epsilon}$ and yield stress $\bar{\sigma} = \sigma(\bar{\epsilon})$. One remarkable feature of Eq. (8) is that it does not only account for the hardening arising from the *deviatoric* part of the overall plastic strain rate $\mathbf{D}^p$, but also, in an approximate way, for that arising from its *hydrostatic* part, that is in fact from void growth.

The extended model thus defined however suffers from the fact that the same parameter $\bar{\sigma}$ enters both the "square" and "cosh" terms of the yield criterion, which means that the effect of strain hardening is implicitly assumed to be the same on the overall yield stresses under purely deviatoric and purely hydrostatic loadings. Leblond et al. (1995), using an extension of the approximate homogenization analysis of Gurson (1975, 1977) to the hardenable case, have shown that this is only an approximation which may lead to significant errors on the value of porosity rate. They have proposed a variant of Gurson's criterion Eq. (1) in which different macroscopic parameters σ_1, σ_2, instead of the single $\bar{\sigma}$, enter the "square" and "cosh" terms; they have evidenced the improvement thus brought to the prediction of the porosity rate through comparison of the model predictions with the results of some micro-

mechanical numerical simulations of a spherical cell, analogous to those of Koplik and Needleman (1988) for a cylindrical one.

Both the strain hardening and the strain rate hardening extensions of the Gurson (1975, 1977) framework are only expected to be reasonable approximations for lightly hardening solids since the form of Eq. (1) presumes a non-hardening, rate independent matrix material. On the other hand, the validity of the expressions governing the evolution of porosity, Eq. (7), and the equivalence of matrix and macro plastic dissipation, Eq. (8), are independent of the matrix material characterization.

Another heuristic modification involving the characterization of the matrix material is to represent the matrix material as a rate dependent viscoplastic solid, (Pan et al. 1983). As for strain hardening, the modification involves the relation between the matrix flow strength $\bar{\sigma}$ and the matrix plastic strain rate $\dot{\bar{\epsilon}}$. Specifically, the matrix plastic strain rate can be written as

$$\dot{\bar{\epsilon}} = \dot{\epsilon}_0 f(\bar{\sigma}, g) \tag{13}$$

where g is a measure of plastic flow resistance of the matrix.

Extensions of the original model of Gurson (1975, 1977) to matrix materials exhibiting kinematic hardening have also been proposed by Mear and Hutchinson (1985), see also Becker and Needleman (1986), Tvergaard (1987), Leblond et al. (1995). But these extensions are somewhat hampered by the ambiguities and difficulties arising, already at the local scale, in the definition of a "good" kinematic hardening rule in the context of large strain plasticity.

Another extension pertains to the adaptation of the model of Gurson (1975, 1977) to more realistic, non-spherical cell shapes. In order to bring the model predictions to better agreement with the results of some micromechanical simulations, Tvergaard (1981) proposed to modify Gurson's original flow potential by including the heuristic parameters q_i in Eq. (1). Most authors have adopted values of q_2 and q_3 equal to 1 and q_1^2, respectively; Tvergaard's proposed modification then simply amounts to multiplying the porosity f by the heuristic factor q_1. Values of this parameter of the order of 1.5 have been proposed both by Tvergaard (1981) as just mentioned, from comparisons with micromechanical simulations, and Perrin and Leblond (1990), from theoretical arguments.

The physical interpretation of the parameter q_1 is however multi-faceted. For instance:

- The study of void growth in an infinite medium (zero porosity) by Huang (1991) led to the conclusion that the prefactor in the Rice and Tracey (1969) exponential void growth law was notably underestimated. Gologanu (1997) noted that correcting this underestimation within the model of Gurson (1975, 1977) required introducing a q_1-parameter of the order of 1.6. The role of this parameter is then to correct inaccuracies occurring in the model in the limit of vanishingly small porosities, and has nothing to do with the shape of the elementary cell.
- The study of Leblond and Morin (2014) has shown that introduction of a q_1-parameter depending on the triaxiality T, and of the order of 1.25 for small T, is necessary to correct the inherent error on the porosity rate made by Gurson's (1977) model, as a result of his truncation of a series at the first order. In this context the introduction of q_1 is necessary even for a spherical elementary cell and a finite, nonzero porosity.

The introduction of the "q_i"-parameters by Tvergaard (1981) was completed (i) by Chu and Needleman (1980) by introducing an extra term connected to void nucleation in the evolution law Eq. (7) of the porosity, see Sect. 3 above; and (ii) by Tvergaard and Needleman (1984) through a heuristic modification of the porosity in the yield criterion Eq. (1) and the associated flow rule Eq. (3), aimed at phenomenologically accounting for coalescence of voids, see Sect. 5 below. The resulting GTN model has been widely used for numerical, finite-element based simulations of ductile rupture of actual, full-size specimens and structures; a few examples will be provided in Sect. 7 below.

An important modification of the evolution law of Gurson (1975, 1977), Eq. (7) of the porosity, was recently proposed by Nahshon and Hutchinson (2008). The aim of this modification was to account in a heuristic way for the development of damage evidenced in micromechanical numerical simulations performed by Tvergaard (2008, 2009, 2012), Dahl et al. (2012), Nielsen et al. (2012) under conditions of low or vanishing triaxiality T. The Nahshon and Hutchinson (2008) modification can be written as

$$\dot{\bar{f}} = \dot{f} + k_\omega \, f \, \omega(\boldsymbol{\sigma}) \frac{\boldsymbol{\sigma}' : \mathbf{D}^p}{\bar{\sigma}} \tag{14}$$

where $\dot{f}$ is given by Eq. (7), k_ω is a heuristic parameter and the function $\omega(\boldsymbol{\sigma})$ is defined by

$$\omega(\boldsymbol{\sigma}) = 1 - \left(\frac{27 J_3}{2\sigma_{eq}^3}\right)^2, \quad J_3 = \det \boldsymbol{\sigma}'. \tag{15}$$

We have used the notation $\dot{\bar{f}}$ in Eq. (14) to emphasize the commonality with the use of f^*, Eq. (2), to incorporate coalescence into the formulation. Indeed, as remarked by Nahshon and Hutchinson (2008), adopting Eq. (14) makes it impossible to retain the interpretation of f as the true void volume fraction; f becomes a heuristic damage parameter analogous to those encountered in the "theory of continuum damage mechanics". But it should be borne in mind that in spite of the limitations of Eq. (15), it represents a convenient, easy-to-implement heuristic way of accounting for the development of ductile damage at low or vanishing triaxiality. The only alternative is to account in a detailed way for the gradual change of shape of the voids under conditions of low triaxiality, and for the resulting softening of the material; models doing such a job are described in Sect. 4.3 below, and offer a more rigorous way of predicting ductile damage at low or vanishing triaxiality, but at the expense of considerably greater complexity.

Numerous other extensions of the analysis of Gurson (1975, 1977) and the resulting model have been proposed; such extensions include incorporation of Eshelby-type velocity fields in the limit-analysis of the hollow sphere (Monchiet et al. 2011), consideration of a matrix obeying Tresca's criterion instead of that of von Mises (Cazacu et al. 2014), etc. These extensions cannot all be cited here.

4.3 Models incorporating void shape effects

4.3.1 The GLD model for spheroidal voids

The GLD (Gologanu–Leblond–Devaux) model developed by Gologanu et al. (1993, 1994, 1997) extends the model of Gurson (1975, 1977) by introducing void shape effects, in the simplest case of spheroidal (axisymmetric ellipsoidal), prolate or oblate voids. It was developed in three steps. First, Gologanu et al. (1993) extended Gurson's limit-analysis of a hollow sphere by considering a prolate spheroidal void enclosed within a confocal spheroidal cell subjected to some axisymmetric loading; the trial velocity fields they used satisfied conditions of homogeneous strain rate on all spheroids confocal with the void and the external boundary.[1] Second, Gologanu et al. (1993) considered oblate voids, using the same type of representative cell and velocity fields. Third, Gologanu et al. (1997) refined the limit-analyses for both prolate and oblate voids by considering more velocity fields, belonging to a general class defined by Lee and Mear (1992). They also extended the model to general loadings in a heuristic way.

In the simpler case of an axisymmetric loading ($\sigma_{xx} = \sigma_{yy} \neq \sigma_{zz}$, other $\sigma_{ij} = 0$, Oz denoting the axis of rotational symmetry of the void), the GLD criterion reads

$$\begin{aligned}\Phi(\boldsymbol{\sigma}, f, w) = {} & \frac{C}{\bar{\sigma}^2}(\sigma_{zz} - \sigma_{xx} + \eta\sigma_h)^2 \\ & + 2(1+g)(f+g)\cosh\left(\frac{\kappa\sigma_h}{\bar{\sigma}}\right) \\ & - (1+g)^2 - (f+g)^2 \leq 0\end{aligned} \tag{16}$$

where w denotes the shape parameter of the void (ratio of its axes in the directions Oz and Ox, respectively), C, η, g (the "second porosity") and κ coefficients depending on the internal parameters f and w, and σ_h some weighted average of σ_{xx} and σ_{zz} also depending on f and w. The expressions and values of the various coefficients are different for prolate and oblate voids:

- For prolate voids C is nearly unity, η is small and g is nil; the criterion thus bears a strong resemblance to that for a spherical void, Eq. (1), and appears as a kind of interpolation between this criterion and that for a cylindrical void, see (Gurson 1975, 1977).
- For oblate voids C may notably differ from unity, and η and g are nonzero; therefore the resemblance with Gurson's criterion Eq. (1) is less marked. The main novelty with respect to this criterion is the appearance of the coefficient g, which plays the role of a kind of additional porosity since it contributes to the reduction of the reversibility domain. For a penny-shaped crack (completely flat void) this "second porosity" equals that defined by a spherical void with the same radius. For such a crack, the appearance of such a quantity in the yield criterion is an obvious necessity, since otherwise it would reduce to that of von Mises, f being zero.

[1] An alternative limit-analysis based on velocity fields orthogonal to these spheroids was proposed by Garajeu et al. (2000).

The GLD model involves extra internal parameters with respect to that of Gurson, namely the shape parameter w of the voids and the orientation of these voids (that is of their axis of rotational symmetry), for which evolution relations are needed.

An expression of $\dot{w}$ based on partially analytical, partially numerical limit-analysis, but also on rigorous results for nonlinear composites derived by Ponte Castaneda (1991), Willis (1991) and Michel and Suquet (1992) from extensions of Hashin–Shtrikman's theory to the nonlinear case, was proposed by Gologanu et al. (1997). This expression notably accounted for the fact first evidenced by Budiansky et al. (1982), and later confirmed by many authors, that a spherical void subjected to some axisymmetric loading with major axial stress ($\sigma_{zz} > \sigma_{xx} = \sigma_{yy}$) tends to become *oblate*, instead of prolate, at high triaxialities, in contradiction with what one would intuitively expect and indeed occurs in an elastic material.

With regard to the orientation of the axis of rotational symmetry of the voids, Gologanu et al. (1997) simply assumed that the rate of rotation of this axis was equal to the global rate of rotation of the material. This meant neglecting the effect of the global strain rate upon the rotation of the void, and represented an oversimplification which has been justifiably criticized and improved by Scheyvaerts et al. (2011).

The GLD model has been used notably to develop coalescence models, for the prediction of the evolution in time of the inter-void distance in the various directions of space; this distance indeed plays an essential role in such models. More details will be provided in Sect. 5 below.

4.3.2 The Madou–Leblond model for ellipsoidal voids

The hypothesis made by Gologanu et al. (1993, 1994, 1997) of spheroidal voids raises difficulties in the application of their model, because the three axes of the voids, even if initially equal, almost always take distinct values upon deformation; thus more or less dubious hypotheses must be introduced to replace the real voids by some "equivalent spheroidal voids" having only two distinct axes. This was the motivation for the extension of the GLD model to general ellipsoidal voids having three distinct axes by Madou and Leblond (2012a,b, 2013), Madou et al. (2013). Again, this extension was done in several steps.

In a first step Madou and Leblond (2012a) extended the approximate limit-analysis of spheroidal cells containing confocal spheroidal voids to ellipsoidal cells containing confocal ellipsoidal voids (Gologanu et al. 1993, 1994); to do so, they used a family of velocity fields just discovered by Leblond and Gologanu (2008), extending those used by Gologanu et al. (1993, 1994), which satisfied conditions of homogeneous strain rate on an arbitrary family of confocal ellipsoids. In a second step Madou and Leblond (2012b) refined the limit-analysis, first for hydrostatic loadings by performing numerical limit-analyses of the ellipsoidal hollow cells considered, second for deviatoric ones by using the results of Ponte Castaneda (1991), Willis (1991) and Michel and Suquet (1992) for nonlinear composites mentioned above. In a third step Madou and Leblond (2013) performed a large number of finite-element-based limit-analyses of ellipsoidal hollow cells aimed at assessing the quality of the approximate yield criterion proposed. In a final paper Madou et al. (2013) proposed evolution equations for the length and orientation of the axes of the voids, by combining "elastic evolution equations" proposed by Ponte Castañeda and Zaidman (1994) and Kailasam and Ponte Castaneda (1998) with heuristic "plastic corrections" determined numerically.

Madou and Leblond (2012a,b) showed that with a number of approximations, one may derive, quite remarkably, a criterion of the same basic type as that in the GLD model, Eq. (16):

$$\Phi(\boldsymbol{\sigma}, f, w_1, w_2) = \frac{\mathcal{Q}(\boldsymbol{\sigma})}{\bar{\sigma}^2} + 2(1+g)(f+g) \cosh\left[\frac{\mathcal{L}(\boldsymbol{\sigma})}{\bar{\sigma}}\right] - (1+g)^2 - (f+g)^2 \leq 0 \tag{17}$$

where w_1 and w_2 are the two shape parameters of the void (ratios of two axes over the third one), $\mathcal{Q}(\boldsymbol{\sigma})$ a quadratic form of the components of the tensor $\boldsymbol{\sigma}$ and $\mathcal{L}(\boldsymbol{\sigma})$ a linear form of its sole diagonal components. The various coefficients involved here depend on f, w_1 and w_2; their expressions do not, in the spheroidal case, exactly match those in the GLD model because the approximations used to derive them are slightly different, but the predictions of the two models, in this specific case, are nevertheless very close.

As an illustration, Fig. 3 compares the yield locus predicted by the model for an elliptic crack (very flat void) to that calculated by the finite element method

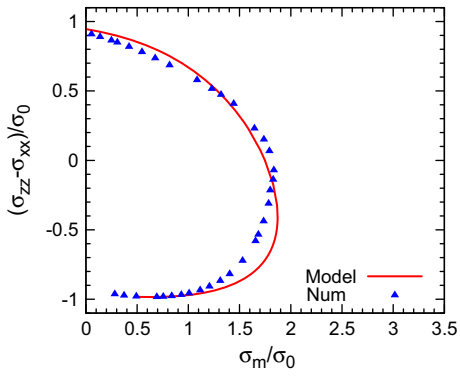

(a)

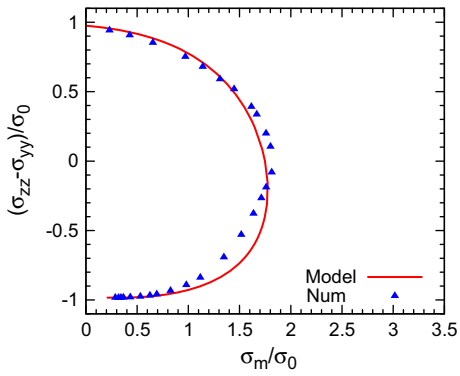

(b)

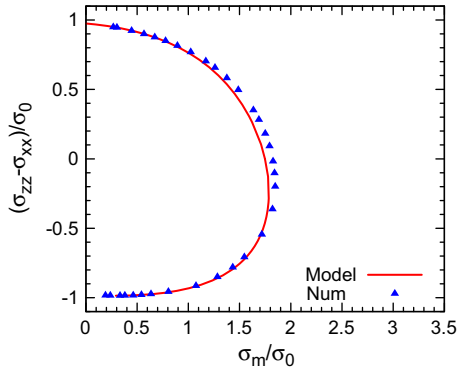

(c)

Fig. 3 Traces in three planes of the yield locus for an elliptic crack of semi-axes in the proportions 5/2/0.2, with second porosity $g = 0.14$ - Finite element results and model predictions. **a** $\sigma_{xx} = \sigma_{yy} \neq \sigma_{zz}$; **b** $\sigma_{xx} = \sigma_{zz} \neq \sigma_{yy}$; **c** $\sigma_{yy} = \sigma_{zz} \neq \sigma_{xx}$. After Madou and Leblond (2013)

considering the same elementary cell as in the derivation of the model (Madou and Leblond 2013). The principal axes of the loading coincide with those of the void and the traces of the yield locus are plotted in three planes. The agreement of theoretical and numerical yield loci is quite satisfactory.

The model of Madou and Leblond (2012a, b, 2013), Madou et al. (2013), as for the GLD model, is supplemented with evolution equations for the length and orientation of the axes of the void. Rather than considering these quantities separately, Madou et al. (2013) have proposed considering the quadratic form $\mathcal{P}(\mathbf{u})$ characterizing the geometry of the ellipsoidal void, defined by

$$\mathcal{P}(\mathbf{u}) = \frac{(\mathbf{u}.\mathbf{e}_x)^2}{a^2} + \frac{(\mathbf{u}.\mathbf{e}_y)^2}{b^2} + \frac{(\mathbf{u}.\mathbf{e}_z)^2}{c^2} \tag{18}$$

where $\mathbf{u}$ denotes an arbitrary vector, a, b, c the principal semi-axes of the void and $\mathbf{e}_x$, $\mathbf{e}_y$, $\mathbf{e}_z$ the corresponding unit vectors. (The boundary of the void is defined by the equation $P(\mathbf{OM}) = 1$ where O denotes its center and M the current point.) At each instant, the semi-axes and orientations of the void may be obtained through elementary diagonalization of the 3×3 symmetric matrix of $\mathcal{P}(\mathbf{u})$, so that it suffices to specify the evolution equation of this quadratic form instead of those of $a, b, c, \mathbf{e}_x$, $\mathbf{e}_y, \mathbf{e}_z$ individually; such an evolution equation is much better adapted to the numerical implementation of the model since it is free of singularities when two axes becomes equal. Madou et al. (2013) showed that the evolution of the matrix $\mathbf{P}$ of the quadratic form $\mathcal{P}(\mathbf{u})$ in Eq. (18) is governed by the equation

$$\dot{\mathbf{P}} + \mathbf{P}.\left(\mathbf{D}^v + \boldsymbol{\Omega}^v\right) + \left(\mathbf{D}^v + \boldsymbol{\Omega}^v\right)^T.\mathbf{P} = \mathbf{0}, \tag{19}$$

where $\mathbf{D}^v$ and $\boldsymbol{\Omega}^v$ denote the strain and rotation rate tensors of the void. This reduced the problem to specifying suitable expressions for $\mathbf{D}^v$ and $\boldsymbol{\Omega}^v$.

Madou et al. (2013) then proposed to adopt the following heuristic extensions of the "elastic expressions" of $\mathbf{D}^v$ and $\boldsymbol{\Omega}^v$ by Ponte Castañeda and Zaidman (1994) and Kailasam and Ponte Castaneda (1998):

$$\begin{cases} \mathbf{D}^v = \mathbf{L}.\mathbf{D} \\ \boldsymbol{\Omega}^v = \boldsymbol{\Omega} + \mathbf{R}.\mathbf{D} \end{cases} \tag{20}$$

where $\mathbf{D}$ and $\boldsymbol{\Omega}$ are the global strain and rotation rate tensors and $\mathbf{L}$ and $\mathbf{R}$ 4-th order "plastic localization tensors". The expressions of these tensors were related to those of their elastic counterparts $\mathbf{L}^e$, $\mathbf{R}^e$ defined by Ponte Castañeda and Zaidman (1994) and

Kailasam and Ponte Castaneda (1998), through multiplication of some of their components by some heuristic correction factors, obtained through a large number of finite element simulations of ellipsoidal hollow cells.

The new features brought by the model of Madou and Leblond (2012a, b, 2013), Madou et al. (2013) with respect to that of Gurson (1975, 1977) will now be illustrated by displaying the predictions it makes for the evolution of the overall stress, the porosity, the orientation of the void's axes and the length of these axes, in a few simple, typical cases. These cases have been considered in some micromechanical finite element simulations of Nielsen et al. (2012), which are independent of any homogenized model and may therefore be used as references to assess the quality of the model predictions. These simulations consider initially parallelepiped elementary cells containing an initially spherical void (Fig. 4). A zero orthogonal displacement is imposed on the faces $X_3 = \pm C_0$ (plane strain condition), whereas rigorous periodic conditions are enforced on the faces $X_1 = \pm A_0$, and uniform displacements U_1 and U_2 are imposed on the face $X_2 = B_0$, the face $X_2 = -B_0$ being clamped (these conditions are almost equivalent to periodic ones if B_0 is large enough). The ratio U_2/U_1 is adjusted at every step of the calculation so as to ensure a constant value of the ratio $\kappa = \sigma_{22}/\sigma_{12}$ characterizing the importance of the overall shear stress. Possible contact between the void faces is accounted for through some classical penalty method. The material obeys a Mises criterion with isotropic hardening; the material data are provided by Nielsen et al. (2012).

The predictions of the model of Madou and Leblond (2012a, b, 2013), Madou et al. (2013) are obtained by considering the entire cell as a single element obeying this model, and calculating the response of this element using the finite element program SYSTUS developed by ESI-Group. Figure 5, borrowed from the thesis of Morin (2015), compares the predictions of Madou and Leblond's model (ML) with the numerical results of Nielsen et al. (2012) (Num), for the normalized overall shear stress σ_{12}/σ_0 (σ_0 = initial yield stress) and the normalized porosity f/f_0 (f_0 = initial porosity). These quantities are plotted versus the "shear angle" defined as $\Psi \equiv \arctan[U_1/(2B_0+U_2)]$. The agreement between numerical and theoretical results is especially good for the shear stress (Fig. 5a). This agreement is not surprising before the sharp decrease of the stress

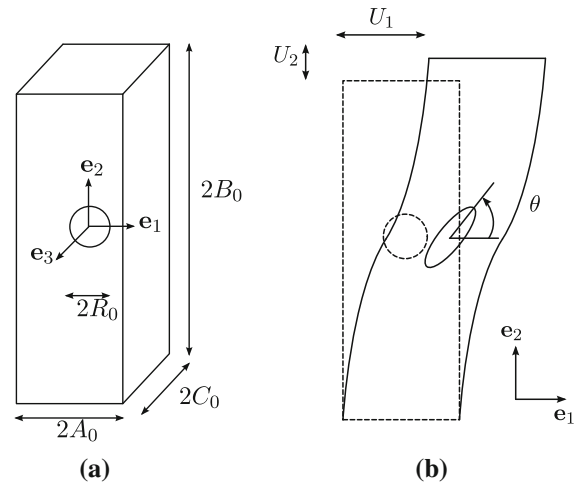

Fig. 4 Elementary cell considered by Nielsen et al. (2012). **a** Initial configuration. **b** Deformed configuration

due to coalescence because the influence of damage is small then; but it is much more significant at and after the onset of this decrease, since it means that the model is able to correctly reproduce coalescence induced by damage due to void shape changes under conditions of low triaxiality, which the model of Gurson (1975, 1977) would completely fail to do. (Coalescence is accounted for using the heuristic suggestion of Tvergaard and Needleman (1984), which introduces two adjustable parameters; but doing so in the context of Gurson's model would not suffice to induce a significant stress drop, in the absence of significant void growth). For the normalized porosity (Fig. 5b), the reproduction of the numerical results by the model is also quite good. Again, the predictions of the model of Gurson (1975, 1977) would not be so good; for $\kappa = 0.25$ for instance, it would predict an increase of the porosity because of the slightly positive triaxiality, in contrast to the numerical results.

Figure 6, again borrowed from the thesis of Morin (2015), compares numerical results and model predictions for the void orientation characterized by the angle θ defined in Fig. 4b, and the normalized axes R_i/R_0 (R_0 = radius of the initially spherical void). (Note that there is no "natural correspondence" between the initial half-dimensions of the cell A_0, B_0, C_0 shown in Fig. 4 and the major, intermediate and minor semi-axes of the void a, b, c shown in Fig. 6b, since the former quantities are defined in the observer's fixed frame and the latter in the void's local principal frame). All fea-

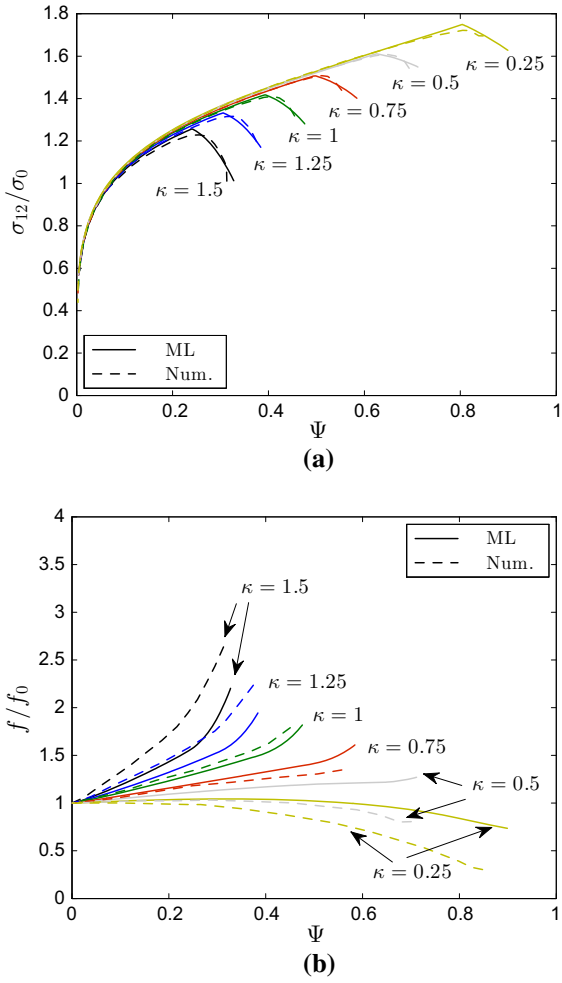

Fig. 5 Comparison of the predictions of the model of Madou and Leblond (2012a, b, 2013), Madou et al. (2013) with the numerical results of Nielsen et al. (2012). From Morin (2015). **a** Shear stress. **b** Normalized porosity

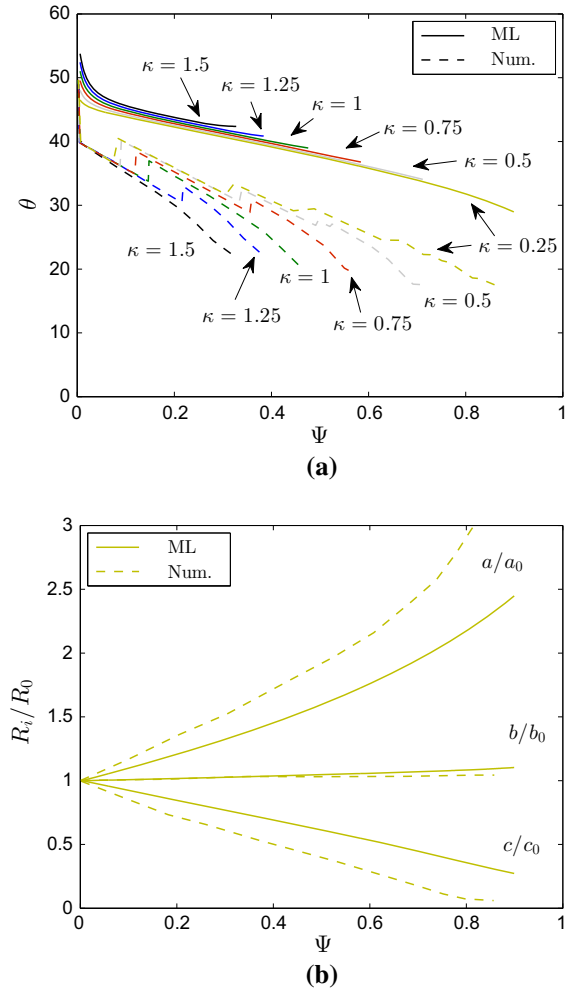

Fig. 6 Comparison of the predictions of the model of Madou and Leblond (2012a, b, 2013), Madou et al. (2013) with the numerical results of Nielsen et al. (2012). From Morin (2015). **a** Void orientation. **b** Normalized void axes ($\kappa = 0.25$)

tures are acceptably reproduced by the model.[2] Also, the markedly different evolution of the void's axes illustrate the impossibility, in such a case, of using the GLD model based on the assumption of equality of two axes.

A final remark on the approach of ductile fracture based on limit-analysis of elementary hollow cells initiated by Gurson (1975, 1977), resulting from what precedes, is that it has in time borrowed more and more results from the parallel approach developed by Ponte-Castaneda et al., based on the pioneering works of Ponte Castaneda (1991), Willis (1991) and Michel and Suquet (1992). Indeed the work of Gurson (1975, 1977) had no connection whatsoever with this (then nonexistent) parallel approach, but Gologanu et al. (1997) employed it to refine their evolution equation for the shape parameter of a spheroidal void, and Madou and Leblond (2012b), Madou et al. (2013) used it twice, first to refine their criterion in the case of predominantly deviatoric loadings, second as a basis for the development of evolution equations for the length and orientation of the void axes.

[2] There is a slight gap between numerical and theoretical results for the orientation angle θ; but this gap is present from the very start of the loading (and not compensated afterwards), which indicates that it may be due to the difficulty, when examining the numerical results, of defining an orientation angle for an almost spherical, but not strictly ellipsoidal cavity.

4.3.3 The models of Ponte-Castaneda and coworkers

As mentioned above, the models developed by Ponte-Castaneda et al. find their origin in extensions of Hashin–Shtrikman's well-known homogenization theory of random elastic composites to nonlinear behaviors, developed independently in the early 1990s by Ponte Castaneda (1991), Willis (1991) and Michel and Suquet (1992). They all rely on a procedure of "comparison" of the real, nonlinear composite with some "reference" linear composite, the number of phases and properties of which may be chosen at will (with some constraints) and optimized, the difficulty being of course that the more complex the reference composite, the harder the resulting calculations. The models proposed have been developed in a number of papers, the most important of which (in the authors' opinion) are mentioned below:

- Ponte Castañeda and Zaidman (1994)'s model first made a relatively simple use of results of Ponte Castaneda (1991), Willis (1991) and Michel and Suquet (1992), to extend a rigorous elastic bound of Willis (1977) for materials having an overall "ellipsoidal symmetry" (extension of the classical spherical symmetry) to nonlinear, plastic or viscoplastic materials. The model was completed by Kailasam and Ponte Castaneda (1998) by defining evolution equations for the length and orientation of the void axes.
  The predictions of this early model were quite accurate for low triaxialities, but for high ones the stresses were considerably overestimated. One possible qualitative explanation of these phenomena lies in the range of variation of the local strains, and therefore of the "secant moduli" (ratios of the local stresses over the local strains), depending on the overall stress state. Indeed it is probable that the comparison with some reference linear material is quite relevant if the spatial fluctuations of the secant moduli are moderate, but less so when they become large. Now the fluctuations of the local strains dictating those of the secant moduli are moderate for essentially deviatoric loadings, but not so for essentially hydrostatic ones because the expansion of the voids generates high strains in their vicinity. This suggests that the comparison with some reference linear material must become less and less pertinent when the triaxiality increases.
- In order to remedy this deficiency of the linear comparison procedure, Ponte Castaneda (2002) devised a "second-order" method which was applied by Danas and Ponte Castañeda (2009a, b) to the case of porous, plastic or viscoplastic materials. The definition of the new model involved an ad hoc scheme of interpolation and extrapolation aimed at enforcing the exact coincidence of its predictions with those of Gurson's model in the case of spherical/cylindrical voids subjected to hydrostatic overall stress states. This meant dropping to some extent the linear comparison procedure and borrowing instead elements from the alternative Gurson-type approach. The result was a considerable improvement of the model predictions for high triaxialities with respect to Ponte Castañeda and Zaidman (1994)'s model. The rigorous "bounding properties" of the model were however lost in the process.
- Very recently, Agoras and Ponte Castañeda (2013, 2014) used an "iterative procedure" just devised by Ponte Castaneda (2012) to generate another model free of the deficiencies of that of Ponte Castañeda and Zaidman (1994) at high triaxialities. The predictions of this model for purely hydrostatic loadings exactly coincided with the exact results known for a Hashin assembly of homothetical hollow spheres on the one hand, and for the so-called "infinite-rank sequentially laminated microstructures" defined and studied by Idiart (2007, 2008) on the other hand. The remarkable point in this new improved model was that it was obtained without any ad hoc adjustment. However it was not clear whether the model did or did not possess rigorous bounding properties applicable in general; these bounding properties were established only for the two special microstructures just mentioned, the second of which is of little practical relevance since the hypothesis of an infinite sequence of separations of scales it makes can obviously never be met.

It may be noted that Danas and Ponte Castañeda (2009a, b) borrowed elements of the approach based on limit-analysis of elementary cells that symmetrically reproduces what Madou and Leblond (2012b), Madou et al. (2013) did when defining their own model, see Sect. 4.3.2 above. A certain degree of convergence of the two approaches in recent years is therefore evident. Whether this convergence will ever be complete and

the two approaches merge into a single one remains uncertain at present.

4.4 Models incorporating plastic anisotropy

Plastic anisotropy has most often, up to now, been accounted for by assuming the sound material to obey the orthotropic criterion of Hill (1948). The focus in this section is on porous solids where the matrix material is characterized by a phenomenological anisotropic theory of plasticity. Studies focusing on porous crystal plasticity, for example (Lebensohn and Cazacu 2012; Han et al. 2013; Paux et al. 2015), will not be discussed here.

4.4.1 Benzerga and Besson's model for spherical voids

Benzerga and Besson (2001) were apparently the first to consider spherical voids embedded in a Hill matrix. Their approach was based on an extension of the limit-analysis by Gurson (1975, 1977) of a hollow sphere made of a Mises material to the case of a Hill material. The criterion they obtained reads

$$\Phi(\boldsymbol{\sigma}, f) = \frac{\sigma_{eq}^2}{\bar{\sigma}^2} + 2f\cosh\left(\frac{\kappa\sigma_m}{\bar{\sigma}}\right) - 1 - f^2 \leq 0 \quad (21)$$

where κ is a coefficient depending on those defining Hill's local criterion.

There are two differences here with respect to Gurson's flow potential Eq. (1) applicable to a Mises matrix. First, the "equivalent stress" σ_{eq} in Eq. (21) must be understood in the sense of Hill instead of that of von Mises (as is obviously required for the criterion to reduce to that of Hill for a zero porosity f). Second, the coefficient κ is not necessarily equal to $3/2$.

It must be noted however that the stress σ_m involved in the "cosh", which governs void growth, is exactly the same as in Gurson's criterion Eq. (1). This notably implies, via the normality property of the plastic flow rule, that the growth of the voids under hydrostatic loading is predicted to be identical in all directions of space, which means that the preferential growth in certain directions induced by plastic anisotropy is neglected. This arises from the fact that the trial velocity fields used by Benzerga and Besson (2001) were exactly identical to those of Gurson (1975, 1977) for a Mises matrix, and thus disregarded any influence of anisotropy upon the solution velocity field. It is not immediately clear why such a procedure should be reasonable.

In spite of this, several numerical assessments of the criterion of Benzerga and Besson (2001), Eq. (21), in particular see (Morin et al. 2014), have evidenced its accuracy, even for purely hydrostatic overall stress states. The probable explanation of this seemingly puzzling success lies in the variational characterization of the overall plastic dissipation and yield locus. Since the overall dissipation is the minimum of the average value of the corresponding local quantity over the space of incompressible and kinematically admissible velocity fields, it is stationary in the vicinity of the solution field. This means that rather large variations of the trial field around the solution field must result in much smaller variations of the overall plastic dissipation and the resulting approximate yield locus, and are therefore tolerable. This remark has played an important role in the development of more refined models summarized below.

4.4.2 Models for spheroidal voids

Similar extensions of the GLD model for spheroidal voids in Mises matrix materials to Hill matrix materials were proposed by Monchiet et al. (2006, 2008) using the velocity fields of Gologanu et al. (1993, 1994) adapted to this geometry, and Keralavarma and Benzerga (2008, 2010) using the richer fields of Gologanu et al. (1997). The criteria they obtained were formally analogous to that of Madou and Leblond (2012a, b, 2013), Madou et al. (2013), Eq. (17) for ellipsoidal voids embedded in a Mises matrix material, albeit with different coefficients. Again, numerical assessment of the criteria of both Monchiet et al. (2006, 2008) and Keralavarma and Benzerga (2008, 2010) evidenced the quality of their predictions in spite, again, of the use of the basically "isotropic" velocity fields of Gologanu et al. (1993, 1994, 1997).

4.4.3 The Morin–Leblond–Kondo model for ellipsoidal voids

The model developed very recently by Morin et al. (2015b) considers general ellipsoidal voids embedded in some anisotropic Hill matrix, without even assuming coincidence of the principal axes of the voids and

those of the material. Using the remark made above about the good results obtained by using "isotropic" velocity fields even for anisotropic matrices, not only for spherical voids (see Sect. 4.4.1) but also spheroidal ones (see Sect. 4.4.2), Morin et al. (2015b) applied the "isotropic" velocity fields of Leblond and Gologanu (2008), adapted to the general ellipsoidal case, to a Hill material, thus extending the work of Madou and Leblond (2012a, b, 2013), Madou et al. (2013) for a Mises material. The criterion they got was formally analogous to that of Madou and Leblond, Eq. (17), with different coefficients.

In order to get explicit expressions of all of these for all possible values of the parameters of Hill's criterion, it revealed necessary to introduce an assumption of small anisotropy and perform a first-order expansion in the deviation of these parameters from their "isotropic" values. In spite of this approximation, the very recent numerical assessment by Morin (2015) of the criterion of Morin et al. (2015b) seems to evidence the accuracy of its predictions, even for moderate, not-so-small anisotropy.

4.5 Second gradient extension of Gurson's model

One common feature of all models mentioned above is that, because they incorporate the softening arising from void growth, they predict a potentially unlimited localization of damage and strain, which generates various problems of both mathematical nature (occurrence of bifurcations with an infinite number of bifurcated branches, making their choice impossible) and numerical nature (mesh sensitivity in finite element calculations). The problem is general in softening models. It invariably results from the fact that such models are basically of "homogenized" nature, so that they cease to be applicable at the smaller and smaller scales over which the strain ultimately concentrates.[3]

Although other solutions are possible—see for instance the proposal by Leblond et al. (1994) to heuristically consider the porosity as a nonlocal variable whose rate is given by some convolution integral, and the application of this approach depicted in Sect. 6—a satisfying, although admittedly complex, solution to this problem was proposed some years ago by Gologanu et al. (1997). Instead of adopting a purely phenomenological approach, Gologanu et al. (1997) proposed to extend the limit-analysis by Gurson (1975, 1977) of a hollow sphere made of a Mises material and subjected to conditions of homogeneous boundary strain rate, (Mandel 1964; Hill 1967), to conditions of *inhomogeneous* boundary strain rate; this meant replacing the linear dependence of the velocity on the elementary cell's boundary upon coordinates, by a quadratic dependence. Although such a dependence is still approximate[4], its aim is to account for possible quick variations of the macroscopic stress and strain rate fields over distances comparable to the size of the cell (that is to the void spacing), precluded by the more usual linear dependence.

In a first step, Gologanu et al. (1997) laid foundations of the model by evaluating the overall virtual powers of forces resulting from the boundary conditions adopted. The main result was that the following expression of the density $\mathcal{P}_i^*$ of the overall virtual power of internal forces:

$$\mathcal{P}_i^* = -\int_\Omega (\boldsymbol{\sigma} : \mathbf{D}^* + \mathbf{M} \vdots \nabla \mathbf{D}^*)\, d\Omega. \tag{22}$$

In this expression Ω denotes the body considered; $\boldsymbol{\sigma}$ and $\mathbf{D}^*$ are the overall stress and virtual strain rate tensors, that is the average values of the corresponding local quantities over the representative cell; $\mathbf{M}$ is the third-rank overall *moment tensor*, defined as the first-order moment of the local stress tensor over the cell; and $\nabla \mathbf{D}^*$ is the macroscopic gradient of the tensor $\mathbf{D}^*$. The equilibrium equations corresponding to this expression of $\mathcal{P}_i^*$ read

$$\sigma_{ij,j} - M_{ijk,jk} = 0 \quad \text{in } \Omega. \tag{23}$$

Equations (22) and (23) make it clear that what is obtained here is a second-gradient theory. Note that since the local material behavior is described by the standard first-gradient theory of von Mises, this is a result of the sole homogenization process, and more specifically of the assumption of a velocity varying

[3] That softening models have their roots in homogenization is very often only implicit, but in the case of Gurson-type models quite clear and explicit.

[4] This means that the homogenization procedure based on such boundary conditions intrinsically remains a *model*, in contrast with other procedures using rigorous, for instance periodic, boundary conditions.

quadratically, instead of linearly, with coordinates on the cell's boundary.

In a second step, Gologanu et al. (1997) extended the limit-analysis of Gurson (1975, 1977) of a hollow sphere by considering extra velocity fields satisfying the extended boundary conditions considered. The output was an overall criterion of the form

$$\Phi(\boldsymbol{\sigma}, \mathbf{M}, f) = \frac{1}{\bar{\sigma}^2}\left(\sigma_{eq}^2 + \frac{Q^2}{b^2}\right) + 2f\cosh\left(\frac{3\sigma_m}{2\bar{\sigma}}\right) - 1 - f^2 \leq 0 \quad (24)$$

where Q^2 denotes some quadratic form of the components of the moment tensor $\mathbf{M}$, and b the radius of the sphere; this quantity physically represents the mean half-distance between neighboring voids and plays the role of some "microstructural distance" in the model.

As an illustration, Fig. 7 compares the yield locus predicted by the model for a spherical void with porosity $f = 0.01$ to that calculated by the finite element method considering boundary conditions on the elementary cell of the same type as in the derivation of the model (Gologanu et al. 1997). The loading is axisymmetric and the traces of the yield locus are plotted in four planes. The agreement of theoretical and numerical yield loci is satisfactory.

Equations (23) and (24) permit to qualitatively understand why the appearance of the moment tensor $\mathbf{M}$ in the model leads to some limitation of the localization of strain and damage. Indeed the equilibrium equations, Eq. (23), imply that the first derivatives of $\boldsymbol{\sigma}$ behave like the second derivatives of $\mathbf{M}$, so that $\boldsymbol{\sigma}$ behaves like the first derivatives of $\mathbf{M}$. Now assume that the damage tends to indefinitely localize in time. Then $\mathbf{M}$ varies from $\mathbf{0}$ (in the completely damaged zone) to some nonzero value (in the sound zone) over a distance which gradually goes to zero; it follows that its first derivatives, and therefore the stress tensor $\boldsymbol{\sigma}$ by what precedes, go to infinity. But this is impossible since the criterion Eq. (24) limits the components of the latter tensor. Hence the damage cannot indefinitely localize; of course in practice the size of the damaged zone will be comparable to the microstructural distance b.

The development of any second-gradient model, if it is to be of any practical use, must necessarily be accompanied by a discussion of its implementation into some finite element code; indeed such an implementation is

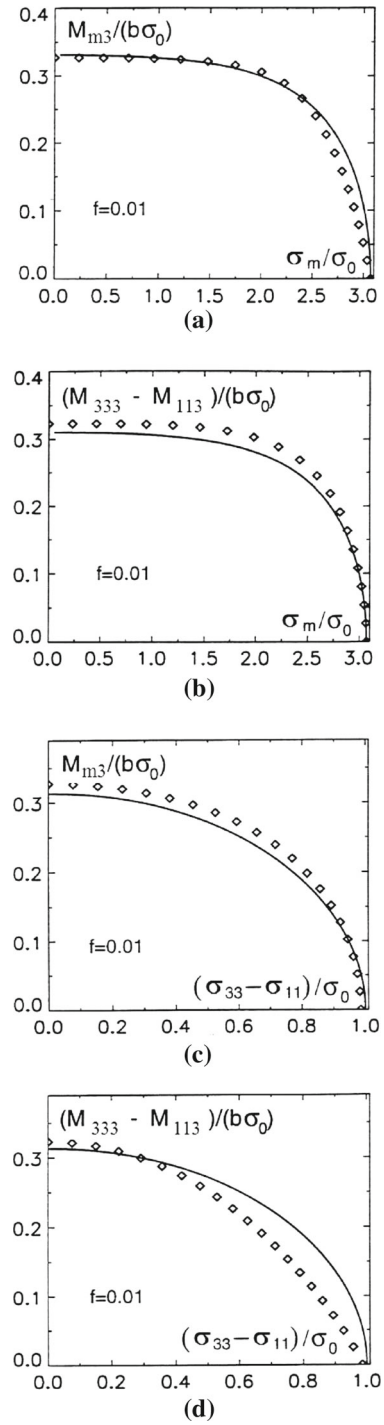

Fig. 7 Traces in four planes of the yield locus for the second-gradient extension of Gurson's model, for a spherical void with porosity $f = 0.01$—finite element results and model predictions. **a** $\sigma_{33} - \sigma_{11} = 0$, $M_{333} - M_{113} = 0$; **b** $\sigma_{33} - \sigma_{11} = 0$, $M_{m3} = 0$; **c** $\sigma_m = 0$, $M_{333} - M_{113} = 0$; **d** $\sigma_m = 0$, $M_{m3} = 0$. After Gologanu et al. (1997)

indispensable for the study of virtually all practically significant problems, and much less straightforward than that of first-gradient models. The main difficulty lies in the necessary evaluation of spatial derivatives of the strains, that is of the second derivatives of the displacements.

Enakoutsa and Leblond (2009) implemented Gologanu et al.'s second-gradient model, following their suggestion, by (i) introducing new nodal degrees of freedom (DOF) aimed at representing the strains; (ii) calculating the derivatives of the strains by using these new DOF in conjunction with the first derivatives of the shape functions; and (iii) enforcing the approximate coincidence of the new DOF and the strains through some penalty method. The drawbacks of such an approach were an awkwardly large number of DOF per node, especially in three dimensions, and the difficulty of choosing a "good" value for the penalty coefficient, which had to be sufficiently large to be effective, but not too much in order not to generate an ill-conditioned tangent matrix.

In view of these difficulties, Bergheau et al. (2014) proposed, in order to calculate the derivatives of the strains, to retain the introduction of new nodal DOF representing strains, but discard the penalty method of Enakoutsa and Leblond (2009), and instead write the equality of these DOF and the strains in a weak sense. The left-hand side of the vectorial relation connecting the new DOF to the nodal displacements then involves a "mass matrix" analogous to that encountered in dynamic problems, which Bergheau et al. (2014) proposed to lump and invert straightforwardly, so as to express the new DOF explicitly in terms of the displacements and finally eliminate them. In this way the unknowns are reduced to the sole displacements, like for a standard first-gradient model, and the risk of an ill-conditioned tangent matrix is eliminated.[5]

An additional advantage of the implementation of the model of Gologanu et al. (1997) by Bergheau et al. (2014) is that unlike most implementations of second-gradient models and especially that of Enakoutsa and Leblond (2009), it permits to easily mix elements obeying first- and second-gradient models, since the nodal DOF of the two types of models are identical. An example of such a mix will be provided in Sect. 7 below. Its practical interest is to reduce the length and cost of calculations by using the second-gradient model only in those zones of the structure where it is really needed, that is where damage develops significantly.

[5] The price to pay is, unfortunately, a larger bandwidth of the stiffness matrix than for a first-gradient model, because this matrix does not only "connect" first-neighbor nodes (contained in the same element), but also "third-neighbor" ones (having first neighbors lying in the same element).

5 Void coalescence

5.1 Preliminary remarks

Two major methods have emerged to model void coalescence in (rate-independent) ductile materials:

- Interpreting coalescence as a plastic flow *localization* phenomenon, at the scale of some homogenized model that accounts for the effect of voids.
- Analyzing coalescence as a phenomenon of strain *concentration* within layers of thickness comparable to the void size.

The first method views the process as an instability that can be predicted in terms of the pre-localization constitutive model (Rudnicki and Rice 1975; Rice 1976). Details about its mathematical formulation and implications will be given in Sect. 6 along with alternative rate-dependent formulations. This method has been followed by several authors, for example by Needleman and Rice (1978), Yamamoto (1978), Perrin (1992), Benzerga et al. (1999) using a Gurson-like constitutive relation, as well as by Ponte Castañeda and Zaidman (1994), Danas and Ponte Castañeda (2012), Song et al. (2015) using the models of Ponte Castaneda et al. described in Sect. 4.3.3. Void coalescence may not be expected to fit this concept. As noted by Rice (1976), "An alternative hypothesis would be that some essentially new physical deformation mechanism comes into play, *abruptly*, and *rapidly degrades the strength* of the material. In such cases the pre-localization constitutive relations cannot be continued analytically at the critical point, and *they provide no basis* for prediction of localization."[6] The second method above addresses precisely this sort of situation. It presumes a sudden shift in the physical deformation mechanism. The micromechanical cell model calculations of Koplik and Needleman

[6] The emphasis is ours.

(1988) provide a solid foundation for that shift, at least for quasi-periodic void distributions. Many more such analyses have been published since, as reviewed by Benzerga and Leblond (2010). These micromechanical analyses have later been supported by empirical evidence, based on mere physical observations of internal necks, see Pineau et al. (2016) for an overview.

Another conceptual difficulty in modeling void coalescence is that conventional homogenization theories do not apply to it either. Indeed, such theories rely on the fundamental assumption of separation of scales. In the case of materials containing voids, this means that the typical void spacing must be much smaller than the distance over which the macroscopic mechanical fields vary significantly. This assumption, therefore, is generally not satisfied in the case of void coalescence whereby the strain rate concentrates in a small zone containing only a few voids. As a consequence, the models based on the second method rely on analyses of elementary mechanisms but do not, strictly speaking, pertain to homogenization because they consider cells of fixed, small dimensions, containing very few voids.

Further, the approach followed in the second method consists of dividing the elementary cell into porous and dense regions. The latter are eventually modeled as rigid and intercepting the lateral sides of the cell so as to mimic the micro-deformation mechanism characteristic of void coalescence by internal necking (uniaxial deformation of the cell). In practice, this method has been implemented in two ways. In the two-step "homogenization" approach, followed mainly by Leblond and co-workers (Gologanu et al. 2001a, b; Leblond and Mottet 2008; Tekoglu et al. 2012), the voids in the porous region are smeared out. In this case, constitutive relations of porous material plasticity are used in the porous zone. Another way is to explicitly account for the voids in the rigid-plastic limit analysis of the cell. This one-step approach was initiated by Thomason (1985), although very little details were provided then, and further developed in recent years (Benzerga and Leblond 2014; Morin et al. 2015a, 2016; Torki et al. 2015). Some advantages of the two-step "homogenization" approach over earlier models were discussed by Benzerga and Leblond (2010). In what follows, only the one-step micromechanical approach is reviewed, as it is seemingly most promising. Prior to undertaking this review, the most commonly used approach in computational modeling of ductile fracture is recalled to set the stage.

5.2 The f^* approach

As indicated in Sect. 4.2.2, Tvergaard and Needleman (1984), Needleman and Tvergaard (1984) have proposed a complete computational methodology for modeling ductile failure with phenomenological constitutive relations for all stages of progressive cavitation. In particular, void coalescence was incorporated in terms of accelerated void growth. This involved replacing the actual porosity in the yield function given by Eq. (1) with some effective porosity f^*, equal to f prior to the onset of void growth acceleration and to a multiple of it beyond some critical stage as in Eq. (2).

Equation (2) is a two-parameter phenomenological description of coalescence. Since the physics underlying void growth acceleration is left unspecified in this model, the involved parameters, f_c and f_f, may be adjusted based on experiments, which is a common practice. Alternatively, they may be inferred from more refined analyses adopting either method mentioned under the preliminary remarks. For example, the critical porosity f_c may be estimated based on localization analyses, as done by Benzerga et al. (1999) on the basis of the application of a localization condition to the original Gurson model by Perrin (1992)[7]. Further, Benzerga (2002) has developed estimates of the second parameter f_f, more precisely δ by rewriting Eq. (2) as $f^* = f_c + \delta(f - f_c)$, on the basis of a limit analysis approach to void coalescence by internal necking. Yet another method would be to infer these parameters from finite-element cell model calculations (Pardoen and Hutchinson 2000).

Thus, in principle the f^* approach can be used in conjunction with the most advanced void growth models with its parameters either adjusted on experiments or inferred from refined analytical or cell models. In subsequent sections, focus is laid on models that incorporate specific physics into the void coalescence phenomenon.

[7] Perrin's work elaborated on earlier work by Yamamoto (1978) by accounting for deformation-induced anisotropy, consistent with the results of Koplik and Needleman (1988), and revisiting the Rice–Rudnicki localization condition (Rudnicki and Rice 1975); see Perrin and Leblond (1993).

5.3 Thomason's condition

5.3.1 Original form

Thomason (1985) posed the problem of rigid-plastic limit analysis of a cylindrical cell of either square or circular section containing a coaxial void of finite height. The matrix material was taken to obey an associated Mises yield criterion. The concentration of plastic strain in the ligaments was represented by various velocity fields. This problem, while well posed, was not solved by Thomason in closed form. Instead, he obtained approximate numerical solutions to which he proposed an empirical fit. Using notation from (Benzerga et al. 1999), the overall criterion thus obtained is

$$\Phi(\boldsymbol{\sigma};\chi,w)=\frac{\sigma_{33}}{\bar{\sigma}}-(1-\chi^2)\left[0.1\left(\frac{\chi^{-1}-1}{w}\right)^2+1.2\sqrt{\chi^{-1}}\right]\leq 0 \tag{25}$$

where the common axis of the void and the cell is taken along x_3, which also defines the normal to the "localization" plane. Also, w refers to the aspect ratio of the cylindrical void and χ to the ratio of lateral void radius to lateral cell radius, the latter radius representing a void spacing in the band of localization. In short, parameter χ shall be referred to as the ligament parameter. In the limit $w\to 0$ (flat void) the second term in Eq. (25) diverges and the criterion is never met. This is clearly a defect in the model, which is however believed to have limited consequences in materials failing after significant void growth (see Sect. 5.4.1 for further discussion).

Note that in order to implement a coalescence criterion such as Eq. (25) a void growth model incorporating void shape effects should be used (see Sect. 4.3). Alternate approximations are also possible. For example, one may assume $w\approx 1$ prior to coalescence and use the GTN model for $f\leq f_c$, and even for $f\geq f_c$ using the equality in Eq. (25) to determine f_c (Zhang et al. 2000).

5.3.2 Extended forms

Thomason's condition has been used as a criterion for the onset of coalescence, mainly in the materials science community; see Pineau et al. (2016) for an overview. For this sort of criterion to be used in computational modeling of ductile failure, evolution equations for the internal parameters have to be supplied. Benzerga (2000, 2002) developed such equations for the void aspect ratio w, the ligament parameter, χ, which plays the role of porosity, and the spacing ratio λ, defined as the out of (localization) plane spacing relative to the in-plane spacing, as follows:

$$\dot{\chi}=\frac{3}{4}\frac{\lambda}{w}\left[\frac{3\gamma}{\chi^2}-1\right]\dot{\varepsilon}_{\rm eq}+\frac{\chi}{2\gamma}\dot{\gamma}, \tag{26}$$

$$\dot{w}=\frac{9}{4}\frac{\lambda}{\chi}\left[1-\frac{\gamma}{\chi^2}\right]\dot{\varepsilon}_{\rm eq}-\frac{w}{2\gamma}\dot{\gamma}, \tag{27}$$

where the shape factor γ was introduced in addition to w and was taken to evolve as the shape of the voids changes from spheroidal ($\gamma=1/2$) at the onset of localization ($\chi=\chi_c$) to conical ($\gamma=1$) at impingement ($\chi=1$):

$$\dot{\gamma}=\frac{1}{2(1-\chi_c)}\dot{\chi} \tag{28}$$

The current void spacing can directly be inferred from the initial void spacing and deformation history. This is straightforward for periodic or random Poisson-like distributions of void centers, not so for clustered ones. Hence λ is updated through the heuristic law:

$$\dot{\lambda}=3\zeta\lambda\,\dot{\varepsilon}_{\rm eq}, \tag{29}$$

where $\zeta=1/2$ for a periodic array of voids in tension, more generally a factor characterizing the nature of void distribution, periodic ($\zeta=1/2$), random ($\zeta=0$) or clustered (presumably $0\leq\zeta\leq 1/2$). The void and cell axes were tacitly taken to rotate with the material. In actual implementations of the model (Benzerga et al. 2002a, 2004) only Eqs. (27), (29) and the evolution of the void axis are needed if the porosity is retained as a primary variable post-localization and χ (hence γ) is updated explicitly through a relationship to f, w and λ.

Similar equations were obtained by Pardoen and Hutchinson (2000). The derivations of Benzerga (2002) stem from the fundamental observation that, except for extremely flat voids, the zones of elastic unloading (modeled as rigid) intercept the poles of the void. Also, in both Pardoen and Hutchinson (2000) and Benzerga (2002) the voids were modeled as spheroidal while assuming that the like of criterion Eq. (25) holds. Pardoen and Hutchinson (2000) and Benzerga (2002) proposed heuristic extensions of the above criterion. Pardoen and Hutchinson's extension focused on incor-

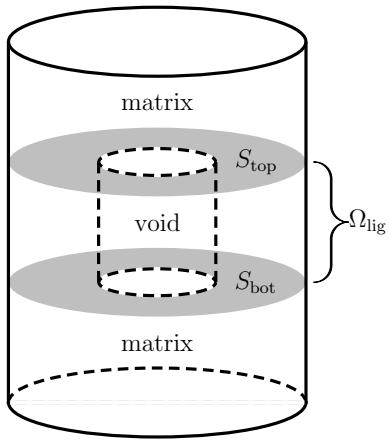

Fig. 8 Elementary cell considered by Benzerga and Leblond (2014)

porating the effect of strain hardening to be fit on cell model calculations. On the other hand, Benzerga's extension of Eq. (25) focused on removing the singularity in the limit of flat voids ($w \to 0$) (Benzerga 2002).

5.4 Models for predominately tensile loads

5.4.1 The Benzerga–Leblond solution

To the extent that a model of void coalescence by strain concentration is appropriate and needed, it has remained elusive. Until recently, the empirical criterion (25) and its heuristic extensions were the only available ones. Benzerga and Leblond (2014) revisited Thomason's analysis for the circular cylindrical cell (Fig. 8) and obtained a fully analytical expression for the coalescence criterion as

$$\begin{aligned}
&\Phi(\boldsymbol{\sigma};\chi,w) = |\sigma_{33}| - \sigma^{\text{vol}} - \sigma^{\text{surf}} \le 0\\
&\sigma^{\text{vol}}(\chi) = \frac{\bar{\sigma}}{\sqrt{3}}\left[2 - \sqrt{1+3\chi^4} + \ln\frac{1+\sqrt{1+3\chi^4}}{3\chi^2}\right]\\
&\sigma^{\text{surf}}(\chi,w) = \frac{\bar{\sigma}}{3\sqrt{3}}\frac{\chi^3 - 3\chi + 2}{\chi w}
\end{aligned} \tag{30}$$

The function $\sigma^{\text{vol}}+\sigma^{\text{surf}}$ has units of stress and specifies the dependence of coalescence upon the internal parameters. Some special cases are worth mentioning:

- In the limit of a dense matrix ($\chi \to 0$) the coalescence stress diverges ($\sigma_{33}^{\text{coal}} \sim 1/\chi$). This is expected since the uniaxial deformation mode is incompatible with matrix incompressibility. In other words, coalescence is impossible in the absence of voids! Thus, for very low porosities, criterion in Eq. (30) is unlikely to be met and a Gurson-like model is more appropriate.
- When $\chi \to 1$ all stress bearing capacity vanishes, as expected, since the ligament has thinned down to zero.
- For sufficiently elongated voids ($w \to \infty$) the coalescence stress $\sigma_{33}^{\text{coal}} \sim \sigma^{\text{vol}}(\chi)$ is independent of the void aspect ratio.
- In the limit of a penny-shape crack ($w \to 0$) the coalescence stress again diverges, as $1/w$; note that the singularity is weaker than in Thomason's imperfect fit underlying Eq. (25). As noted above, this singularity is unphysical as the coalescence of microcracks is often observed. However, not only an internal necking approach to this special case seems inadequate, length scale effects may play a role, which are ignored here.

Evolution equations, Eqs. (26–29), can be used along with the coalescence criterion of Eq. (30).

5.4.2 Improved models

Benzerga and Leblond's criterion, Eq. (30), was obtained on the basis of a velocity field that has two disadvantages. First, the criterion could not be optimized by performing some minimization over the parameters entering the velocity field, as these were completely determined by boundary conditions. Second, it suffered from a discontinuity at the rigid–plastic interface. Morin et al. (2015a) introduced two general families of velocity fields: a family of generalized discontinuous fields which considers the shape of the plastic/rigid interface as a parameter; and continuous velocity fields. For special choices of the velocity fields they obtained improved criteria, although not in complete closed form. In addition, Morin et al. carried out a series of finite element based limit analyses, following the method described by Madou and Leblond (2012b), for various combinations of the internal parameters w and χ. Figure 9 illustrates some of their results. The numerical limit-analysis results were used to assess the coalescence criterion developed by Benzerga and Leblond (2014), referred to as Φ_1 in the figure, as well as two new criteria, Φ_2 and Φ_3 based on the generalized

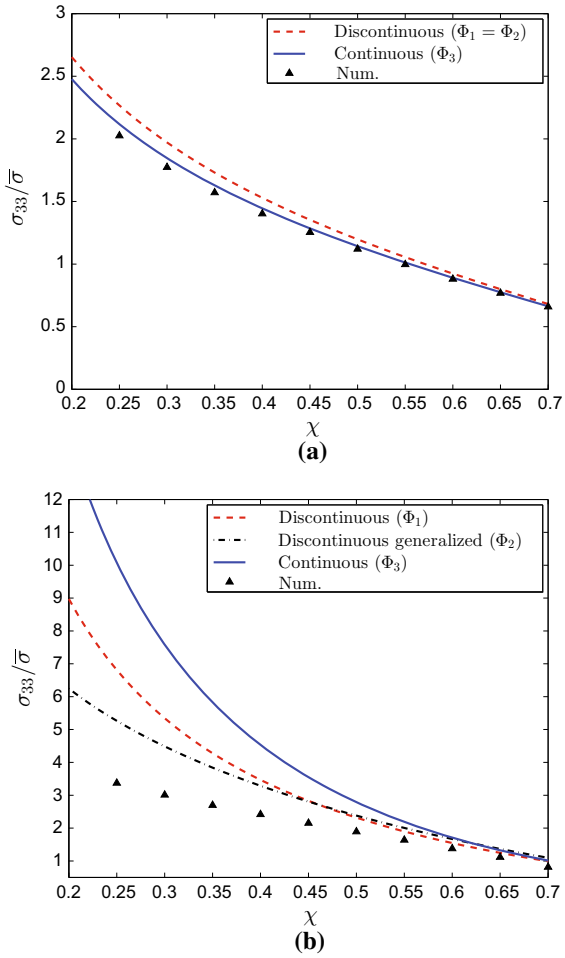

Fig. 9 Numerical results and predictions of the model by Benzerga and Leblond (2014) (criterion Φ_1) and two models by Morin et al. (2015a) for the limit-load in tension of the cell in Fig. 8 plotted in terms of $\sigma_{33}/\bar{\sigma}$ as a function of ligament parameter χ. **a** $w = 3$, **b** $w = 0.2$. Adapted from Morin et al. (2015a)

discontinuous and the continuous fields, respectively. The improved models provide, in general, tighter upper bounds, albeit for different ranges of internal parameters. For sufficiently elongated voids (Fig. 9a, $w = 3$), the Benzerga–Leblond criterion and the "generalized discontinuous" criterion of Morin et al. are indistinguishable while the criterion based on continuous fields clearly provides a tighter upper bound. It is remarkable that all models do quite well, without any adjustable parameter. This suggests that details about the shape of the plastic zone do not matter in that range. The situation shown in Fig. 9a is representative of spherical as well as prolate voids in general. On the other hand, for sufficiently flat voids (Fig. 9b, $w = 0.2$), all models suffer from the $1/w$ singularity, thus leading to an overestimation of the limit load. However, the generalized discontinuous model provides a significant improvement over the criterion (30).

5.5 Models for combined tension and shear

An early attempt at modeling void coalescence in shear bands was essentially a void impingement model by McClintock et al. (1966). There, approximate equations of isolated void growth were used to estimate strains to failure under various mean tensile stress to shear stress ratios. Fracture was taken to occur when the void touched the boundaries of the elementary cell. This model was used by Xue (2008) to motivate a heuristic modification to the GTN model by means of a damage variable that is purely plastic strain driven in the absence of hydrostatic tension. Xue's model thus bears some resemblance to the Nahshon-Hutchinson model described in Sect. 4.2.2. None of these models address the phenomenon of void coalescence per se. Important fundamental questions are: does linkage between voids occur under pure shear loading? If so what is the mechanism? The cell model calculations of Tvergaard (2008, 2009, 2012) and Nielsen et al. (2012) begin to shed some light on possible mechanisms. The models of void coalescence described below presume that, with some superposed hydrostatic tension, the same mechanism of strain concentration in ligaments operates thus leading to accelerated drop of stress carrying capacity of the elementary cell.

5.5.1 The model of Tekoglu et al.

As mentioned under preliminary remarks, a two-level "homogenization" procedure can be applied to incorporate the effect of shear on void coalescence, still essentially viewed as an internal necking mechanism. This was indeed achieved by Leblond and Mottet (2008) extending earlier models of this kind (Gologanu et al. 2001a, b). Tekoglu et al. (2012) have recently improved upon this model through some suitable extension of Thomason's treatment of coalescence to non-axisymmetric loadings. In doing so, they accounted for both the extensional and shear components of the microscopic deformation field. However, only that corresponding to shear was expressed in explicit, analyti-

cal form. Their model is therefore intermediate between the two-step homogenization technique used by Gologanu et al. (2001a, b), Leblond and Mottet (2008) and the models dealing with fully explicit velocity fields (Thomason 1985; Benzerga and Leblond 2014).

They arrived at a quadratic coalescence criterion which reads

$$\Phi(\boldsymbol{\sigma};\chi,w,\boldsymbol{e}_3)=\frac{\sigma_{33}^2}{{\sigma^A}^2}+\frac{\sigma_{31}^2+\sigma_{32}^2}{\tau^2}-1\leq 0 \qquad (31)$$

where σ^A refers to either the coalescence stress in Eq. (25) or Benzerga's heuristic modification (Benzerga 2002) and $\tau(\chi)$ is a function of the ligament parameter defined as:

$$\tau(\chi)=\frac{\bar{\sigma}}{\sqrt{3}}(1-\chi^2) \qquad (32)$$

Hence, in the absence of any shear loading, criterion Eq. (31) reduces to either Thomason's Eq. (25) or its variant by Benzerga (2002).

5.5.2 The model of Torki et al.

More recently, Torki et al. (2015) extended the analysis by Benzerga and Leblond (2014) to incorporate the effect of remote shear loading. Their analysis explicitly considers the microscopic deformation field around the void in fully analytical form. Their coalescence criterion is given by $\Phi(\boldsymbol{\sigma};\chi,w,\boldsymbol{e}_3)\leq 0$ with

$$\Phi=\begin{cases}\dfrac{(|\sigma_{33}|-t\sigma^{\mathrm{surf}})^2}{b{\sigma^{\mathrm{vol}}}^2}+\dfrac{\sigma_{31}^2+\sigma_{32}^2}{l\tau^2}-1 & |\sigma_{33}|\geq\sigma^{\mathrm{surf}}\\[2ex] \dfrac{\sigma_{31}^2+\sigma_{32}^2}{l\tau^2}-1 & |\sigma_{33}|\leq\sigma^{\mathrm{surf}}\end{cases} \qquad (33)$$

where $\sigma^{\mathrm{vol}}(\chi)$, $\sigma^{\mathrm{surf}}(\chi,w)$ and $\tau(\chi)$ are the functions given in Eqs. (30) and (32). Torki et al. have also introduced heuristic parameters t, b and l based on comparisons with cell model calculations. In general b is close to unity and the primary motivation for t was to obtain a finite limit load, hence coalescence, under pure tension of penny-shaped cracks, as would be relevant to materials failing after limited void growth (e.g., Babout et al. 2004; Kondori and Benzerga 2014). Criteria (31) and (33) both predict that the effective yield stress in pure shear is reduced by a factor $(1-f_b)$ where $f_b=\chi^2$ is the porosity in the localization band; compare with a reduction by $1-f$ in Gurson-like models.

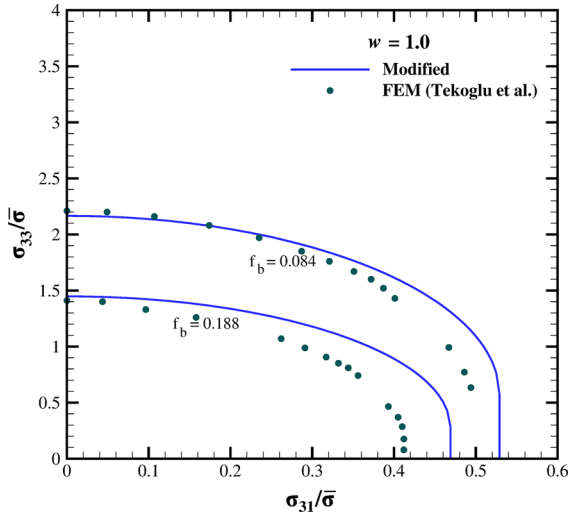

Fig. 10 Yield loci corresponding to the coalescence model of Torki et al. (2015) (*lines*) and the finite element results of Tekoglu et al. (2012) (*points*)

Figure 10 illustrates a result obtained by Torki et al. (2015) for the case of cylindrical voids with a height to diameter ratio $w=1$. For this case, the modified model, Eq. (33), predicts an effective yield locus that is very close to the original one (setting $t=b=l=1$) as can be inferred from Fig. 9c of Torki et al. (2015). It is worth noting that the model was derived for the cylindrical cell shown in Fig. 8 whereas the finite element calculations of Tekoglu et al. (2012) were for spherical voids in an orthorhombic cell. For this reason, comparison is made for the same values of the porosity in the band, f_b. In addition, the coalescence criterion, Eq. (33), was developed based on approximations that did not guarantee the upper-bound character of the yield locus. Further work is needed to address the uncertainties involved in comparing both sets of results. Nevertheless, the predictions of the model in Fig. 10 appear to be quite good.

5.6 Models incorporating plastic anisotropy

To account for plastic anisotropy, Benzerga et al. (2004) extended the coalescence criterion for plastically isotropic matrices of Benzerga (2002) using the

heuristics:

$$\Phi(\boldsymbol{\sigma}, \chi, w, \boldsymbol{e}_3) = \frac{\sigma_{\text{eq}}}{\bar{\sigma}} + \frac{3}{2}\frac{|\sigma_{\text{m}}|}{\bar{\sigma}} - \frac{3}{2}\frac{\sigma^{\text{coal}}}{\bar{\sigma}} \leq 0 \quad (34)$$

where σ_{eq} was interpreted as Hill's equivalent stress as in Eq. (21) and $\sigma^{\text{coal}}(\chi, w)$ is the coalescence stress from (Benzerga 2002). Following this idea, Eq. (30) may be written in a similar form with $\sigma^{\text{coal}} = \sigma^{\text{vol}} + \sigma^{\text{surf}}$. This enables writing the coalescence criterion for arbitrary orientations of the localization band. The rationale for Eq. (34) is that for the isotropic matrix, the tensile stress normal to the localization plane can be expressed for axisymmetric loadings in terms of the Mises equivalent stress and mean normal stress.

Obviously, the format Eq. (34) is approximate. Quite recently, Keralavarma and Chockalingam (2016) extended the Benzerga-Leblond analysis in Sect. 5.4.1 by considering a plastically anisotropic matrix and continuous velocity fields belonging to the family introduced by Morin et al. (2015a), but different from the particular choice made by Morin et al. (2015a). Through a judicious choice of the velocity fields, they developed a coalescence criterion for predominately tensile loads applicable to anisotropic materials in closed form.

5.7 Concluding remarks on void coalescence

Because scale separation does not hold *stricto sensu* during void coalescence, the phenomenon is most appropriately modeled by considering elementary cells containing a few voids. Even at such a scale, coalescence may occur in three ways: (i) by internal necking of the intervoid ligament; (ii) by a micro-shear band leading to void sheet formation; or (iii) in columns of ruined material leading to so-called necklace coalescence (see Fig. 33 in the overview by Pineau et al. (2016)). Recent progress in the analytical modeling of void coalescence addresses type (i).

Coalescence criteria Eqs. (30), (31) or (33) are associated models of porous material plasticity obtained by averaging the behavior of cells that accommodate localized or concentrated modes of plastic flow. As such, they may not apply to the behavior of a porous material from the outset of deformation. This is certainly true under predominately tensile stress states. Note that under predominately shear states of loading, yielding may be more favorable according to the coalescence

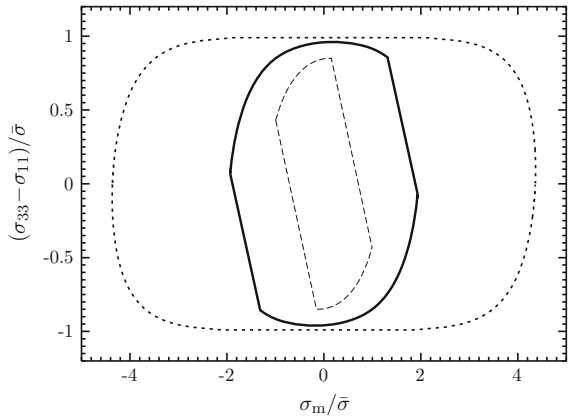

Fig. 11 Yield surfaces for axisymmetric loadings resulting from the intersection of the yield domains defined by (16) and (30): $(\cdots)$ initial surface corresponding to $f = 0.00075$ and $w = 15$; (—) at the onset of coalescence with $f = 0.04$, $w = 5$ and $\chi = 0.34$; (–) during coalescence with $f = 0.15$, $w = 2.2$ and $\chi = 0.75$

type criteria compared with Gurson-like criteria. By way of consequence, these criteria are expected to be used concurrently with Gurson-like models. As the two types of models have essentially dealt with different cell geometries the effective domain of elasticity is eventually viewed as the intersection of two domains so that the effective yield surface exhibits vertices near stress states where both deformation mechanisms are possible. This sort of hybrid approach is illustrated in Fig. 11. It has been used to model fracture in initially crack-free three-dimensional notched specimens (Benzerga et al. 2004) as well as plastic flow localization in plane strain bars (Benzerga et al. 2002a). The flat parts on the yield surface correspond to void coalescence. Indeed when coalescence occurs, the components of the macroscopic strain rate parallel to the localization band become nil. This implies *via* the normality property of the macroscopic flow rule that the macroscopic yield function becomes independent of the in-plane stresses. For axisymmetric loadings, the slope of the straight part in Fig. 11 is $-3/2$. For more general loadings, the $-3/2$ slope should be replaced with a Lode-parameter dependent factor.

Hybrid models have vertices as in Fig. 11. If the two fundamental modes of plastic deformation accompanying void growth and void coalescence are indeed viewed as independent plastic mechanisms, then this situation is not unlike what is encountered in crystal plasticity near stress states where two or more slip systems are activated. However, in the hybrid models ver-

tices are built-in by means of the separate treatments of void growth and coalescence. This raises the issue of the physical nature of such vertices. This issue ultimately rests on the fact that the localized deformation mode is presumed in the models reviewed above. To address this, Morin et al. (2015a) have recently determined effective yield loci of porous cells containing voids of various shapes (spherical versus cylindrical) without the kinematic constraints of zero strain rate in the directions of the plane of localization pertaining to void coalescence. Their results, which were obtained using a finite-element based limit analysis technique, are illustrated in Fig. 12 along with the Gurson yield surface for $f = 0.01$. Three lessons are drawn:

- The so computed yield surface consists of two parts. The curved part corresponds to solutions for which the plastic strain rate is non-zero in the entire cell, that is to the growth phase. On the other hand, the straight part corresponds to solutions for which the plastic strain rate is concentrated in the inter-void ligament, that is to the coalescence phase. The flat parts do not always exist, as similar calculations (not included) for a porosity of 0.001 clearly show.
- The computed surfaces do not reveal any corners, although the transition from growth to coalescence is characterized by a strong yield surface curvature.
- At fixed void aspect ratio, the void shape (cylindrical versus spherical) has little effect. This finding supports the use of finite-height cylindrical shapes in developing analytical models for void coalescence.

Gurson's yield locus does not have any similar straight portion corresponding to coalescence, since the boundary conditions of homogeneous strain rate considered in its derivation prevent strain localization. Quite recently, Morin et al. (2016) have developed a model unifying void growth and coalescence which mimics key features of the computational results in Fig. 12.

With the above in mind, several issues are yet to be clarified. In the available models, hybrid and unified alike, the directions of localization are not predicted. Instead, they are assumed to be set by the void distribution. If the latter is periodic, there is a finite number of localization planes defined by the available ligaments. All proportions kept, this is analogous to crystal plasticity again where the slip systems are set by the underlying atomic order and are not predicted per se. In such

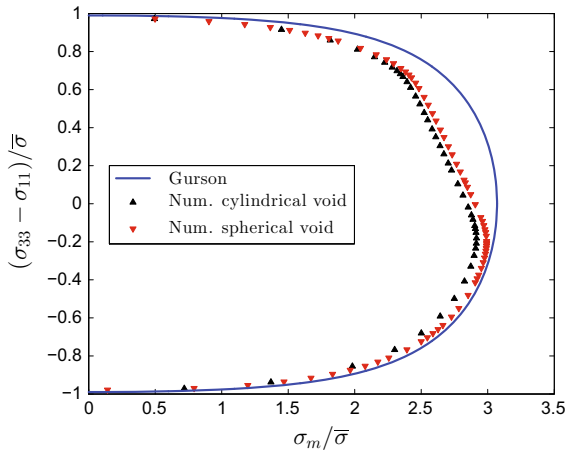

Fig. 12 Yield loci of cylindrical cells containing spherical or finite-height cylindrical voids, for $w = 1$, $\lambda = 1$ and $f = 0.01$. From Morin et al. (2015a)

cases, the effective yield surface may have as many flat parts as there are localization systems. Hence, for a uniformly random distribution of voids, there may be an infinite number of localization systems and it is not obvious that the yield surface would exhibit such flat parts. Of course, if the elementary cell contains only a few voids, the distribution is likely not random but at best clustered. In this case, it may be argued that the number of localization systems is indeed finite.

The approach initiated by Benzerga and Leblond (2014) and further pursued by Morin et al. (2015a, 2016), Torki et al. (2015), Keralavarma and Chockalingam (2016) defines a modeling framework and opens the door to several improvements. The coalescence of penny-shape cracks can be addressed by considering localization zones that extend above and below the cavity, as inferred from finite element simulations. The unifying model of Morin et al. (2016) could be improved by considering void/cell geometries other than cylindrical. Alternative mechanisms of coalescence in columns and by micro-shear bands should be addressed as well. While many issues are still open, the coalescence conditions may be used in minimal form to predict the values of critical parameters entering the f^* approach.

6 Localization

Localization, in the sense of a deformation pattern involving one or more intense deformation bands, occurs in a wide variety of solids, e.g. structural metals,

rocks and concrete, and under a wide variety of loading conditions, e.g. quasi-static and dynamic. In some circumstances, a deformation band arises due to geometric constraints, while in other circumstances the concentration of deformation is an outcome of the material response, rather than a consequence of boundary constraints. In this section, focus on localization that is primarily a consequence of the material response. The significance of localization of deformation for ductile fracture is that such localization often plays a key role in the ductile fracture process. In some circumstances, the large local strains and high stresses in a band can precipitate void nucleation, growth and coalescence. In other circumstances, the softening arising from void nucleation and/or growth leads to localization of deformation.

There is a large literature on localization of deformation with porosity playing either a primary or secondary role in precipitating that localization. No attempt will be made to review that literature but a recent study is presented by Mansouri et al. (2014) where additional references can be found. The focus here is on three issues: (i) the role of void nucleation in precipitating localization; (ii) the role of material heterogeneity; and (iii) the use of a localization analysis to enhance finite element calculations.

We begin by reviewing the classical analysis where a band of localized deformation emerges more or less abruptly from a homogeneous deformation state, (Hadamard 1903; Thomas 1961; Hill 1962; Mandel 1966; Rice 1976). If the material constitutive relation is modeled as rate independent, the onset of localization can emerge as a bifurcation. It is a special bifurcation in that it involves conditions at a material point.

Defining the onset of localization of deformation for materials with a rate dependent constitutive description is more subtle and less precise. Incremental wave speeds remain real and the solution to the all around displacement boundary value problem is unique. However, with an initial imperfection or a perturbation, deformations can (and do) localize into a narrow band.

An element of a solid is considered subject to displacement boundary conditions that in a homogeneous (and homogeneously deformed) solid would give rise to a uniform deformation gradient field. In the current state, the deformations, stresses and material properties are presumed to be independent of position. The conditions for a deformation state consistent with a narrow localized band are sought.

Two requirements must be satisfied across the band interfaces. First, compatibility requires

$$\dot{\mathbf{F}}^b = \dot{\mathbf{F}}^o + \dot{\mathbf{q}} \otimes \mathbf{n} \tag{35}$$

where $\mathbf{F}$ is the deformation gradient, $(\,)^b$ denotes field quantities inside the band, $(\,)^o$ denotes corresponding quantities outside the band, the n_i are the components of the band normal and $\dot{\mathbf{q}}$ is the jump in the deformation gradient rate across a surface with normal $\mathbf{n}$.

Rate equilibrium across the band interfaces implies

$$\mathbf{n} \cdot (\dot{\mathbf{s}}^b - \dot{\mathbf{s}}^o) = 0 \tag{36}$$

where $\mathbf{s}$ is the unsymmetric nominal stress tensor related to the Cauchy stress by

$$\mathbf{s} = \det(\mathbf{F})\mathbf{F}^{-1} \cdot \boldsymbol{\sigma} \tag{37}$$

Using standard kinematic relations to relate $\dot{\mathbf{s}}$ to the Jaumann rate of Cauchy stress $\hat{\boldsymbol{\sigma}}$, the constitutive relation for a rate independent solid can be written in component form as

$$\dot{s}_{ij} = \begin{cases} K^{tan}_{ijkl}\dot{F}_{lk} & \text{for plastic loading} \\ K^{el}_{ijkl}\dot{F}_{lk} & \text{for elastic unloading} \end{cases} \tag{38}$$

while for a rate dependent solid the constitutive relation has the form

$$\dot{s}_{ij} = K^{el}_{ijkl}\dot{F}_{lk} - \dot{P}_{ij} \tag{39}$$

where $\dot{P}_{ij}$ is obtained from the term $-\mathbf{L}^{el} : \mathbf{D}^p$ after appropriate kinematic transformations.

Inside the band $\dot{s}^b_{ij} = K^b_{ijkl}\dot{F}^b_{lk}$ and outside the band $\dot{s}^o_{ij} = K^o_{ijkl}\dot{F}^o_{lk}$. For a broad class of elastic-plastic solids and for loadings corresponding to continued plastic deformation, the bifurcation analysis can be carried out for a fictitious 'linear comparison solid' that has moduli that are independent of $\dot{F}_{ij}$ and that correspond to the loading branch of the moduli of the elastic-plastic solid, (Hill 1958; Raniecki and Bruhns 1981). Using the plastic loading branch of Eq. (38) together with Eqs. (35) and (36), the condition for a localization bifurcation becomes, see Hill (1958), Rice (1976), Raniecki and Bruhns (1981)

$$\left[n_i K^{tan}_{ijkl} n_k\right]\dot{q}_l = 0 \tag{40}$$

For a non-trivial solution to exist, the determinant of coefficients in Eq. (40) must vanish. Hence, a localization bifurcation requires

$$\det(\mathbf{M}) = 0 \tag{41}$$

where

$$M_{jl} = n_i K^{tan}_{ijkl} n_k \tag{42}$$

Satisfaction of Eq. (41) coincides with the loss of ellipticity of the equations governing continuing quasi-static deformation.

What is of interest is the orientation for which $\det(\mathbf{M}) = 0$ at the earliest point in the deformation history. When Eq. (41) is satisfied, Eq. (40) can be used to determine the associated $\dot{q}_i$.

For the rate dependent relation Eq. (39), the plasticity is contained in $\dot{P}_{ij}$ and $\dot{P}_{ij}$ only depends on quantities evaluated at time t and not on their rates. Hence, for a homogeneous solid $\dot{P}_{ij}$ has the same value both inside and outside the band. The counterpart to Eq. (40) is

$$\left[n_i K^{el}_{ijkl} n_k\right]\dot{q}_l = 0 \tag{43}$$

As long as stress levels remain small compared to elastic stiffnesses, the only solution to Eq. (43) is $\dot{q}_l = 0$ and a localization bifurcation does not occur.

Now suppose that there is a band where the deformations differ from those outside the band from the outset, say due to some initial heterogeneity. Then, combining Eqs. (35), (36) and the constitutive relation written as

$$\dot{s}_{ij} = K_{ijkl}\dot{F}_{lk} - \dot{P}_{ij} \tag{44}$$

gives

$$\left[n_i K^{b}_{ijkl} n_k\right]\dot{q}_l = n_i\left(K^{b}_{ijkl} - K^{o}_{ijkl}\right)\dot{F}^{o}_{lk} + n_i\left(\dot{P}^{b}_{ij} - \dot{P}^{o}_{ij}\right) \tag{45}$$

Once initial conditions and the deformation history outside the band, $\dot{F}^{o}_{lk}$ are specified, Eq. (45) can be solved to determine the $\dot{q}_l$ and the deformation and stress histories inside the band at each time step. Equation (45) can be used for rate independent solids (in which case the P_{ij} terms do not appear), until $\det\left(n_i K^{b}_{ijkl} n_k\right)$ vanishes, to determine imperfection sensitivity.

In practice, an issue with using Eq. (45) is that a deformation history needs to be determined for all band orientations n_i (in practice the range of possible orientations is spanned and results interpolated between those). The orientation that leads to localization occurring earliest in the deformation history is then determined. For rate independent solids there is no guarantee that the critical orientation for bifurcation is critical for a specified inhomogeneity.

Identifying the onset of localization using Eq. (45) is an issue. For rate independent solid, the onset of localization in Eq. (45) is $\det\left(n_i K^{b}_{ijkl} n_k\right) = 0$. However for a rate dependent solid (assuming stresses remain small compared to elastic moduli), there may be no abrupt transition to identify with the onset of localization. Generally the value of the ratio of some measure of deformation rate inside the band to that outside the band becoming greater than a specified number is used to identify the onset of localization. If this ratio increases fairly rapidly at some time, the state identified with the onset of localization is not very sensitive to that choice, but it is possible for the build up of deformation in the band to be fairly gradual. In such a case, identification of a particular state as corresponding to the onset of localization is somewhat arbitrary.

Analyses of localization bifurcations in rate independent solids, see Rice (1976), have identified several constitutive features that play a key role in promoting localizations: (i) softening. i.e. loss of strain hardening capacity; (ii) non-normality, i.e, the direction, in stress space, of the plastic strain rate and the direction associated with the loading condition not coinciding, as in Eq. (48) below; and (iii) a yield surface corner. The first of these is obviously an attribute of void nucleation, growth and coalescence. It also turns out that, when void nucleation is modeled as governed by a stress controlled criterion the second of these can trigger early localization. Such analyses have also shown that the onset of localization is stress state sensitive with earlier localization occurring for plane strain stress states than for axisymmetric stress states.

The onset of localization is also very sensitive to the nucleation criterion. First, consider a strain controlled nucleation criterion, so that

$$\dot{f}_{\text{nuc}} = \mathcal{D}\dot{\bar{\varepsilon}}$$

where $\bar{\varepsilon}$ is the matrix plastic strain. Then using the original Gurson yield function, neglecting terms of order stress/elastic modulus and building on the analyses of Rudnicki and Rice (1975), it was found by Needleman and Rice (1978) that with strain controlled nucleation and in a plane strain stress state, the critical value of the matrix hardening $\bar{h}$ normalized by the matrix flow strength $\bar{\sigma}$ is given by

$$\left(\frac{\bar{h}}{\bar{\sigma}}\right)_{\text{crit}} = \frac{3}{2} f \cosh\left(\frac{3\sigma_m}{2\bar{\sigma}}\right) \sinh\left(\frac{3\sigma_m}{2\bar{\sigma}}\right) + \mathcal{D} \cosh\left(\frac{3\sigma_m}{2\bar{\sigma}}\right) \tag{46}$$

whereas in an axisymmetric state the critical value of $\bar{h}/\bar{\sigma}$ is

$$\left(\frac{\bar{h}}{\bar{\sigma}}\right)_{\text{crit}} = -\frac{1}{4}\frac{E}{\bar{\sigma}} + \mathcal{D} \cosh\left(\frac{3\sigma_m}{2\bar{\sigma}}\right) + \frac{3}{2} f \cosh\left(\frac{3\sigma_m}{2\bar{\sigma}}\right) \sinh\left(\frac{3\sigma_m}{2\bar{\sigma}}\right) \tag{47}$$

In Eqs. (46) and (47) $\sigma_{\text{m}} = \sigma_{kk}/3$.

Equation (46) shows that in plane strain localization can take place while the matrix is still hardening ($\bar{h} > 0$). Both void growth (through the current value of f) and void nucleation (through the value of $\mathcal{D}$) promote the onset of localization so that porosity induced localization can occur at relatively small strains in lightly hardening materials. On the other hand, the large negative value of the first term on the right hand side of Eq. (47) indicates that porosity induced localization in an axisymmetric stress state will require large strains.

Next, consider a stress controlled nucleation criterion of the form in Eqs. (10) and (12) with $c_1 = 0$ and $c_2 = 1$, so that

$$\dot{f}_{\text{nuc}} = \mathcal{B}\dot{\sigma}_{\text{m}}$$

For a rate independent solid, the plastic multiplier $\dot{\Lambda}$ is determined by the consistency condition $\dot{\Phi} \equiv 0$ during plastic flow. The plastic flow rule, Eq. (3), then takes the form (Needleman and Rice 1978),

$$\mathbf{D}^p = \frac{1}{H}\frac{\partial \Phi}{\partial \boldsymbol{\sigma}}\left[\frac{\partial \Phi}{\partial \boldsymbol{\sigma}} + \frac{\mathcal{B}}{3}\frac{\partial \Phi}{\partial f}\mathbf{I}\right] : \hat{\boldsymbol{\sigma}} \tag{48}$$

Thus, as a consequence of the hydrostatic stress dependence of the void nucleation criterion, the flow rule exhibits plastic non-normality in that the term in brackets on the right hand side of Eq. (48) is not just $\partial\Phi/\partial\boldsymbol{\sigma}$. As shown by Rudnicki and Rice (1975), plastic non-normality can play a significant role in promoting localization.

With stress controlled nucleation, the critical matrix hardening rate in plane strain is given by Needleman and Rice (1978),

$$\left(\frac{\bar{h}}{\bar{\sigma}}\right)_{\text{crit}} = \frac{1}{1 - \mathcal{B}\bar{\sigma}\cosh\left(\frac{3\sigma_m}{2\bar{\sigma}}\right)} \times \left[\frac{3}{2} f \cosh\left(\frac{3\sigma_m}{2\bar{\sigma}}\right) \sinh\left(\frac{3\sigma_m}{2\bar{\sigma}}\right) + \frac{1}{6}\frac{1+\nu}{1-\nu}\mathcal{B}\bar{\sigma}\cosh\left(\frac{3\sigma_m}{2\bar{\sigma}}\right) \times \left\{1 + \frac{1}{6}E\mathcal{B}\cosh\left(\frac{3\sigma_m}{2\bar{\sigma}}\right)\right\}\right] \tag{49}$$

The term involving $\mathcal{B}$ in the denominator on the right hand side of Eq. (49) can be strongly destabilizing. In particular, when stress controlled nucleation takes place over a narrow range the value of $\mathcal{B}$ can be very large. The destabilizing effect of a burst of nucleation with a stress controlled nucleation criterion is illustrated in the numerical localization results of Pan et al. (1983).

Xu and Needleman (1992) carried out localization analyses based on Eq. (45) for a material with a nucleation criterion of the form

$$\dot{f}_{\text{nuc}} = \mathcal{B}\left(\dot{\bar{\sigma}} + c\dot{\sigma}_{\text{m}}\right) \tag{50}$$

The form of Eq. (50) is suggested by the micromechanical analysis of particle debonding of Needleman (1987).

Figure 13 shows the computed localization strain as a function of the parameter c for two imposed deformation histories: (i) plane strain tension and (ii) plane strain tension with a superposed hydrostatic stress modeling the conditions in the neck of a plane strain tension specimen. As seen in Fig. 13 the dependence on c is not monotonic. This is because the strain at which the peak nucleation rate occurs decreases with increasing values of c. For larger values of c, the burst of nucleation occurs at a small strain where the hardening rate is high and localization takes place after some void growth, while smaller values of c give rise to nucleation at larger values of overall strain. The location of the value of c for which the minimum localization strain occurs will depend on the matrix material properties.

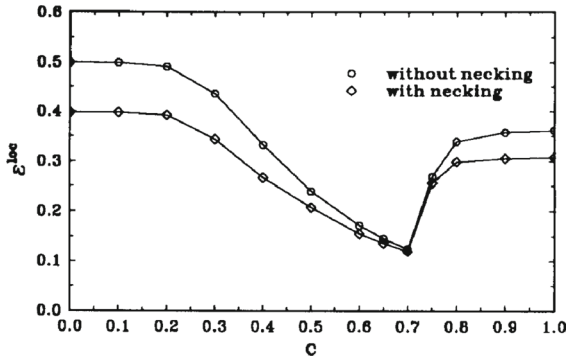

Fig. 13 Localization in plane strain tension with and without necking. From Xu and Needleman (1992)

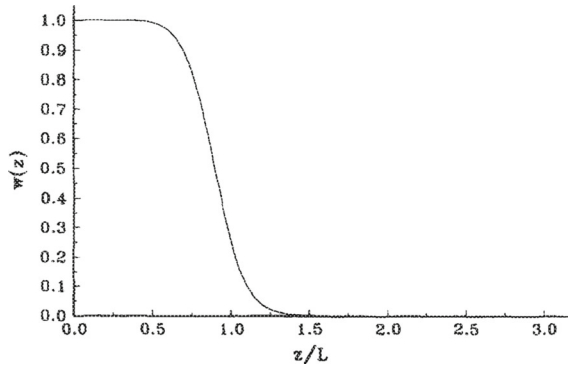

Fig. 14 The function $w(\mathbf{z})$ with $p = 8$ and $q = 2$. From Tvergaard and Needleman (1995)

The results in Fig. 13 illustrate the importance of the localization criterion for the prediction of localization.

Localization of deformation can be and, in fact often is encountered in the solution of boundary value problems. With a rate independent characterization of the matrix material, the localization condition, Eqs. (41) and (42) is met, at some point in the configuration being analyzed, the governing quasi-static equations lose ellipticity and then are ill-posed. With a rate dependent matrix material, loss of ellipticity does not occur, but the numerical stability of the governing equations can become problematic. One consequence of the loss of ellipticity for mesh based numerical methods such as the finite element method is that the energy dissipation in the post-localization regime depends on the length scale associated with the numerical grid and vanishes as the grid length goes to zero. Whether or not this becomes an issue with a rate dependent matrix material depends on the degree of rate dependence, the specific boundary value problem being analyzed and the stability of the numerical scheme, as discussed in a simple context by Needleman (2015).

For ductile failure modeling, this issue stems from the fact that the GTN relation and its various modifications do not contain a length scale. One way to modify the Gurson framework to incorporate a length scale, based on a micromechanics analysis, was proposed by Gologanu et al. (1997) as discussed in Sect. 4.5. Another, simpler but purely phenomenological approach, is to regard the porosity f as a non-local variable via an integral formulation (Leblond et al. 1994). An example of the implications for such a formulation for localization is given by Tvergaard and Needleman (1995) who carried out two dimensional quasi-static analyses of localization for a periodic array of soft spots with the usual local porosity f replaced by a non-local one $\hat{f}$ whose time-derivative is given by

$$\dot{\hat{f}}(\mathbf{x}) = \frac{\mathbf{1}}{\mathbf{W}(\mathbf{x})} \int_{\mathbf{V}} \dot{\mathbf{f}}(\bar{\mathbf{x}}) \mathbf{w}(\mathbf{x} - \bar{\mathbf{x}}) \mathbf{dV} \tag{51}$$

with

$$W(\mathbf{x}) = \int_{\mathbf{V}} \mathbf{w}(\mathbf{x} - \bar{\mathbf{x}}) \mathbf{dV} \tag{52}$$

and

$$w(z) = \left[\frac{1}{1 + \left(\frac{z}{L}\right)^p} \right]^q \ , \ z = \sqrt{\mathbf{z} \cdot \mathbf{z}} \tag{53}$$

where $\mathbf{z} = \mathbf{x} - \bar{\mathbf{x}}$ and the form of $w(z)$ used by Tvergaard and Needleman (1995) is shown in Fig. 14.

The results of Tvergaard and Needleman (1995) illustrate the significance of accounting for a material length scale in grid based numerical solutions involving localization. Figure 15 shows results obtained from finite element calculations using a conventional GTN constitutive relation. The width of the localization band clearly depends on the mesh resolution. On the other hand, using a formulation based on Eqs. (51) to (53), Fig. 16, the width of the localization band is essentially independent of the mesh resolution for a wide range of discretizations.

Another approach to introducing a length scale into finite element calculations involving localization was introduced by Huespe et al. (2009, 2012). Their formulation is aimed at circumstances where a finite element

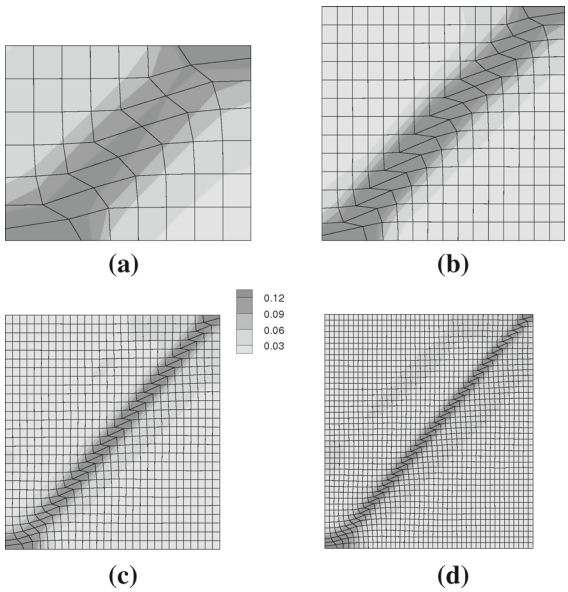

Fig. 15 Contours of f for $L = 0$ **a** a 7×7 mesh. **b** a 14×14 mesh. **c** a 28×28 mesh. **d** a 42×42 mesh. From Tvergaard and Needleman (1995)

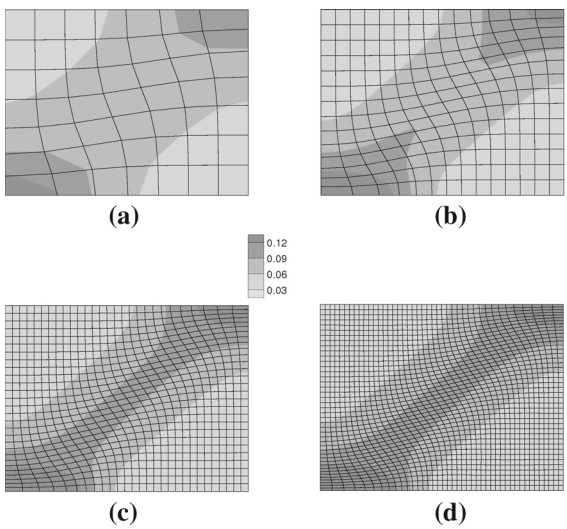

Fig. 16 Contours of f for $L = 0.1B_0$ **a** a 7×7 mesh. **b** a 14×14 mesh. **c** a 28×28 mesh. **d** a 42×42 mesh. From Tvergaard and Needleman (1995)

calculation of a structure or component is carried out and localization of deformation occurs on a scale that is much smaller than the size of a finite element. In the formulation of Huespe et al. (2009, 2012) additional functions representing the band are added to the usual finite element shape functions. A finite thickness embedded weak discontinuity is introduced when the

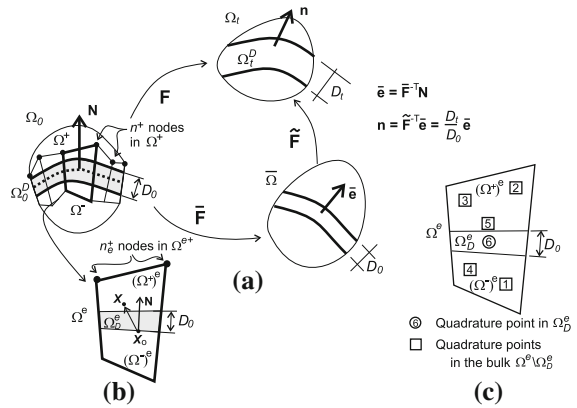

Fig. 17 Finite deformation weak discontinuity kinematics. **a** The multiplicative decomposition of the deformation gradient. **b** A quadrilateral finite element with an embedded weak discontinuity. **c** Quadrature points within a quadrilateral finite element. From Huespe et al. (2012)

condition Eq. (41) is met for some band orientation **n** as illustrated in Fig. 17. After the localization condition is met, the band is required to deform homogeneously and follow the specified constitutive relation. The specified band thickness D_0 is regarded as a material length scale. As a consequence, convergent calculations of the history of deformation through localization and the creation of new free surfaces can be carried out.

Figure 18 shows results for plane strain tension with various finite element meshes and for various values of the length parameter D_0. A very similar shear band is obtained for the three mesh resolutions shown and the overall stress-strain response near failure is nearly the same for all three discretizations. With a fixed finite element mesh, the post-localization response depends on D_0 as seen in Fig. 18d.

The formulation of Huespe et al. (2009, 2012) is limited to rate independent materials. Arriaga et al. (2015) have proposed a stability analysis that could be applied for a rate dependent porous plastic solid and so permit this type of enhanced finite element analysis to be used more generally.

7 Applications

7.1 GTN analyses for welded joints

In a number of analyses the ductile fracture models have been applied to study the failure evolution in welded joints. The examples to be considered here will focus

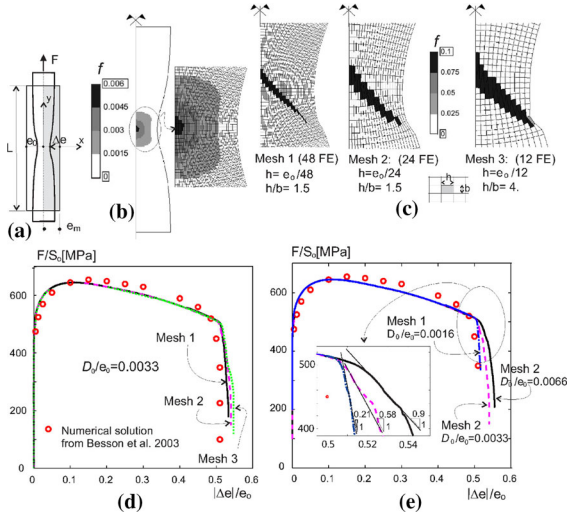

Fig. 18 Localization and failure in a plane strain specimen. **a** A sketch illustrating the boundary value problem. **b** Void volume fraction distribution, in the deformed configuration, when the first material point (which is at the specimen center) satisfies the bifurcation condition. **c** Contours of void volume fraction in the deformed configuration for meshes with 48, 24 and 12 finite elements in the horizontal direction. **d** The specimen load versus normalized width reduction obtained using the three meshes. **e** A comparison of the specimen load versus normalized width reduction curves obtained with three values of band width D_0. From (Huespe et al. 2012)

on fusion welded specimens, on friction stir welding and on resistance welding, in particular spot-welded specimens.

7.1.1 Charpy testing of fusion welded specimens

The Charpy V-notch test is a standard procedure for characterizing the ductile-to-brittle transition in steels, as has been discussed in Ritchie (1978), François and Pineau (2002). The use of a micromechanically based material model to analyze the failure mode transition in the Charpy test has been proposed by Tvergaard and Needleman (1986, 1988), Benzerga et al. (2002b). In these studies the GTN model has been used to represent ductile fracture by void growth to coalescence, and this is combined with a model for cleavage failure in grains, which represents the brittle mode of failure. Several investigations of cleavage fracture in body-centered-cubic metals have shown that a constant critical stress is a realistic criterion for slip induced cleavage failure in the low temperature range, and it has been assumed in the cited works that such a constant critical value σ_c is a sufficiently good criterion in the whole range of temperatures. Then the temperature dependence of the failure mode results from the fact that at lower temperatures the initial yield stress is higher, so that it is more likely to reach the critical stress σ_c for cleavage before the amount of plastic yielding is sufficient to develop ductile fracture. The effect of a high loading rate on fracture results from the material strain-rate sensitivity, accounted for by a visco-plastic GTN model, which makes it more likely to reach the critical stress σ_c before void coalescence when the Charpy specimen is subjected to an impact load; also see (Tanguy et al. 2005) for statistical aspects in cleavage fracture.

This combination of material models has been applied to Charpy specimens for welded joints, first as a plane strain analysis (Tvergaard and Needleman 2000) and subsequently as full three dimensional analyses (Tvergaard and Needleman 2004). In fusion welding new weld material is melted into the joint and on each side of the weld the base material is separated from the weld material by a narrow heat affected zone (HAZ). Usually the material properties are different in these three material zones along the fusion line. In particular the HAZ material tends to have a higher initial yield stress, which makes it more likely that the cleavage stress σ_c will be reached before ductile fracture, and this more brittle response of the HAZ material is a characteristic feature of the mechanical properties of welds.

To test the weld, Charpy specimens are cut out so that they are perpendicular to the weld and parallel to the surface of the welded piece. The specimen can be cut at various depths below the surface of the welded piece, and the notched face of the Charpy specimen is chosen to be either parallel to the surface of the welded piece or perpendicular to this surface. In the first type of specimen Fig. 19 illustrates how the V-notch is offset by the distance x_c^2 from the center of the weld to test the notch-sensitivity of each of the three materials in the weld zone. This geometry can be reasonably well approximated by a plane strain analysis (Tvergaard and Needleman 2000) and is also analyzed in three dimensions (Tvergaard and Needleman 2004). Both the two dimensional and three dimensional analyses show that the most critical situation, i.e. the lowest work of fracture corresponding to the most brittle response, occurs when the specimen is cut such that the region slightly below the notch falls inside the HAZ.

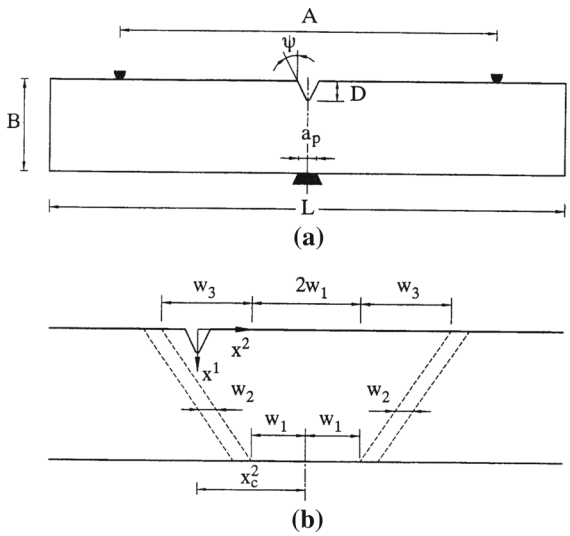

Fig. 19 **a** In-plane geometry of the Charpy specimen. **b** Geometry of the fusion-weld. From Tvergaard and Needleman (2004)

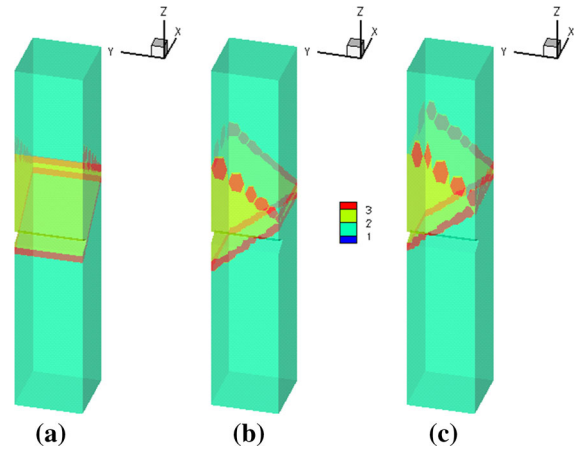

Fig. 20 Examples of weld configurations analyzed, *1* is the base material, *2* is the weld material, *3* is HAZ. **a** $x_c^2 = 6.5$ mm, **b** $x_c^2 = 4$ mm (rotated 90°), **c** x_c^2 =7 mm (rotated 90 °). From Tvergaard and Needleman (2004)

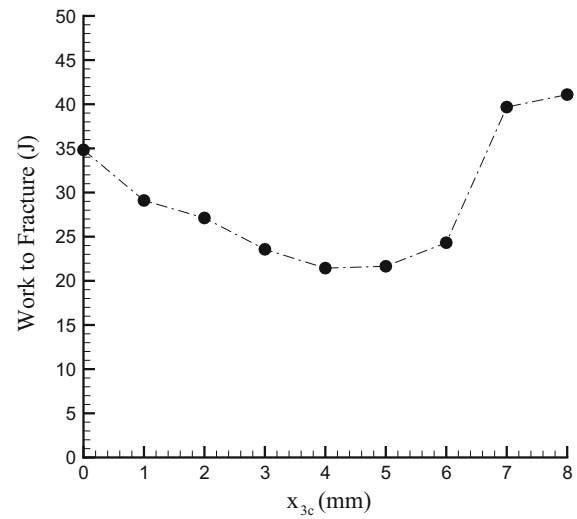

Fig. 21 Work to fracture vs. the distance x_c^2 from the center of the weld to the notch (rotated 90°). From Tvergaard and Needleman (2004)

Figure 20b, c show two situations where the notched face of the Charpy specimen is perpendicular to the surface of the welded piece. Clearly these situations are fully three dimensional and cannot be approximated by a planar analysis. Wherever the notch is located inside the weld zone some of the material slightly below the notch is inside the HAZ, but still the absorbed energy varies with the location of the notch, as illustrated in Fig. 21. The stress state is more constrained in the center of the specimen than near the free sides, so the stresses tend to be higher near the center, where brittle fracture might initiate in the HAZ below the notch.

7.1.2 Failure in friction stir welded joints

Friction stir welding is a relatively new solid state process for joining a variety of different materials. The basis of the process is a spinning tool consisting of a pin and a shoulder plate which is lowered into the weldline between two metal sheets until the shoulders are pressed in contact with the sheets to be welded. When the spinning tool is moved forward along the weldline a joint is created due to friction heating and extensive deformation of the material in the stir zone. The heat and deformation created between the shoulder plate and the material to be welded, result in a difference in the microstructure and thereby the mechanical properties between the top and bottom of the weld.

Ductile fracture in a friction stir welded aluminum plate has been analyzed by Nielsen (2008b), Nielsen and Tvergaard (2009). This has been done by studying tensile test specimens cut out of the plate perpendicular to the weld, and it is found that the damage development and the position of the final fracture are strongly affected by variations in the yield stress profile transverse to the weldline. Figure 22 shows typical variations of the yield stress near the weld, normalized by the yield stress of the base material. The three curves

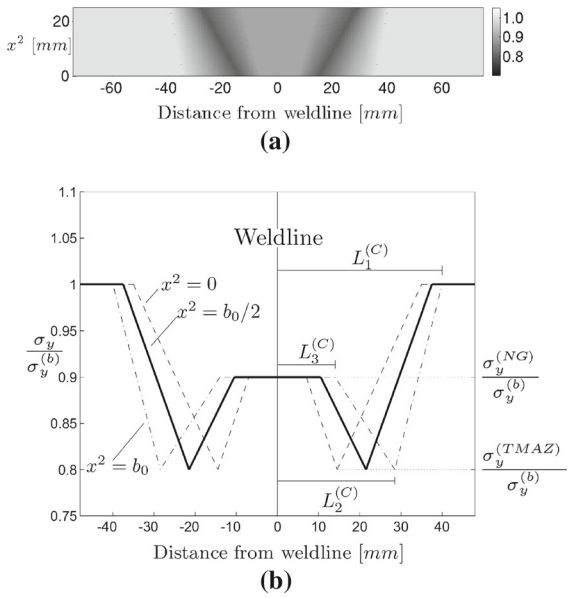

Fig. 22 Characteristic yield stress variation transverse to the weldline for friction stir welded aluminum alloy; **a** yield stress in weld cross-section; **b** modeled yield stress profile at the top, bottom and middle of the weld cross-section. From Nielsen and Tvergaard (2009)

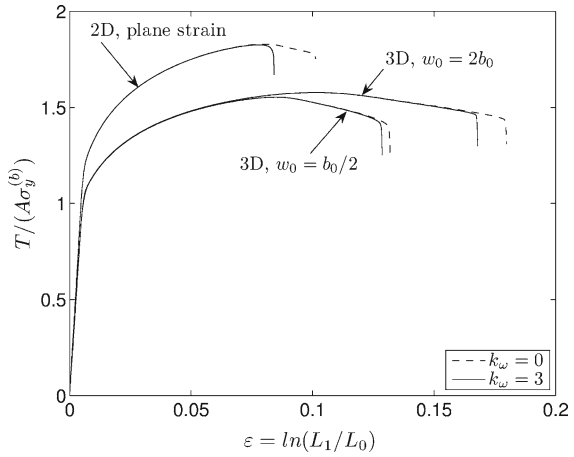

Fig. 23 Load versus axial strain curves for friction stir welded specimens. From Nielsen and Tvergaard (2009)

shown in Fig. 22b give the yield stress variation at the bottom of the weld ($x^2 = 0$) and at the middle and the top. As is seen in Fig. 22 the central part of the weld is called the nugget zone (NG), while the edge parts with lowest yield stress are called the thermo-mechanically affected zones (TMAZ). The rotating weld tool moving along the weldline will tend to give a difference between the advancing and the retreating sides of the weld, but in Nielsen (2008b), Nielsen and Tvergaard (2009) the resulting slight non-symmetry of the yield stress profiles has been neglected, thus assuming the symmetric distributions shown in Fig. 22. Also the power hardening exponent is assumed to vary with the yield stress, by using an empirical relationship. The volume fraction of void nucleating particles is assumed to be the same throughout the welded plate.

The analyses of Nielsen (2008b) are based on the viscoplastic version of the GTN model, assuming that voids nucleate according to a plastic strain controlled rule, and that fracture occurs when the voids have grown to coalescence. Nielsen and Tvergaard (2009) used the same constitutive model for some computations, but here the predictions are compared with results of the modified material model proposed by Nahshon and Hutchinson (2008) and discussed in Sect. 4.2.2, in which an extra damage term has been introduced to be able to predict failure at low stress triaxiality.

Figure 23 shows load vs. axial strain curves both for plane strain calculations and for full three dimensional calculations, in cases where $\sigma_y^{(TMAZ)}/\sigma_y^{(b)} = 0.8$ and $\sigma_y^{(NG)}/\sigma_y^{(b)} = 1.0$. In the two dimensional analyses ductile failure is predicted noticeably later by the GTN model than by the modified model, because here a rather dominant localized shearing develops in the TMAZ region where the initial yield stress is lower. The difference is smaller in the three dimensional analyses.

In Fig. 23 b_0 denotes the initial plate thickness. The tensile test with half length $L_0 = 3b_0$ is cut out of the plate perpendicular to the weld. The width w_0 of the 3D specimen in Fig. 23 is either $2b_0$ or $b_0/2$.

Contours of the damage parameter f are shown in Fig. 24 for the material properties also considered in Fig. 23 (with $k_\omega = 3$, see Eq. (14) for the meaning of this parameter), but for a wider three dimensional specimen than those considered in Fig. 23 (the figure shows the full plate thickness but only half of the width, due to symmetry). At the first stage the localized shearing in the TMAZ region is clearly visible by the concentrated damage, while in the later stage a broad through-thickness shear region has developed from the center of the weld part of the specimen.

7.1.3 Resistance spot welded specimens

Resistance spot welding is a well known method for joining a variety of thin sheet metals. One of the meth-

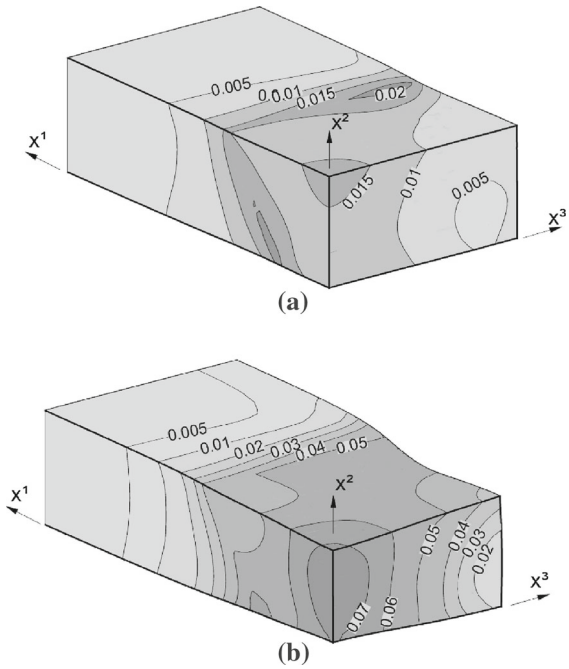

Fig. 24 Damage development, f, in a wide test specimen, $w_0 = 4b_0$; **a** at $\epsilon = 0.1648$; **b** at $\epsilon = 0.2139$ ($k_\omega = 3$). From Nielsen and Tvergaard (2009)

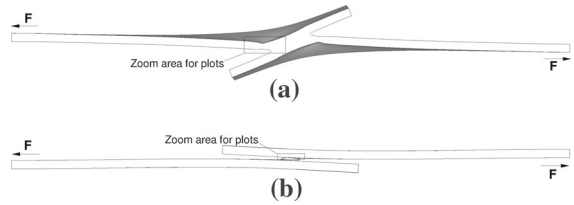

Fig. 25 Examples of modeled shear-lab specimens; **a** the plug failure mode; **b** the interfacial failure mode. From Nielsen and Tvergaard (2010)

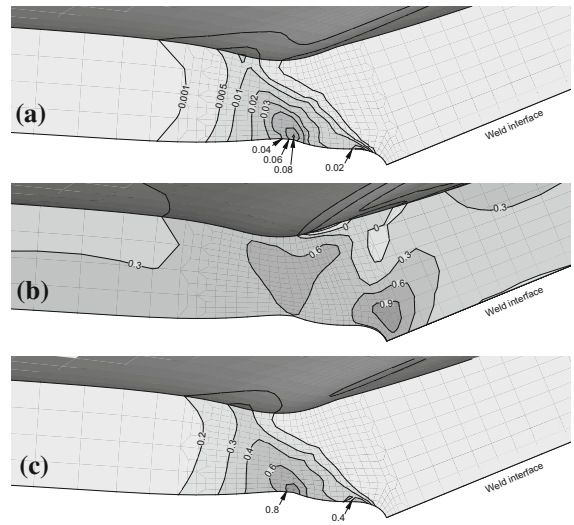

Fig. 26 Plug failure of single spot welded shear-lab specimen with weld radius $a = 4$ mm, specimen width $2w = 25$ mm, and sheet thickness $t = 1.5$ mm—for model D ($k_\omega = 0$); **a** void volume fraction f; **b** stress triaxiality T; **c** microscopic plastic strain ϵ_M^p. From (Nielsen and Tvergaard 2010)

ods used for testing the strength of spot welds is a tensile test for a shear-lab specimen, where two plate strips are welded together by a single spot weld. The failure of such a shear-lab test made of DP600-steel has been analyzed in Nielsen (2008a), using the GTN model. Vickers hardness measurements on the cross-section of welds have been used in an experimental investigation to measure the distribution of the initial yield stress. Around the circular weld there is a weld nugget, approximately shaped as an ellipsoid, which has significantly higher yield stress than that in the base material.

Nielsen and Tvergaard (2010) analyzed the ductile fracture of shear-lab specimens using the GTN model as well as the modified model from Nahshon and Hutchinson (2008). Figure 25 shows the two types of failure modes that are predicted by the ductile fracture analyses, and also found in experiments. Results of a numerical solution obtained by the GTN model ($k_\omega = 0$) are shown in Fig. 26, presented as variations of field variables in the central cross-section along the specimen. As is seen from Fig. 25a, this situation where plug failure is developing is highly nonlinear and three dimensional, not only in terms of large strains but also the weld nugget undergoes large rotations and the material beside the weld nugget deforms in ways very different from that in the nugget. As seen in Fig. 26 there is practically no straining and no void growth inside the weld nugget, where the yield stress is higher, and failure is growing in the softer material beside the nugget, which is going to develop into the shear failure that will separate the nugget from the rest of the specimen, as is characteristic for plug failure.

Figure 27 shows curves of tensile force vs. end displacement as predicted by four different material models, where D is the GTN model, and A the modified model from Nahshon and Hutchinson (2008). Models B and C are versions of A, where the extra damage term is only activated in intervals of low stress triaxiality T, in the vicinity of $T = 0$. The curve for model D corresponds to the computation also illustrated in Fig. 26.

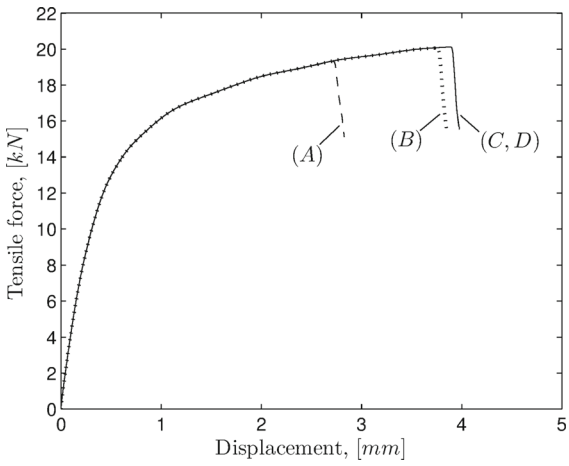

Fig. 27 Modeled tensile curves for single spot welded shear-lab specimen with weld radius $a = 4$ mm, specimen width $2w = 25$ mm, and sheet thickness $t = 1.5$ mm—in all cases ductile plug failure was predicted. From Nielsen and Tvergaard (2010)

Since the stress triaxialities in Fig. 26b are rather low, this is in the range where the extra damage term introduced in Nahshon and Hutchinson (2008) is expected to play a noticeable role, and therefore it is not surprising that material A predicts failure a great deal earlier than material D. It is noted that by Nielsen (2010) computations like those in Fig. 27 have also been carried out for the GLD model, thus accounting for the effect of void shape changes, and these computations have predicted later failure than that for model D in Fig. 27.

The computations illustrated in Figs. 26 and 27 are carried out for a specimen with weld radius $a = 4$ mm, specimen width $2w = 25$ mm, and sheet thickness $t = 1.5$ mm. Nielsen and Tvergaard (2010) also carried out computations for a lower weld radius, $a = 1.5$ mm, on the same shear-lab specimen. Here the area of the weld is so small that the force needed to shear off the weld nugget is not sufficient to bend the plates in the shear-lab specimen near the weld and therefore the interfacial failure mode occurs as illustrated in Fig. 25b. The material in the weld nugget undergoes essentially simple shear with the stress triaxiality $T = 0$, and as expected model D (the GTN model) predicts no failure, as there is no void growth, while model A predicts failure at an end displacement and a tensile force much smaller than found in Fig. 27.

In the comparison with experiments for DP600-steel Nielsen (2008a) only considered the GTN model, corresponding to D in Fig. 27. In the range of sufficiently large weld radius, where the failure mode is like that in Fig. 25a, the GTN model gave a good approximation of the experiments, which means according to Fig. 27 that also models B and C would give good approximations, while model A would underestimate the failure elongation somewhat. For a smaller weld radius, where interfacial failure was observed (Fig. 25b), the GTN model could not predict the shear failure, but here incorporating the shear modification of Nahshon and Hutchinson (2008) does result in failure.

The ability to predict deformation and failure at welds underlies the safe and economical design of pipelines particularly in hostile environments where earthquakes, soil liquefaction, frost heave, thaw settlement, and ice gouging can occur. In such circumstances, the pipeline needs to be able to undergo relatively large plastic strains without failing. GTN based calculations are used in developing design rules for such welded pipelines as described in Tang et al. (2015).

7.2 Analyses using the hybrid model of coalescence

As indicated in Sect. 5, fundamental issues are encountered in any micromechanical approach to void coalescence. It has notably been said that the phenomenon may not be adequately described within the confines of classical localization theory (Rice 1976). This does not mean that it is hopeless to attempt to predict coalescence by applying strain localization theory to some "homogenized" model. It just emphasizes the need, in order to do so, for a model incorporating the mesoscopic mechanism of coalescence, that is strain concentration at a scale of the order of the void size, not the void spacing. Enabled by the availability of hybrid models a first attempt at this was made by Benzerga et al. (2002a). They did not apply Rice's localization analysis per se. Instead, they provided full boundary-value problem solutions to the problem of plastic flow localization using constitutive relations for porous metal plasticity of the hybrid kind. Their study focused on discussing the interplay between plastic anisotropy and a yield vertex inherent to the hybrid model. The vertex developed for relatively low porosity levels, as small as 0.05 or thereabout, concurrent with the first instance of coalescence at the location of highest stress triaxiality. Benzerga et al. found a striking synergistic effect of plastic anisotropy and a yield vertex in triggering localization, as illustrated in Fig. 28a.

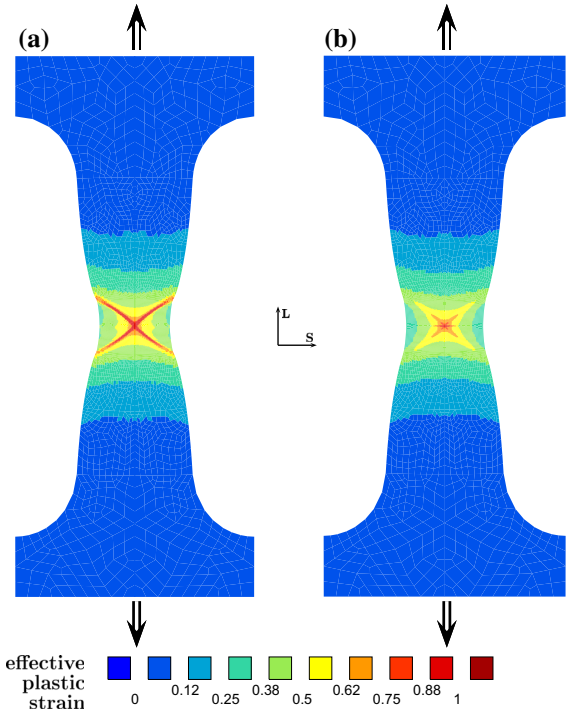

Fig. 28 Plastic flow localization in plane strain bars using the GLD model of void growth, heuristically extended to plastic anisotropy, and a variant of the coalescence criterion (34) (hybrid approach; see Fig. 11) for: **a** a plastically anisotropic matrix, $f_0 = 0.0075$, $w_0 = 1$, and $\lambda_0 = 1$; and **b** isotropic matrix, $f_0 = 0.0075$, $w_0 = 1$, and $\lambda_0 = 1.5$. Adapted from Benzerga et al. (2002a)

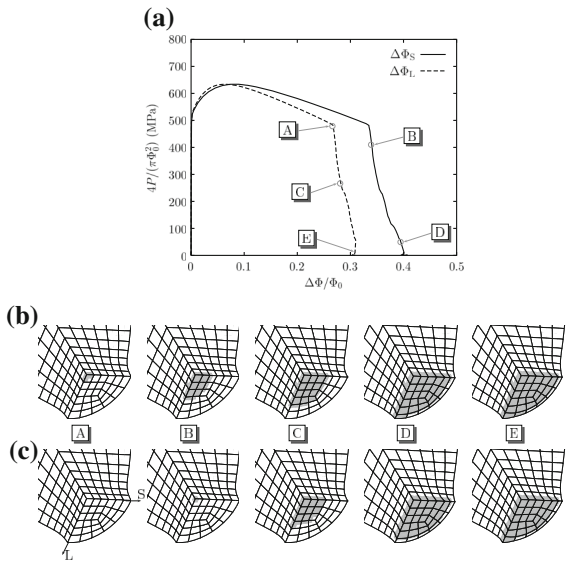

Fig. 29 Application of a hybrid model to anisotropic crack initiation and growth in round notched vars. **a** Force versus diameter reduction along two perpendicular transverse directions displaying various stages A to E using $f_0 = 0.00075$, ln $w_0 = 3$, $\lambda_0 = 1$ and an initial void orientation perpendicular the loading axis. **b** Elements undergoing coalescence (flat part in Fig. 11) are painted *gray*. **c** Broken elements are painted *Gray*. A: Onset of coalescence; B: crack initiation; C: anisotropy in extent of coalescence and crack growth; D: last element along L undergoing coalescence; E: last element along L broken. After Benzerga et al. (2004)

They also found that the presence of the vertex does not necessarily lead to flow localization in the specimen, Fig. 28b (initial values of the internal parameters are indicated using the subscript 0). Clearly, more work is needed in this area, especially with the development of unified models of void growth and coalescence.

Figure 29 illustrates the application of a hybrid-type model, namely a GLD model heuristically extended to incorporate plastic anisotropy and the void coalescence criterion (34), to three-dimensional crack initiation and propagation in initially round notched bars. The bars were loaded in the transverse direction of a steel plate in which the voids were initially modeled as "cigars" normal to the loading direction. The difference between the two (load versus diameter reduction) curves is due to plastic anisotropy as the initially round sections develop into an oval shape. The calculations were carried out using quadratic elements with reduced integration and an implementation of the hybrid model in an in house code (ZeBuLon). The knee in the load-deflection curves corresponds to the first instance of void coalescence at the center of the bar where the triaxiality is highest. When coalescence sets in at the current integration point, the material has not yet lost all stress bearing capacity. The latter occurs for the first time at stage B, which may be referred to as crack initiation. The subsequent crack growth process is anisotropic due to the plastic anisotropy of the material.

Quite recently, this type of hybrid approach has been used by Shinohara et al. (2016) who employed the GTN model for void growth and a three-dimensional coalescence model that heuristically accounts for void spacing anisotropy.

7.3 Simulations of Dunand and Mohr's experiments on "butterfly" specimens

Dunand and Mohr (2011a, b) have recently developed a technique for experimental study of thin structures. The optimized "butterfly" specimens this technique is based on are basically plates, the central region of

which is made thinner in order to concentrate the strain and control the location of the crack. These specimens are subjected to combined tension and shear; the loading may be proportional or non-proportional, and vary between the extremes of tension in transverse plane strain and pure shear. Details may be found in the papers of Dunand and Mohr (2011a, b).

In the experiments considered hereafter, the ratio F_V/F_H of the vertical (tensile) to horizontal (shear) forces is kept constant. Four values of the angle $\beta \equiv \arctan(F_V/F_H)$ are considered, $\beta = 90°$ (tension in transverse plane strain), 63°, 25° and 0° (pure shear). For each experiment, two load-displacement curves are recorded: vertical force versus vertical displacement and horizontal force versus horizontal displacement. Photographs of the fractured specimens are also taken. The material used is a high resistance TRIP780 steel. Again, details are provided by Dunand and Mohr (2011a, b).

The simulations are performed using the ABAQUS finite element program. The three dimensional mesh consists of 71986 trilinear, selectively subintegrated (C3D8) elements and 82479 nodes. Controlled displacements are imposed on the lower and upper surfaces of the specimen. The model used is that of Madou and Leblond (2012a, b, 2013), Madou et al. (2013) accounting for void shape effects, well adapted to conditions of low triaxiality, see Sect. 4.3.2 above. Coalescence of voids is accounted for in the heuristic manner suggested by Tvergaard and Needleman (1984). The main uncertainties in the simulations arise from the fact that void nucleation is disregarded; this phenomenon is known to be important in the type of steel considered although the relevant parameters are not known precisely.

Figure 30 shows the experimental (Exp) and computed (ML) load-displacement curves for various values of the angle β defined above (the case $\beta = 0°$ is disregarded in Fig. 30a because the vertical force and displacement are zero then, and the case $\beta = 90°$ is similarly disregarded in Fig. 30b). All experimental curves are acceptably reproduced [the agreement could be improved by accounting for the plastic anisotropy of the material through use of the model of Morin et al. (2015b), see Sect. 4.4.3]. The most remarkable point here is the reproduction of the experimental final instability: the computed load-displacement curve becomes more or less suddenly vertical, and the elastoplastic iterations cease to converge. This occurs even for very

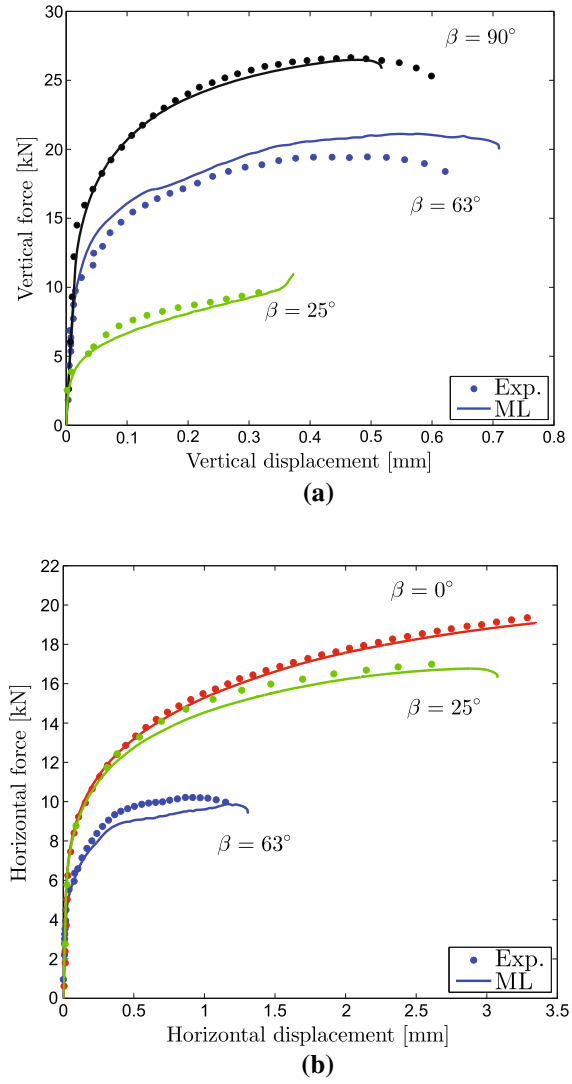

Fig. 30 Butterfly specimen—vertical force versus vertical displacement and horizontal force versus horizontal displacement. **a** Vertical force versus vertical displacement. **b** Horizontal force versus horizontal displacement

low triaxialities ($\beta = 0°$ or 25°), because of the damage induced by void shape changes. The prediction of this type of damage is a typical feature of the model of Madou and Leblond (2012a, b, 2013), Madou et al. (2013)—simulations performed with the GTN model not accounting for void shape effects have been performed and checked to fail to reproduce, for low triaxialities, the final experimental instability.

Figure 31 compares, in the case $\beta = 25°$, the photograph of the fractured specimen and the distribution of the maximum principal strain computed at the last

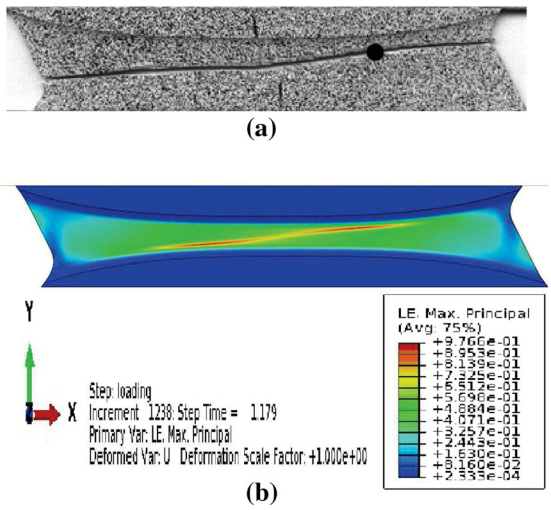

Fig. 31 Butterfly specimen—photograph of the fractured specimen and computed distribution of the maximum principal strain. **a** Fractured specimen. **b** Distribution of maximal principal strain

available instant, just prior to the instability, on the deformed configuration (without any amplification of the displacements). The location of the yellow and red region where the computed maximum principal strain takes its highest values coincides quite well with that of the experimentally observed crack. More, the black circle of Fig. 31a, which marks the probable actual point of initiation of the crack, lies precisely within the red zone of Fig. 31b where the strain is maximum.

Numerical simulations of these experiments have also been successfully performed by Dunand and Mohr (2011a) using the model of Gurson (1975, 1977) with the heuristic modification of the evolution equation of the porosity of Nahshon and Hutchinson (2008), see Sect. 4.2.2. The simulations just presented show that use of the model of Madou and Leblond (2012a, b, 2013), Madou et al. (2013) accounting for void shape effects represents a viable alternative, more rigorous albeit more complex, way of reproducing the experiments of Dunand and Mohr (2011a, b).

7.4 Two applications of Gologanu et al.'s second-gradient extension of Gurson's model

The predictions of the second gradient extension of the model of Gurson (1975, 1977) by Gologanu et al. (1997), aimed at solving the problem of unlimited localization of strain and damage, see Sect. 4.5, will now be illustrated through two numerical examples due to Bergheau et al. (2014). All computations described in this section have been performed using the SYSTUS finite element program developed by ESI-Group.

The first example pertains to the two dimensional axisymmetric simulation of a fracture test performed on a pre-notched and precracked TA30 specimen (TA = Tensile Axisymmetric, 30 = diameter in mm). The geometry and one of its discretizations are represented in Fig. 32. Advantage is taken of symmetry about the horizontal mid-plane to model only the upper half of the specimen, and the axis of rotational symmetry coincides with the left boundary of the mesh; note the triangular notch at the lower-right corner, from which the horizontal fatigue pre-crack (invisible in the figure) originates. Two meshes are in fact used, so as to permit a study of the mesh sensitivity of the results; they differ through the size of the square elements used in the region of the propagating crack, 0.3 mm and 0.1 mm, the mesh represented in Fig. 32 corresponding to the former value. The specimen is made of A 508 Class 3 steel (used in nuclear components); the material parameters are provided by Bergheau et al. (2014). In particular, various values of the heuristic parameters of f_c (the "critical porosity" at the onset of coalescence) and $\delta = (f_u - f_c)/(f_f - f_c)$ (the "accelerating factor") of Tvergaard and Needleman (1984) are used, and the value of the "microstructural distance" b (see Sect. 4.5) is 0.55 mm.

Figure 33 compares the experimental load-displacement curve (in dark blue) to various numerical ones:

- The yellow and green curves have been obtained with the same coalescence parameters, $f_c = 0.08$ and $\delta = 4$ but the two meshes having element sizes of 0.3 and 0.1 mm in the region of the crack, respectively. The curves are very close, showing that the influence of the discretization is minimal. Results obtained with the standard first-gradient model of Gurson (1975, 1977) would exhibit a much larger mesh sensitivity in the descending portion of the curve.
- The red curve corresponds to the best agreement obtained with the experimental results; it has been obtained with the mesh having an element size of 0.3 mm in the region of the crack and the parameters $f_c = 0.04$ and $\delta = 2$. The agreement with the experimental results is quite acceptable considering the inherently imperfect reproducibility of experi-

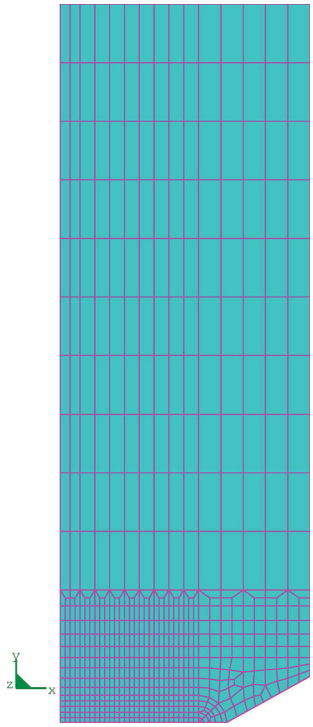

Fig. 32 Mesh of a TA30 specimen. From Bergheau et al. (2014)

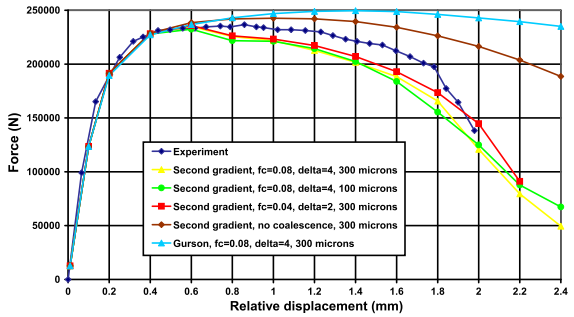

Fig. 33 Load-displacement curves of a TA30 specimen. From Bergheau et al. (2014)

mental results. This result is remarkable in view of the qualitative compatibility of the value of f_c used with the theoretical ones, of the order of a few percent, obtained by various authors through micromechanical finite element simulations of representative porous cells, see the pioneering work of Koplik and Needleman (1988) and its many successors. Such a result could never be obtained with Gurson's model which was always observed to necessitate much smaller, and unrealistic values of f_c to warrant satisfactory reproduction of experimental load-displacement curves of cracked specimens.

– The brown curve has been obtained with the same mesh but coalescence has been suppressed here by adopting a high value for f_c (or equivalently a unity value for δ). The large discrepancy with the experimental curve, especially in its descending portion, illustrates the necessity of accounting for coalescence to satisfactorily reproduce the test.
– Finally the light blue curve has been obtained with the same mesh and coalescence parameters as the red one, but using the original model of Gurson (1975, 1977) instead of the second gradient extension of Gologanu et al. (1997). The much-too-modest decrease of the load illustrates the incapacity of Gurson's model to reproduce experimental results for such high values of f_c, and the necessity of using much lower, unrealistic values.

The second example pertains to the two dimensional plane strain simulation of a fracture test performed on a CT12 specimen (CT = Compact Test, 12 = thickness in mm). The discretized geometry is shown in Fig. 34. (A single mesh is used this time). Advantage is taken of symmetry about the vertical mid-plane of the specimen to model only its right half. A vertical fatigue pre-crack (invisible in the figure) originates from the notch root. Square elements of size 0.3 mm are used in the region of the propagating crack. The specimen is made of SS 316L stainless steel; the material parameters are provided by Bergheau et al. (2014). In particular, various values of the "critical porosity" at the onset of coalescence f_c and "accelerating factor" δ of Tvergaard and Needleman (1984) are used again, and the value of the "microstructural distance" b is 0.5 mm.

Figure 35 shows the experimental load-displacement curve (in dark blue) together with three numerical ones:

– The red curve has been obtained with the second gradient model of Gologanu et al. (1997), including coalescence with the values $f_c = 0.05$ and $\delta = 2$. The agreement with the experimental curve is excellent, again illustrating the model's capability to reproduce experimental results using relatively high values of f_c compatible with the available theoretical estimates.
– The brown curve has been obtained with the same model but disregarding coalescence. Again, the large discrepancy with the experimental curve illus-

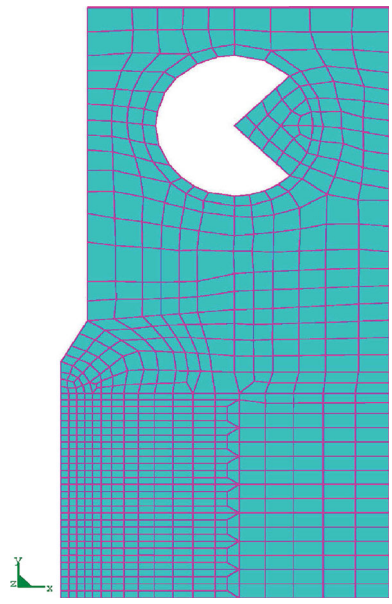

Fig. 34 Mesh of a CT12 specimen. From Bergheau et al. (2014)

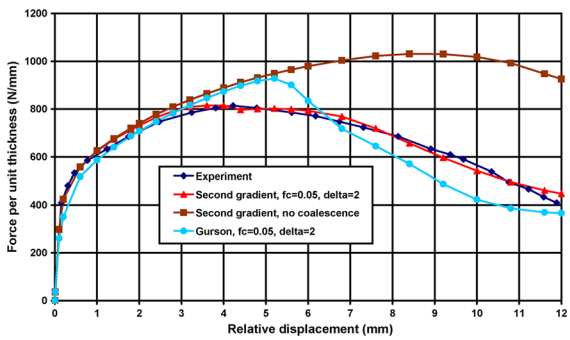

Fig. 35 Load-displacement curves of a CT12 specimen. From Bergheau et al. (2014)

trates the necessity of accounting for coalescence to satisfactorily reproduce the test.

– The light blue curve has been obtained with the same coalescence parameters as the red one but using the Gurson (1975, 1977) model. The large gap between this curve and the experimental one again illustrates the incapacity of Gurson's model to reproduce experimental results for high, realistic values of f_c.

Figure 36 shows the distribution of the opening stress (perpendicular to the crack plane) on the deformed configuration of the specimen (without any magnification of the displacements), at the last instant

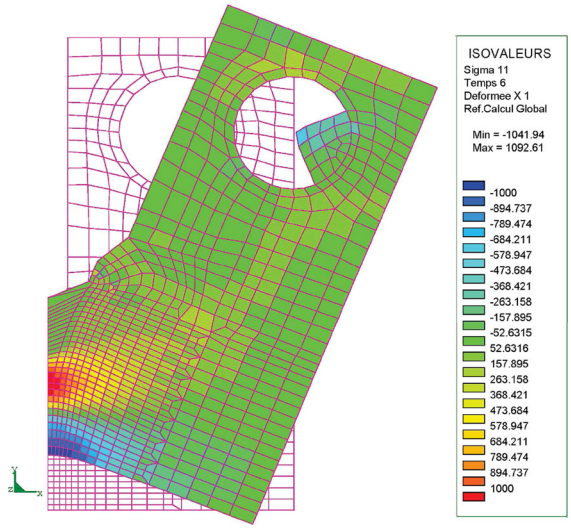

Fig. 36 Opening stress field in a CT12 specimen. From Bergheau et al. (2014)

of the simulation corresponding to the red curve in Fig. 36. (The undeformed mesh is shown in the background for reference.) The important propagation of the crack and the large ensuing deformation of the specimen are quite conspicuous here. On the vertical plane of symmetry, the opening stress is zero in the region of the crack, positive just ahead of the crack tip and negative beyond, as expected since the total moment of external forces must be zero.

Calculations have also been performed very recently using a mix of elements obeying a Mises standard first-gradient model and the second-gradient extension of the Gurson model by Gologanu et al. (1997), the idea being to reduce the CPU time by using the second-gradient model only in the region of the propagating crack where strain gradients are maximum. As explained in Sect. 4.5, the very recent numerical implementation by Bergheau et al. (2014) of the second gradient model of Gologanu et al. (1997) is especially fit to such a mix. Figure 37a shows three possible zones for the "second-gradient region", and Fig. 37b compares the corresponding load-displacement curves to that obtained using the second-gradient model in the whole structure, which serves as a reference. As can be seen, results virtually identical to the reference ones are obtained by confining second-gradient elements to "Zone 3" of Fig. 37a, with a CPU-time reduction of 24 %, and quite acceptable ones by confining second-gradient elements to "Zone 2", with a CPU-time reduc-

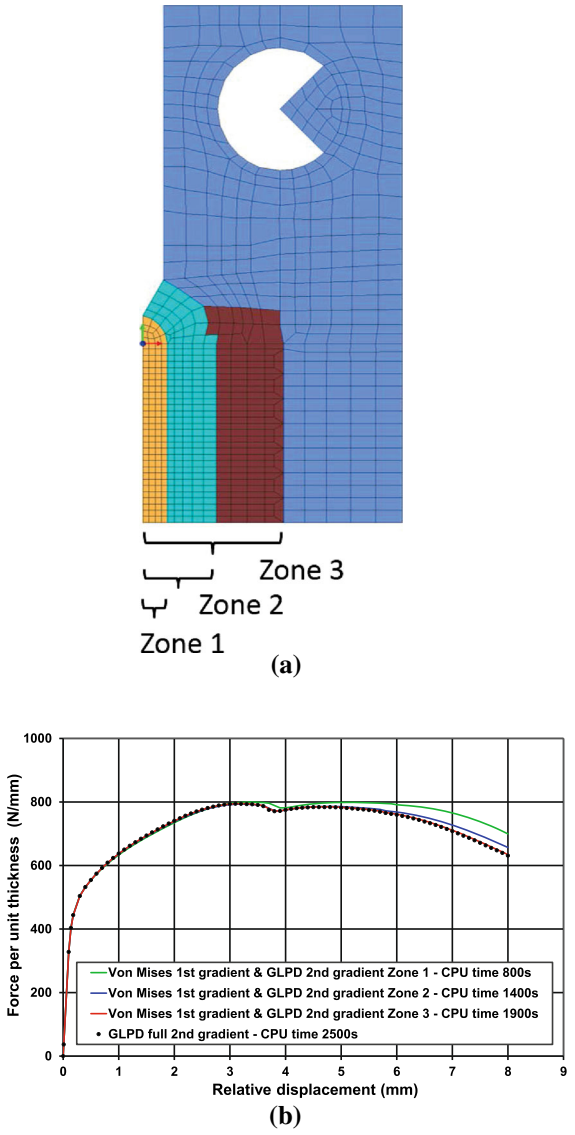

Fig. 37 CT specimen—comparison of simulations using a second-gradient and a mix of first- and second-gradient models. **a** Second gradient zones. **b** Load-displacement curves

tion of 44 %. A more detailed inspection of results (not displayed here) shows that the same conclusions hold for local quantities such as stresses.

7.5 Crack growth

The focus here is on analyses of ductile crack growth aimed at relating the micromechanics of porosity evolution to a material's crack growth resistance. More specifically, the aim is to relate measures of a material's crack growth resistance, such as J_{Ic} and the tearing modulus, T_R, to microstructural quantities governing void nucleation, growth and coalescence, e.g. the stress or strain required for void nucleation, the spacing of void nucleation sites, etc. No attempt is made here to review the extensive literature on porosity induced crack growth. An extensive review of failure of metals, from a materials science perspective, that discusses key issues of ductile crack growth is given by Pineau et al. (2016).

The pioneering analyses of ductile crack growth (which were two dimensional) are those of Rice and Johnson (1970) and McMeeking (1977). Rice and Johnson (1970)'s approximate analysis of void growth in front of a blunting crack tip revealed the importance of blunting on the stress triaxiality in the immediate crack tip vicinity and, since void growth is strongly dependent on stress triaxiality, the importance of blunting for void growth in this region. McMeeking (1977) subsequently carried out finite deformation plane strain finite element analyses of a blunting crack tip to quantify this effect and its dependence on material parameters for materials characterized by a J_2-flow theory of plasticity. In the analyses of Rice and Johnson (1970) and McMeeking (1977), the spacing between initially present voids provides the length scale. In France, this sort of approach was termed the local approach to fracture and first developed for cleavage fracture and then extended to include ductile fracture. Hom and McMeeking (1989) subsequently carried out the pioneering three dimensional analysis of void growth ahead of a crack tip.

Three dimensional analyses of ductile crack growth resistance using the Gurson framework began in the mid 1990s, (e.g. Ruggieri et al. 1996; Mathur et al. 1996). A fundamental difficulty with using a porous plastic constitutive relation like the original Gurson constitutive relation or the GTN modified relation in a local analysis of ductile fracture is the lack of a material length scale. As emphasized by Rice (1976) the prediction of a material's resistance to crack initiation and growth must involve a material length, if only from dimension considerations. Hence, with no length scale in the formulation quantities like J_{Ic}, K_{Ic}, etc. cannot be determined. Also, since softening inevitably precedes material failure, with a rate independent formulation, the governing equations become ill-posed. Therefore, a length scale must somehow be introduced.

Indeed, there are a variety of possible length scales associated with the ductile fracture process. These include the void or void nucleating particle spacing, the void or void nucleating particle size, the void spacing at which void coalescence occurs, the width of shear bands that can precede void coalescence, and the grain size in a polycrystal. In addition, as is well-known there are length scales associated with plastic flow of the matrix and, in some circumstances these can play a role (under dynamic loading conditions inertia can introduce a length scale). The approach to using a length scale by Ruggieri et al. (1996) was through the use of a so-called cell model where each finite element is regarded as a "cell" and the finite element length size is associated with a material length scale. The approach of Needleman and Tvergaard (1991), Tvergaard and Needleman (1994), Mathur et al. (1996) was to introduce "inclusions," actually islands of a void nucleation function, and to identify the material length scale with the inclusion spacing. This is closely related to the initial void spacing length scale of Rice and Johnson (1970) and McMeeking (1977).

A wide variety of calculations of ductile crack growth and ductile-brittle transitions have been carried out using physically based models of the ductile fracture process. Here, we focus on recent calculations of crack growth where the length scale arises from the spacing of the void nucleating particles. It is clear that such a length scale can only govern over a range of length scales: if the void nucleating particles are too close together, the response is as if the material consisted entirely of particles so that the length scale disappears, while on the other hand if the particles are too far apart then fracture is governed only by the size independent material description and, again, the length scale disappears. In grid based numerical methods such as the finite element method, the grid provides a length scale so that if the only material length scale is the void nucleating particle spacing, when that length scale no longer governs, the grid spacing becomes the governing length scale. In such a case, the predictions are an artifact of the numerics rather than an outcome of the model of the fracture process. Needleman and Tvergaard (1994) analyzed a two dimensional plane strain quasi-static crack growth problem with different levels of mesh refinement near the crack tip. Crack growth predictions in cases where the large scale voids dominate showed practically no mesh sensitivity, whereas cases dominated by the small scale voids showed a clear mesh sensitivity. This at least provides the hope that in some circumstances the spacing between such void nucleating inclusions can set a length scale.

In engineering materials such as structural steels and aluminum alloys, the ductile crack growth mechanism can involve two populations of void nucleating particles; larger particles that nucleate voids at relatively small strains and smaller particles that nucleate voids at much larger strains. In a variety of crack growth analyses, including those of Needleman and Tvergaard (1994), this situation is analyzed by modeling the large particles as "islands" of a stress controlled void nucleation function so that they nucleate voids in the vicinity of a crack tip at a fairly early stage of the deformation history, while the small scale particles are taken to be uniformly distributed and nucleate voids by a plastic strain controlled mechanism.

Presuming that the spacing of initially present voids or void nucleating particles provides the governing length scale, the question arises as to how the material's fracture resistance depends on their distribution. All other things being equal, the fracture resistance, as expected, decreases with increasing volume fraction. On the other hand, the dependence on other characteristics of the distribution are not so straightforward.

In order to explore the effect of void nucleating particle distribution, Needleman and Tvergaard (1991) analyzed dynamic crack growth for various distributions with the large particles confined to lying along the initial crack line. They found that more non-uniform distributions can lead to increased crack growth resistance. A possible mechanism for this is that a non-uniform distribution will have some closely spaced particles that the crack can grow through quickly but then will have to grow through a region where the larger void nucleating particles are rather widely spaced. Then, as the crack is delayed at the beginning of this interval, the crack blunts which reduces the stress concentration ahead of the crack to nucleate the next large particle. This non-linear blunting effect leads to an overall slower speed of crack growth. Of course, this is a highly idealized situation and in more general circumstances the crack can grow off the crack line as analyzed in plane strain by Tvergaard and Needleman (1994). However, it illustrates that enhanced crack blunting associated with regions of widely spaced void nucleating particles can result in enhanced crack growth resistance. Thus, in contrast to localization, the crack growth resistance for a non-uniform dis-

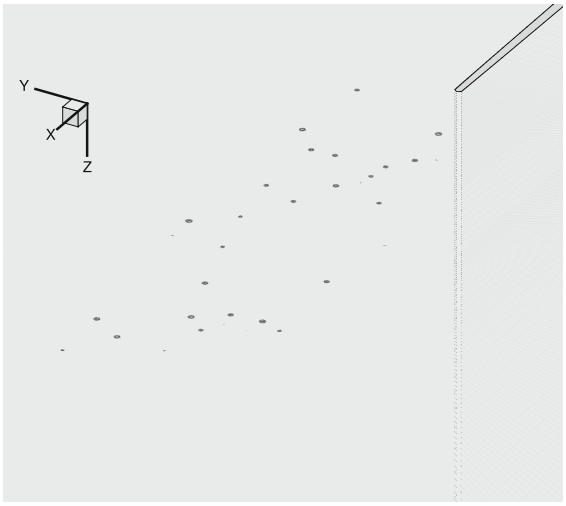

Fig. 38 A slice through the slab thickness (z = constant) showing the inclusion distribution in that plane. From Srivastava et al. (2014)

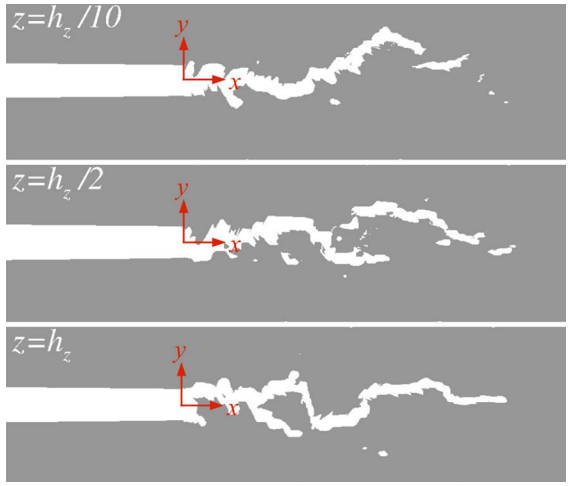

Fig. 39 Crack profiles in three z = constant cross sections for one random distribution with an inclusion volume fraction of 2.4 % in the uniform mesh region. From Srivastava et al. (2014)

tribution can be greater than for a uniform distribution.

Srivastava et al. (2014) carried out three dimensional analyses of the effect of inclusion distribution on crack growth. Both measures of crack growth resistance and of fracture surface roughness were calculated. There were several reasons for this: (i) the parameters characterizing crack growth resistance, such as J_{Ic} and the tearing modulus, T_R, are macro-scale parameters so that theories that give similar values for such parameters can predict significantly different local details; and (ii) there is the basic question as to whether or not there is a quantitative relation between measures of crack growth resistance and fracture surface roughness.

Srivastava et al. (2014) analyzed a mode I small scale yielding boundary value problem for a slice of material with an initial crack. A dynamic finite element analysis was carried out with displacements corresponding to the quasi-static mode I isotropic elastic singular displacement field imposed on the remote boundaries. The initial conditions and the rate of application of the imposed loading was taken to minimize wave effects and to simulate quasi-static loading conditions.

There was a uniform finite element mesh region in front of the initial crack with a specified density (or mean spacing) of the inclusions (the islands of stress controlled nucleation) with a three dimensional random distribution of inclusion centers. Figure 38 shows a through thickness slice of one distribution. Eight inclusion volume fractions were analyzed ranging from 1.2 to 19 %, with calculations carried out for seven realizations of each. The inclusion distributions were characterized by their volume fraction in the uniform mesh region and, equivalently, by the value of their mean spacing (Srivastava et al. 2014). The only length that varied in the cases considered was the mean inclusion spacing. Since for quasi-static loading, only relative lengths matter, all length dimensions were normalized by the dimension of an element side in the uniform mesh region and this length was denoted by e_x; for example, the mean inclusion spacing is denoted by ℓ_0/e_x.

The mode of crack growth for one case is shown in Fig. 39. The white regions indicate where the void volume fraction f exceeds 0.10 so that in the white region essentially all stress carrying capacity is lost. The border of the $f = 0.10$ contour is identified as the crack surface. Crack growth clearly varies through the thickness of the slice.

Crack growth resistance curves, i.e. curves of J versus crack advance Δa, where J is obtained from the value of the applied stress intensity factor K_I, by the small scale yielding relation (Rice 1968)

$$J = K_I^2 \frac{1-\nu^2}{E} \tag{54}$$

were calculated for seven values of mean inclusion spacing (or inclusion volume fraction). Figure 40

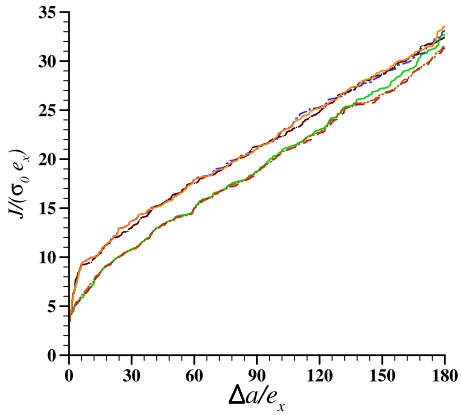

Fig. 40 Applied normalized J, $J/(\sigma_0 e_x)$, versus normalized crack extension, $\Delta a/e_x$, for seven random distributions of inclusions for an inclusion volume fraction $n = 0.024$ ($\ell_0 = 8.41 e_x$). From Srivastava et al. (2014)

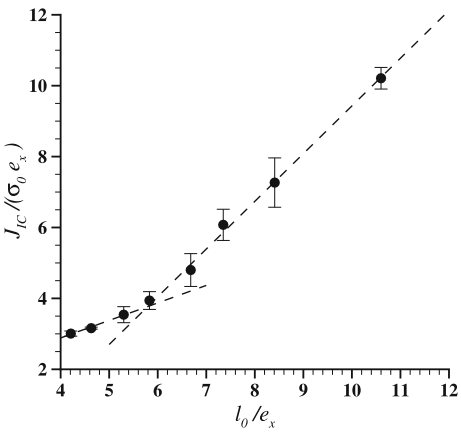

Fig. 41 Variation of $J_{IC}/(\sigma_0 e_x)$ with mean inclusion spacing ℓ_o/e_x. From Srivastava et al. (2014)

shows curves of J, computed from the applied value of K_I from Eq. (54) versus crack length Δa, where Δa is average value through the thickness. The variation between realizations is largest for small inclusion volume fractions (large inclusion spacings) and decreases with increasing inclusion volume fraction. Sufficient crack growth was obtained so that the procedure for calculating J_{Ic} in the ASTM E1820-11 could be simulated.

Figure 41 shows the computed curves of J_{Ic} versus mean inclusion spacing ℓ_0 (normalized by e_x). There is a clear change in the dependence at around $\ell_0/e_x \approx 7$. As noted by Srivastava et al. (2014), this is related to the two modes of ductile crack advance discussed by Tvergaard and Hutchinson (2002). One mode, dominant at

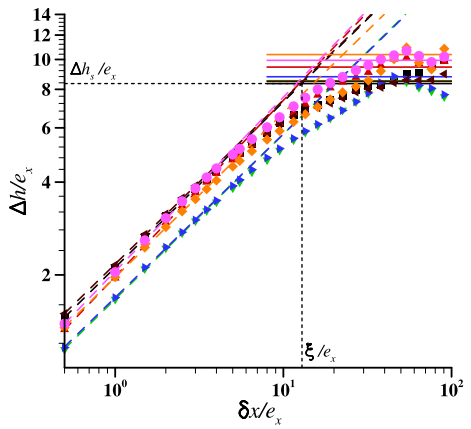

Fig. 42 Height-height correlation functions of the fracture surface roughness for the seven realizations with inclusion volume fraction $n = 0.024$ ($\ell_0/e_x = 8.41$). From Srivastava et al. (2014)

larger inclusion spacings, is a void-by-void mode of crack growth and the other mode, dominant at small inclusion spacings, is a multiple void interaction mode of crack growth.

Statistical measures of the fracture surface roughness were also calculated by Srivastava et al. (2014). Figure 42 shows a plot of the correlation function of the height fluctuations of the fracture surface, Δh given by

$$\Delta h\,(\delta x) = \sqrt{\left\langle [h\,(x+\delta x, z) - h\,(x, z)]^2 \right\rangle_{x,z}} \qquad (55)$$

where $\langle\ \rangle_{x,z}$ denotes the average over x and z, with x being the coordinate in the main crack growth direction and z the coordinate in the slab thickness direction. As seen in Fig. 42, there is a range of values of δx for which a log-log plot of the correlation function exhibits a linear slope, implying a power law relation of the form

$$\Delta h\,(\delta x) \propto \delta x^{\beta} \qquad (56)$$

Here, β is termed the Hurst exponent which necessarily lies between 0 and 1. A self-affine function with Hurst exponent β is a fractal object with dimension $2 - \beta$ when viewed at sufficiently small length scales, but is an ordinary one dimensional object ($\beta = 1$) when viewed over a sufficiently large length scale. The value $\beta = 1/2$ corresponds to a random walk (an increase in Δh is as likely as a decrease); with $\beta > 1/2$, an increase (decrease) is likely to be followed by an increase (decrease); while with $\beta < 1/2$

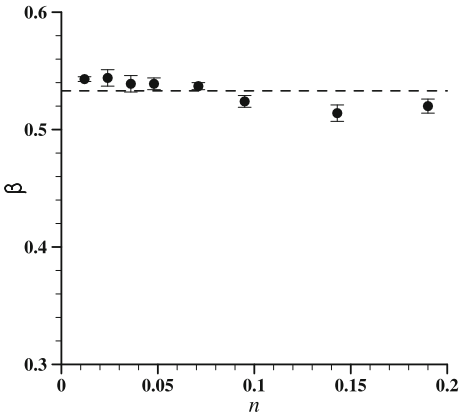

Fig. 43 Variation of the Hurst exponent β with inclusion volume fraction n. From Srivastava et al. (2014)

an increase (decrease) is likely to be followed by a decrease (increase), see the references in Srivastava et al. (2014) for a more complete description.

Figure 43 shows the computed values of the Hurst exponent versus inclusion volume fraction n for the range of volume fractions computed, i.e. from 1.2 to 19 %. The value of the Hurst exponent is essentially independent of inclusion volume fraction (and, equivalently, independent of the mean void spacing). This independence is consistent with the contention of Bouchaud et al. (1990) that the value of the Hurst exponent is independent of the material and nature of the loading, i.e. quasi-static, dynamic, etc.

In the finite element calculations, the fracture surface is identified with the contour $f = 0.10$ and the values of void volume fraction are known at element Gauss points. The correlation function is computed on a uniform grid (as in experiments). This requires extrapolation and the value of β does depend on the extrapolation procedure to some extent, a variation of about 0.02 to 0.03. However, the lack of dependence of the Hurst exponent β on the inclusion volume fraction (or equivalently, the inclusion mean spacing) is independent of the extrapolation procedure used.

The scaling in Eq. (56) holds for a range of values of δx and for $\delta x = \xi$, the height correlation function becomes independent of δx which corresponds to $\beta = 0$ in Eq. (56). The values $\beta = 0$ and $\beta = 1$ correspond to a straight line. In the work of Osovski et al. (2015), a closer look at the character of the correlation function revealed that for small δx, a Hurst exponent with a more or less universal value greater than 0.5 prevails, for somewhat larger values of δx, the value of β is less than 0.5 and finally for sufficiently large δx, $\beta = 0$ or 1. This can be rationalized by noting that the roughness in a random microstructure is close to a random walk (for which $\beta = 0.5$) but biased to a larger value of β by the tendency of cracks (and micro-cracks) to continue growing, at least for a while, in the same direction (possibly providing an explanation of why β has an essentially universal value for a wide range of materials and loading conditions). Then, under mode I loading, the crack is expected to eventually change direction to continue growing, on average, in the initial crack plane. Finally, for sufficiently large δx, the mode I crack appears to be growing straight.

Since the Hurst exponent β is not sensitive to material microstructure, its value cannot be related to any measure of crack growth resistance. On the other hand, the length scale ξ, the length scale at which the crack appears to be straight ($\beta = 0$ or 1) is sensitive to the mean inclusion spacing as shown in Fig. 44. As in Fig. 41 there is a clear change in the variation at a mean inclusion spacing of $\ell_0 \approx 7e_x$.

Figure 45 shows that for ℓ_0 greater than about $7e_x$ there is a clear linear relation between J_{Ic} and ξ. As discussed by Srivastava et al. (2014), the crack growth mode for $\ell_0 \geq 7$ is predominantly what Tvergaard and Hutchinson (2002) termed a void-by-void crack growth mode. Hence, the results of Srivastava et al. (2014) suggest that when the crack growth mode is void-by-void dominated, measures of crack growth resistance and fracture surface roughness can be quantitatively related. What relation, if any, exists in other circumstances is an open question.

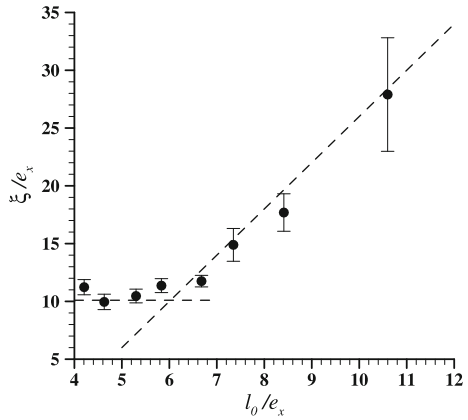

Fig. 44 Variation of the normalized cut-off length, ξ/e_x, with mean inclusion spacing ℓ_o/e_x. From Srivastava et al. (2014)

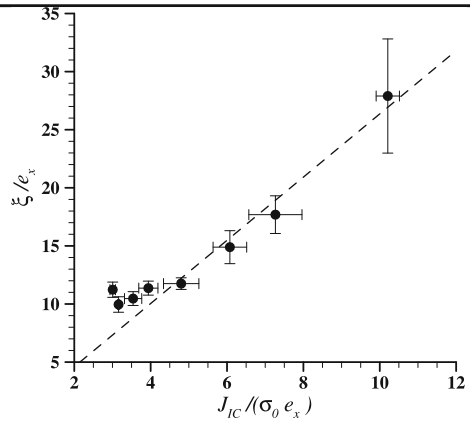

Fig. 45 Variation of the normalized cut-off length ξ/e_x with $J_{IC}/(\sigma_0 e_x)$. From Srivastava et al. (2014)

An increasing number of three dimensional analyses of crack growth are being carried out including the effects of loading rate, (Osovski et al. 2015), micro-inertia (Jacques et al. 2012), matrix strain gradient plasticity (Tang et al. 2013) and flat to slant transitions (Besson et al. 2013).

The results of Srivastava et al. (2014) and those of Osovski et al. (2015) for the relation between crack growth resistance measures and fracture surface roughness measures have been based on the GTN model. Recent advances in void nucleation, growth and coalescence modeling are not incorporated. While the qualitative features of the predictions are in accord with experiment, it is likely that a quantitative agreement will need to incorporate features of the ductile fracture formulations process as in the models presented in Sects. 3, 4, 5.

In addition to fracture surface roughness measurements, there have been great recent advances in three dimensional imaging, such as tomography, so that predictions of internal, as well as surface, local field values can be compared with experimental measurements. Local field predictions are, in general, a more discerning test of predictability than overall quantities such as J_{Ic} or the tearing modulus, T_R.

Two extensions where a micromechanically based, or at least motivated, formulation of the type used to model fracture could have a significant impact are ductile-brittle transition modeling and incorporation of environmental effects into the constitutive framework. The coupling of plasticity with diffusion of various chemical species could follow the formulation for coupled heat conduction with plasticity. The main issue is

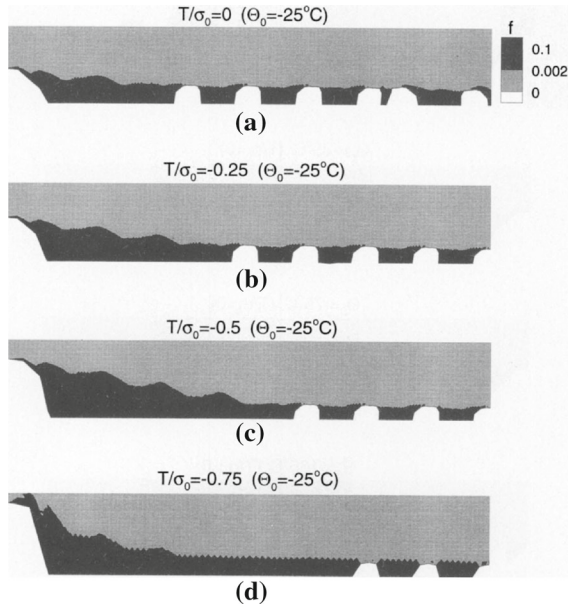

Fig. 46 Contours of porosity f with various values of the T-stress at temperature $\Theta_0 = -25\,^{\circ}\mathrm{C}$ showing the effects of constraint on the transition from a ductile mode of crack growth to brittle cleavage. The 'grains' where cleavage occurred are shown in *white*. The loading is mode I and the crack is constrained to grow straight ahead from its initial location. From Gao et al. (1996)

incorporating the effects of chemistry on void nucleation and possibly growth and coalescence in a predictive yet computationally efficient way.

Various two dimensional calculations of ductile-brittle transitions have been carried out using a phenomenological model for brittle fracture where 'cleavage grains' are introduced as in the analysis of Gao et al. (1996). Figure 46 shows circumstances where crack growth begins via ductile failure but transitions to brittle cleavage after a certain amount of crack growth. The analyses of Gao et al. (1996) were carried out for mode I small scale yielding conditions. In Fig. 46 Θ_0 is the initial temperature and T is an initial stress acting parallel to the crack line. Three dimensional predictive analyses of the ductile-brittle transition could give insight into a material design to preclude, or at least significantly delay, this type of failure transition.

8 Concluding remarks

We have presented an overview of the most widely used continuum framework, generally referred to as the GTN model, for analyzing the ductile fracture of

structural metals by the nucleation, growth and coalescence of voids. The limitations of this modeling framework have been discussed and recent work on improving the modeling framework has been reviewed. Areas where particular recent advances have been made are in the modeling of porosity evolution at low stress triaxiality and in the development of a unified constitutive framework including void growth and coalescence. The inclusion of void nucleation in such a unified framework remains a challenge.

Porous plastic materials are prone to localization of deformation due to porosity induced softening. Localization of deformation can arise as a material instability or it can be induced by material heterogeneity or geometry induced stress and deformation gradients. Localization analyses are useful for exploring the implications of various proposed constitutive relations and can be exploited in numerical implementations. Localization analyses also highlight the need for incorporation of a material length scale into analyses of the response of porous plastic solids whether through direct incorporation into the constitutive relation or through material heterogeneity or both.

We have concluded by showing the capabilities of the current theoretical framework in a variety of applications and the opportunities that exist for the enhanced modeling frameworks to improve the quantitative predictive capabilities of ductile failure modeling. There are opportunities for these advances to have an impact on the design of engineering components and structures as well as on the design of materials with improved ductile failure resistance.

Acknowledgments AAB acknowledges the support of the National Science Foundation under Grant Number CMMI-1405226. AN is grateful for the support provided by the National Science Foundation under Grant Number CMMI-1200203.

References

Agoras M, Ponte Castañeda P (2013) Iterated linear comparison bounds for viscoplastic porous materials with ellipsoidal microstructures. J Mech Phys Solids 61:701–725

Agoras M, Ponte Castañeda P (2014) Anisotropic finite-strain models for porous viscoplastic materials with microstructure evolution. Int J Solids Struct 51:981–1002

Argon AS, Im J, Safoglu R (1975) Cavity formation from inclusions in ductile fracture. Met Trans A 6A:825–837

Arriaga M, McAuliffe C, Waisman H (2015) Onset of shear band localization by a local generalized eigenvalue analysis. Comput Methods Appl Mech Eng 289:179–208

Babout L, Bréchet Y, Maire E, Fougères R (2004) On the competition between particle fracture and particle decohesion in metal matrix composites. Acta Mater 52:4517–4525

Bao Y, Wierzbicki T (2004) On fracture locus in the equivalent strain and stress triaxiality space. Int J Mech Sci 46:81–98

Barsoum I, Faleskog J (2007a) Rupture mechanisms in combined tension and shear-experiments. Int J Solids Struct 44:1768–1786

Barsoum I, Faleskog J (2007b) Rupture mechanisms in combined tension and shear-micromechanics. Int J Solids Struct 44:5481–5498

Barsoum I, Faleskog J (2011) Micromechanical analysis on the influence of the lode parameter on void growth and coalescence. Int J Solids Struct 48:925–938

Beachem CD (1963) An electron fractographic study of the influence of plastic strain conditions upon ductile rupture processes in metals. Trans ASM 56:318–326

Becker R, Needleman A (1986) Effect of yield surface curvature on necking and failure in porous solids. J Appl Mech 53:491–499

Benallal A, Desmorat R, Fournage M (2014) An assessment of the role of the third stress invariant in the Gurson approach for ductile fracture. Eur J Mech A/Solids 47:400–414

Benzerga AA (2000) Rupture ductile des tôles anisotropes. PhD thesis, Ecole Nationale Supérieure des Mines de Paris

Benzerga AA (2002) Micromechanics of coalescence in ductile fracture. J Mech Phys Solids 50:1331–1362

Benzerga AA, Besson J (2001) Plastic potentials for anisotropic porous solids. Eur J Mech A/Solids 20:397–434

Benzerga AA, Leblond JB (2010) Ductile fracture by void growth to coalescence. Adv Appl Mech 44:169–305

Benzerga AA, Leblond JB (2014) Effective yield criterion accounting for microvoid coalescence. J Appl Mech 81(3):031009

Benzerga AA, Besson J, Pineau A (1999) Coalescence-controlled anisotropic ductile fracture. J Eng Mat Tech 121:221–229

Benzerga AA, Besson J, Batisse R, Pineau A (2002a) Synergistic effects of plastic anisotropy and void coalescence on fracture mode in plane strain. Modell Simul Mater Sci Eng 10:73–102

Benzerga AA, Tvergaard V, Needleman A (2002b) Size effects in the Charpy V-notch test. Int J Frac 116:275–296

Benzerga AA, Besson J, Pineau A (2004) Anisotropic ductile fracture. Part II: theory. Acta Mater 52:4639–4650

Beremin FM, Pineau A, Mudry F, Devaux J, DEscatha Y, Ledermann P (1981a) Experimental and numerical study of the different stages in ductile rupture: application to crack initiation and stable crack growth. In: Nemat-Nasser S (ed) Three-dimensional constitutive relations of damage and fracture. Pergamon Press, North Holland, pp 157–172

Beremin FM, Pineau A, Mudry F, Devaux J, DEscatha Y, Ledermann P (1981b) Cavity formation from inclusions in ductile fracture. Met Trans A 12A:723–731

Bergheau JM, Leblond JB, Perrin G (2014) A new numerical implementation of a second-gradient model for plastic porous solids, with an application to the simulation of ductile rupture tests. Comput Methods Appl Mech Eng 268:105–125

Besson J (2010) Continuum models of ductile fracture: a review. Int J Damage Mech 19:3–52

Besson J, McCowan CN, Drexler ES (2013) Modeling flat to slant fracture transition using the computational cell methodology. Eng Frac Mech 104:80–95

Bishop RF, Hill R, Mott NF (1945) The theory of indentation and hardness tests. Proc Phys Soc Lond 57:147–159

Bouchaud E, Lapasset G, Planes J (1990) Fractal dimension of fractured surfaces: a universal value? Eur Phys Lett 13:73–79

Budiansky B, Hutchinson JW, Slutsky S (1982) Void growth and collapse in viscous solids. In: Hopkins HG, Sowell MJ (eds) Mechanics of Solids, The Rodney Hill 60th Anniversary Volume, Pergamon Press, North Holland, pp 13–45

Cazacu O, Revil-Baudard B, Chandola N, Kondo D (2014) New analytical criterion for porous solids with Tresca matrix under axisymmetric loadings. Int J Solids Struct 51:861–874

Chu C, Needleman A (1980) Void nucleation effects in biaxially stretched sheets. J Eng Mat Tech 102:249–256

Cox TB, Low JR (1974) An investigation of the plastic fracture of AISI 4340 and 18 nickel-200 grade maraging steels. Met Trans 5:1457–1470

Dahl J, Nielsen KL, Tvergaard V (2012) Effect of contact conditions on void coalescence at low stress triaxiality shearing. J Appl Mech 79(021):003

Danas K, Ponte Castañeda P (2009a) A finite-strain model for anisotropic viscoplastic porous media: I-theory. Eur J Mech A/Solids 28:387–401

Danas K, Ponte Castañeda P (2009b) A finite-strain model for anisotropic viscoplastic porous media: II-applications. Eur J Mech A/Solids 28:402–416

Danas K, Ponte Castañeda P (2012) Influence of the Lode parameter and the stress triaxiality on the failure of elasto-plastic porous materials. Int J Solids Struct 49:1325–1342

Dunand M, Mohr D (2011a) On the predictive capabilities of the shear modified gurson and the modified Mohr–Coulomb fracture models over a wide range of stress triaxialities and lode angles. J Mech Phys Solids 59:1374–1394

Dunand M, Mohr D (2011b) Optimized butterfly specimen for the fracture testing of sheet materials under combined normal and shear loading. Eng Frac Mech 78:2919–2934

Enakoutsa K, Leblond JB (2009) Numerical implementation and assessment of the GLPD micromorphic model of ductile rupture. Eur J Mech A/Solids 28:445–460

Fleck NA, Hutchinson JW, Tvergaard V (1989) Softening by void nucleation and growth in tension and shear. J Mech Phys Solids 37:515–540

François D, Pineau A (2002) From Charpy to present impact testing. Elsevier, Oxford

Gao X, Shih CF, Tvergaard V, Needleman A (1996) Constraint effects on the ductile–brittle transition in small scale yielding. J Mech Phys Solids 44:1255–1282

Garajeu M, Michel JC, Suquet P (2000) A micromechanical approach of damage in viscoplastic materials by evolution in size, shape and distribution of voids. Comput Methods Appl Mech Eng 183:223–246

Garrison WM, Moody NR (1987) Ductile fracture. J Phys Chem Solids 48:1035–1074

Gologanu M (1997) Etude de quelques problèmes de rupture ductile des métaux. PhD thesis, Université Paris 6

Gologanu M, Leblond JB, Devaux J (1993) Approximate models for ductile metals containing non-spherical voids—case of axisymmetric prolate ellipsoidal cavities. J Mech Phys Solids 41:1723–1754

Gologanu M, Leblond JB, Devaux J (1994) Approximate models for ductile metals containing non-spherical voids—case of axisymmetric oblate ellipsoidal cavities. J Eng Mat Tech 116:290–297

Gologanu M, Leblond JB, Perrin G, Devaux J (1997) Recent extensions of Gurson's model for porous ductile metals. CISM lectures series. In: Suquet P (ed) Continuum micromechanics. Springer, New York, pp 61–130

Gologanu M, Leblond JB, Perrin G, Devaux J (2001a) Theoretical models for void coalescence in porous ductile solids—I: coalescence in "layers". Int J Solids Struct 38:5581–5594

Gologanu M, Leblond JB, Perrin G, Devaux J (2001b) Theoretical models for void coalescence in porous ductile solids–II: coalescence in "columns". Int J Solids Struct 38:5595–5604

Goods SH, Brown LM (1979) The nucleation of cavities by plastic deformation. Acta Metal 27:1–15

Gurland J, Plateau J (1963) The mechanism of ductile rupture of metals containing inclusions. Trans ASM 56:442–454

Gurson AL (1975) Plastic flow and fracture behavior of ductile materials incorporating void nucleation, growth and interaction. PhD thesis, Brown University, Providence

Gurson AL (1977) Continuum theory of ductile rupture by void nucleation and growth: part I—yield criteria and flow rules for porous ductile media. J Eng Mat Tech 99:2–15

Hadamard J (1903) Leçons sur la propagation des ondes et les équations de l'hydrodynamique, Librairie Scientifique, A. Herrmann, Paris, chap 6

Haltom SS, Kyriakides S, Ravi-Chandar K (2013) Ductile failure under combined shear and tension. Int J Solids Struct 50:1507–1522

Han X, Besson J, Forest S, Tanguy B, Bugat S (2013) A yield function for single crystals containing voids. Int J Solids Struct 50:2115–2131

Hill R (1948) A theory of yielding and plastic flow of anisotropic solids. Proc R Soc Lond A 193:281–297

Hill R (1958) A general theory of uniqueness and stability in elastic–plastic solids. J Mech Phys Solids 6:236–249

Hill R (1962) Acceleration waves in solids. J Mech Phys Solids 10:1–16

Hill R (1967) The essential structure of constitutive laws for metal composites and polycrystals. J Mech Phys Solids 15:79–95

Hom CL, McMeeking RM (1989) Three-dimensional void growth before a blunting crack tip. J Mech Phys Solids 37:395–415

Horstemeyer MF, Gokhale AM (1999) A void-crack nucleation model for ductile metals. Int J Solids Struct 36:5029–5055

Hu C, Ghosh S (2008) Locally enhanced voronoi cell finite element model (LE-VCFEM) for simulating evolving fracture in ductile microstructures containing inclusions. Int J Numer Meths Eng 76:1955–1992

Huang Y (1991) Accurate dilatation rates for spherical voids in triaxial stress fields. J Appl Mech 58:1084–1085

Huespe A, Needleman A, Oliver J, Sánchez P (2012) A finite strain, finite band method for modeling ductile fracture. Int J Plast 28:53–69

Huespe AE, Needleman A, Oliver J, Sánchez PJ (2009) A finite thickness band method for ductile fracture analysis. Int J Plast 25:2349–2365

Hussein MI, Borg U, Niordson CF, Deshpande VS (2008) Plasticity size effects in voided crystals. J Mech Phys Solids 56:114–131

Idiart MI (2007) Nonlinear sequential laminates reproducing hollow sphere assemblages. C R Mecanique 335:363–368

Idiart MI (2008) Modeling the macroscopic behavior of two-phase nonlinear composites by infinite-rank laminates. J Mech Phys Solids 56:2599–2617

Jacques N, Mercier S, Molinari A (2012) Effects of microscale inertia on dynamic ductile crack growth. J Mech Phys Solids 60:665–690

Johnson GR, Cook WH (1985) Fracture characteristics of three metals subjected to various strains, strain rates, temperatures and pressures. Eng Frac Mech 21:31–48

Joly P, Cozar R, Pineau A (1990) Effect of crystallographic orientation of austenite on the formation of cleavage cracks in ferrite in an aged duplex stainless steel. Scripta Metall Mater 24:2235–2240

Kailasam M, Ponte Castaneda P (1998) A general constitutive theory for linear and nonlinear particulate media with microstructure evolution. J Mech Phys Solids 46:427–465

Keralavarma SM, Benzerga AA (2008) An approximate yield criterion for anisotropic porous media. C R Mecanique 336:685–692

Keralavarma SM, Benzerga AA (2010) A constitutive model for plastically anisotropic solids with non-spherical voids. J Mech Phys Solids 58:874–901

Keralavarma SM, Chockalingam S (2016) A criterion for void coalescence in anisotropic ductile materials. Int J Plast (in press)

Kondori B, Benzerga AA (2014) Effect of stress triaxiality on the flow and fracture of Mg alloy AZ31. Metall Mater Trans A 45:3292–3307

Koplik J, Needleman A (1988) Void growth and coalescence in porous plastic solids. Int J Solids Struct 24:835–853

Lebensohn R, Cazacu O (2012) Effect of single-crystal plastic deformation mechanisms on the dilatational plastic response of porous polycrystals. Int J Solids Struct 49:3838–3852

Leblond JB, Gologanu M (2008) External estimate of the yield surface of an arbitrary ellipsoid containing a confocal void. C R Mecanique 336:813–819

Leblond JB, Mottet G (2008) A theoretical approach of strain localization within thin planar bands in porous ductile materials. C R Mecanique 336:176–189

Leblond JB, Morin L (2014) Gurson's criterion and its derivation revisited. J Appl Mech 81(051):012

Leblond JB, Perrin G, Devaux J (1994) Bifurcation effects in ductile metals with nonlocal damage. J Appl Mech 61:236–242

Leblond JB, Perrin G, Devaux J (1995) An improved Gurson-type model for hardenable ductile metals. Eur J Mech A/Solids 14:499–527

Lee BJ, Mear ME (1992) Axisymmetric deformation of power-law solids containing a dilute concentration of aligned spheroidal voids. J Mech Phys Solids 40:1805–1836

Lee BJ, Mear ME (1999) Stress concentration induced by an elastic spheroidal particle in a plastically deforming solid. J Mech Phys Solids 47:1301–1336

Madou K, Leblond JB (2012a) A Gurson-type criterion for porous ductile solids containing arbitrary ellipsoidal voids—I: limit-analysis of some representative cell. J Mech Phys Solids 60:1020–1036

Madou K, Leblond JB (2012b) A Gurson-type criterion for porous ductile solids containing arbitrary ellipsoidal voids—II: determination of yield criterion parameters. J Mech Phys Solids 60:1037–1058

Madou K, Leblond JB (2013) Numerical studies of porous ductile materials containing arbitrary ellipsoidal voids—I: yield surfaces of representative cells. Eur J Mech A/Solids 42:480–489

Madou K, Leblond JB, Morin L (2013) Numerical studies of porous ductile materials containing arbitrary ellipsoidal voids—II: evolution of the length and orientation of the void axes. Eur J Mech A/Solids 42:490–507

Mandel J (1964) Contribution théorique à l'étude de l'écrouissage et des lois d'écoulement plastique. 11th international congress on applied mechanics. Springer, Berlin, pp 502–509

Mandel J (1966) Conditions de stabilité et postulat de Drucker. In: Krautchenko J, Sirieys PM (eds) Rheology and soil mechanics. Springer, Berlin, pp 58–68

Mansouri LZ, Chalal H, Abed-Meraim F (2014) Ductility limit prediction using a GTN damage model coupled with localization bifurcation analysis. Mech Mater 76:64–92

Mathur KK, Needleman A, Tvergaard V (1996) Three dimensional analysis of dynamic ductile crack growth in a thin plate. J Mech Phys Solids 44:439–464

McClintock FA (1968) A criterion for ductile fracture by the growth of holes. J Appl Mech 35:363–371

McClintock FA, Kaplan SM, Berg CA (1966) Ductile fracture by hole growth in shear bands. Int J Frac Mech 2:614–627

McMeeking RM (1977) Finite deformation analysis of crack-tip opening in elastic-plastic materials and implications for fracture. J Mech Phys Solids 25:357–381

Mear ME, Hutchinson JW (1985) Influence of yield surface curvature on flow localization in dilatant plasticity. Mech Mater 4:395–407

Michel JC, Suquet P (1992) The constitutive law of nonlinear viscous and porous materials. J Mech Phys Solids 40:783–812

Monchiet V, Gruescu C, Charkaluk E, Kondo D (2006) Approximate yield criteria for anisotropic metals with prolate or oblate voids. C R Mecanique 334:431–439

Monchiet V, Cazacu O, Charkaluk E, Kondo D (2008) Macroscopic yield criteria for plastic anisotropic materials containing spheroidal voids. Int J Plast 24:1158–1189

Monchiet V, Charkaluk E, Kondo D (2011) A micromechanics-based modification of the gurson criterion by using Eshelby-like velocity fields. Eur J Mech A/Solids 30:940–949

Morin L (2015) Influence des effets de forme et de taille des cavités, et de l'anisotropie plastique sur la rupture ductile. PhD thesis, Université Pierre et Marie Curie—Paris VI

Morin L, Madou K, Leblond JB, Kondo D (2014) A new technique for finite element limit-analysis of Hill materials, with an application to the assessment of criteria for anisotropic plastic porous solids. Int J Eng Sci 74:65–79

Morin L, Leblond JB, Benzerga AA (2015a) Coalescence of voids by internal necking: theoretical estimates and numerical results. J Mech Phys Solids 75:140–158

Morin L, Leblond JB, Kondo D (2015b) A Gurson-type criterion for plastically anisotropic solids containing arbitrary ellipsoidal voids. Int J Solids Struct 77:86–101
Morin L, Leblond JB, Benzerga AA, Kondo D (2016) A unified criterion for the growth and coalescence of microvoids. J Mech Phys Solids (in press)
Nahshon K, Hutchinson JW (2008) Modification of the Gurson model for shear failure. Eur J Mech A/Solids 27:1–17
Needleman A (1972) A numerical study of necking in circular cylindrical bars. J Mech Phys Solids 20:111–127
Needleman A (1987) A continuum model for void nucleation by inclusion debonding. J Appl Mech 54:525
Needleman A (2015) The effect of rate dependence on localization of deformation and failure in softening solids. J Appl Mech 82(021):002
Needleman A, Rice JR (1978) Limits to ductility set by plastic flow localization. In: Koistinen DP, Wang NM (eds) Mechanics of sheet metal forming. Plenum Press, Berlin, pp 237–267
Needleman A, Tvergaard V (1984) An analysis of ductile rupture in notched bars. J Mech Phys Solids 32:461–490
Needleman A, Tvergaard V (1991) A numerical study of void distribution effects on dynamic, ductile crack growth. Eng Frac Mech 38:157–173
Needleman A, Tvergaard V (1994) Mesh effects in the analysis of dynamic ductile crack growth. Eng Frac Mech 47:75–91
Nielsen KL (2008a) 3D modelling of plug failure in resistance spot welded shear-lab specimens (DP600-steel). Int J Frac 153:125–139
Nielsen KL (2008b) Ductile damage development in friction stir welded aluminum (AA2024) joints. Eng Frac Mech 75:2795–2811
Nielsen KL (2010) Predicting failure response of spot welded joints using recent extensions to the Gurson model. Comput Mater Sci 48:71–82
Nielsen KL, Tvergaard V (2009) Effect of a shear modified Gurson model on damage development in a few tensile specimen. Int J Solids Struct 46:587–601
Nielsen KL, Tvergaard V (2010) Ductile shear failure or plug failure of spot welds modelled by modified gurson model. Eng Frac Mech 77:1031–1047
Nielsen KL, Dahl J, Tvergaard V (2012) Collapse and coalescence of spherical voids subject to intense shearing: studied in full 3D. Int J Frac 177:97–108
Ortiz M, Molinari A (1992) Effect of strain hardening and rate sensitivity on the dynamic growth of a void in a plastic material. J Appl Mech 59:48–53
Osovski S, Srivastava A, Ponson L, Bouchaud E, Tvergaard V, Ravi-Chandar K, Needleman A (2015) The effect of loading rate on ductile fracture toughness and fracture surface roughness. J Mech Phys Solids 76:20–46
Pan J, Saje M, Needleman A (1983) Localization of deformation in rate sensitive porous plastic solids. Int J Frac 21:261–278
Papasidero J, Doquet V, Mohr D (2015) Ductile fracture of aluminum 2024–t351 under proportional and non-proportional multi-axial loading: Bao-wierzbicki results revisited. Int J Solids Struct 69–70:459–474
Pardoen T, Hutchinson JW (2000) An extended model for void growth and coalescence. J Mech Phys Solids 48:2467–2512
Paux J, Morin L, Brenner R, Kondo D (2015) An approximate yield criterion for porous single crystals. Eur J Mech A/Solids 51:1–10
Perrin G (1992) Contribution à l'étude théorique et numérique de la rupture ductile des métaux. PhD thesis, Ecole Polytechnique
Perrin G, Leblond JB (1990) Analytical study of a hollow sphere made of plastic porous material and subjected to hydrostatic tension—application to some problems in ductile fracture of metals. Int J Plast 6:677–699
Perrin G, Leblond JB (1993) Rudnicki and Rice's analysis of strain localization revisited. J Appl Mech 60:842–846
Pineau A, Benzerga AA, Pardoen T (2016) Failure of metals I. brittle and ductile fracture. Acta Mater 107:424–483
Ponte Castaneda P (1991) The effective mechanical properties of nonlinear composites. J Mech Phys Solids 39:45–71
Ponte Castañeda P, Zaidman M (1994) Constitutive models for porous materials with evolving microstructure. J Mech Phys Solids 42:1459–1495
Ponte Castaneda P (2002) Second-order homogenization estimates for nonlinear composites incorporating field fluctuations: I—theory. J Mech Phys Solids 50:737–757
Ponte Castaneda P (2012) Bounds for nonlinear composites via iterated homogenization. J Mech Phys Solids 60:1583–1604
Puttick KE (1959) Ductile fracture in metals. Phil Mag 4:964–969
Raniecki B, Bruhns OT (1981) Bounds to bifurcation stresses in solids with non-associated plastic-flow law at finite strain. J Mech Phys Solids 29:153–172
Rice J (1976) The localization of plastic deformation. In: Koiter W (ed) 14th International congress theoretical and applied mechanics, North–Holland, Amsterdam, pp 207–220
Rice JR (1968) A path independent integral and the approximate analysis of strain concentration by notches and cracks. J Appl Mech 35:379–386
Rice JR, Johnson MA (1970) The role of large crack tip geometry changes in plane strain fracture. In: Inelastic behavior of solids, Mc Graw Hill, New York, pp 641–672
Rice JR, Tracey DM (1969) On the enlargement of voids in triaxial stress fields. J Mech Phys Solids 17:201–217
Ritchie RO (1978) On the relationship between fracture toughness and Charpy V-Notch energy in ultrahigh strength steels. In: Rosenfield AR, Gegel HL, Hasson DF (eds) What does the Charpy test really tell us?. American Society for Metals, Metals Park, pp 54–73
Rodriguez AK, Ayoub GA, Mansoor B, Benzerga AA (2016) Effect of strain rate and temperature on fracture of AZ31B magnesium alloy. Acta Mater 112:194–208
Rogers HC (1960) Tensile fracture of ductile metals. Trans Met Soc AIME 218:498–506
Rousselier G (1981) Finite deformation constitutive relations including ductile fracture damage. In: Nemat–Nasser (ed) Three-dimensional constitutive equations of damage and fracture. Pergamon Press, North Holland, pp 331–355
Rousselier G (1987) Ductile fracture models and their potential in local approach of fracture. Nucl Eng Design 105:97–111
Rudnicki JW, Rice JR (1975) Conditions for the localization of deformation in pressure–sensitive dilatant materials. J Mech Phys Solids 23:371–394

Ruggieri C, Panontin TL, Dodds RH (1996) Numerical modeling of ductile crack growth in 3-D using computational cell elements. Int J Frac 82:67–95

Scheyvaerts F, Onck PR, Tekoglu C, Pardoen T (2011) The growth and coalescence of ellipsoidal voids in plane strain under combined shear and tension. J Mech Phys Solids 59:373–397

Segurado J, Llorca J (2009) An analysis of the size effect on void growth in single crystals using discrete dislocation dynamics. Acta Mater 57:1427–1436

Shabrov MN, Needleman A (2002) An analysis of inclusion morphology effects on void nucleation. Modell Simul Mater Sci Eng 10:163–183

Shima S, Oyane M (1976) Plasticity theory for porous metals. Int J Mech Sci 18:285–291

Shinohara Y, Madi Y, Besson J (2016) Anisotropic ductile failure of a high-strength line pipe steel. Int J Frac 197:127–145

Song D, Agoras M, Ponte Castaneda P (2015) The evolution of pore shape and orientation in plastically deforming metals: implications for macroscopic response and shear localization. Mech Mater 90:47–68

Srivastava A, Ponson L, Osovski S, Bouchaud E, Tvergaard V, Needleman A (2014) Effect of inclusion density on ductile fracture toughness and roughness. J Mech Phys Solids 63:62–79

Tang S, Kopacz AM, Chan O'Keeffe S, Olson GB, Liu WK (2013) Three-dimensional ductile fracture analysis with a hybrid multiresolution approach and microtomography. J Mech Phys Solids 61:2108–2124

Tang H, Fairchild DP, Cheng W, Kan W, Cook M, Macia ML (2015) Development of surface flaw interaction rules for strain-based pipelines. Int J Offshore Polar Eng 25:45–55

Tanguy B, Besson J, Piques R, Pineau A (2005) Ductile to brittle transition of an A508 steel characterized by charpy impact test. Part II: modeling of the charpy transition curve. Eng Frac Mech 72:413–434

Tekoglu C, Leblond JB, Pardoen T (2012) A criterion for the onset of void coalescence under combined tension and shear. J Mech Phys Solids 60:1363–1381

Thomas TY (1961) Plastic flow and fracture in solids. Academic Press, New York

Thomason PF (1985) Three-dimensional models for the plastic limit-loads at incipient failure of the intervoid matrix in ductile porous solids. Acta Metal 33:1079–1085

Tipper CF (1949) The fracture of metals. Metall 39:133–137

Torki ME, Benzerga AA, Leblond JB (2015) On void coalescence under combined tension and shear. J Appl Mech 82(7):071005

Tvergaard V (1981) Influence of voids on shear band instabilities under plane strain conditions. Int J Frac 17:389–407

Tvergaard V (1982a) Ductile fracture by cavity nucleation between larger voids. J Mech Phys Solids 30:265–286

Tvergaard V (1982b) On localization in ductile materials containing spherical voids. Int J Frac 18:237–252

Tvergaard V (1987) Effect of yield surface curvature and void nucleation on plastic flow localization. J Mech Phys Solids 35:43–60

Tvergaard V (1990) Material failure by void growth to coalescence. Adv Appl Mech 27:83–151

Tvergaard V (2008) Shear deformation of voids with contact modeled by internal pressure. Int J Mech Sci 50:1459–1465

Tvergaard V (2009) Behaviour of voids in a shear field. Int J Frac 158:41–49

Tvergaard V (2012) Effect of stress-state and spacing on voids in a shear-field. Int J Solids Struct 49:3047–3054

Tvergaard V, Hutchinson JW (2002) Two mechanisms of ductile fracture: void by void growth versus multiple void interaction. Int J Solids Struct 39:3581–3597

Tvergaard V, Needleman A (1984) Analysis of the cup-cone fracture in a round tensile bar. Acta Metal 32:157–169

Tvergaard V, Needleman A (1986) Effect of material rate sensitivity on the failure modes in the Charpy V-notch test. J Mech Phys Solids 34:213–241

Tvergaard V, Needleman A (1988) An analysis of the temperature and rate dependence of Charpy V-notch energies for a high nitrogen steel. Int J Frac 37:197–215

Tvergaard V, Needleman A (1994) Effect of crack meandering on dynamic, ductile fracture. J Mech Phys Solids 38:447–471

Tvergaard V, Needleman A (1995) Effects of nonlocal damage in porous plastic solids. Int J Solids Struct 32:1063–1077

Tvergaard V, Needleman A (2000) Analysis of the Charpy V-notch test for welds. Eng Frac Mech 65:627–643

Tvergaard V, Needleman A (2004) 3d analyses of the effect of weld orientation in Charpy specimens. Eng Frac Mech 71:2179–2195

Tvergaard V, Nielsen KL (2010) Relations between a micromechanical model and a damage model for ductile failure in shear. J Mech Phys Solids 58:1243–1252

Van Stone RH, Cox TB, Low JR, Psioda JA (1985) Microstructural aspects of fracture by dimpled rupture. Int Met Rev 30:157–179

Willis JR (1977) Bounds and self-consistent estimates for the overall properties of anisotropic composites. J Mech Phys Solids 25:185–202

Willis JR (1991) On methods for bounding the overall properties of nonlinear composites. J Mech Phys Solids 39:73–86

Wilner B (1988) Stress analysis of particles in metals. J Mech Phys Solids 36:141–165

Xu XP, Needleman A (1992) The influence of nucleation criterion on shear localization in rate-sensitive porous plastic solids. Int J Plast 8:315–330

Xu XP, Needleman A (1993) Void nucleation by inclusion debonding in a crystal matrix. Model Simul Mater Sci Eng 1:111–132

Xue L (2008) Constitutive modeling of void shearing effect in ductile fracture of porous materials. Eng Frac Mech 75:3343–3366

Xue Z, Faleskog J, Hutchinson JW (2013) Tension-torsion fracture experiments—Part II: simulations with the extended Gurson model and a ductile fracture criterion based on plastic strain. Int J Solids Struct 50:4258–4269

Yamamoto H (1978) Conditions for shear localization in the ductile fracture of void-containing materials. Int J Frac 14:347–365

Zhang ZL, Thaulow C, Odegard J (2000) A complete Gurson model approach for ductile fracture. Eng Frac Mech 67:155–168